Surface Modification of Carbonaceous Materials Toward Direct Air Capture of Carbon Dioxide

A Thesis Presented for the
Master of Science
Degree
The University of Tennessee, Knoxville

Narges Mokhtarinori
August 2025

DEDICATION

To my beloved husband Alireza, my precious son Parham, and my sweet daughter Hannah; My greatest sources of love, strength, and inspiration.

ACKNOWLEDGEMENTS

I would like to express my deepest gratitude to my advisor, Professor Sheng Dai, for his guidance throughout my graduate studies. His profound knowledge and scientific vision have been a constant source of inspiration. Under his supervision, I have grown not only as a researcher but also as a more thoughtful and resilient individual. I am truly honored to have been part of his distinguished research group, where I was continuously challenged and supported by a dynamic team of dedicated scientists. I am especially grateful to the knowledgeable postdoctoral researchers, graduate students, and colleagues in Dr. Dai's group, from whom I have learned immensely. I will always value the meaningful teamwork and camaraderie that defined my experience in this lab.

A special thank-you goes to Dr. Zhenzhen Yang for her invaluable mentorship and collaboration. Her scientific guidance, consistent encouragement, and thoughtful feedback have had a tremendous impact on the progress and direction of my research. I would like to thank my thesis committee members, Dr. Victor Nemykin, Dr. Konstantinos Vogiatzis, and Dr. David Keffer, for their valuable insights throughout my academic journey. In addition, I express my sincere thanks to the collaborators, colleagues, and co-authors from other departments, universities, and institutions whose contributions and partnerships significantly advanced my work; especially thankful to Dr. De-en Jiang from the Department of Chemical and Biomolecular Engineering at Vanderbilt University, Dr. Danielle J. Chun and Dr. Michael Kilbey from the Department of Chemistry, and Dr. Mahshid Mokhtarnejad and Dr. Bamin Khomami from the Department of Chemical and Biomolecular Engineering at the University of Tennessee, for their interdisciplinary collaboration.

Internationally, I am thankful to Dr. Zaneta Wojnarowska from the University of Silesia in Katowice, Poland, and Dr. Neil Vasdev from the University of Toronto for their scientific engagement and contributions to the projects.

I would like to express my deepest thanks to my beloved husband, Alireza, for his steadfast support and unwavering belief in me. Thank you for standing beside me through

every long night and uncertain step, for sharing the sacrifices and successes of this journey, and for being my anchor in both life and work.

To my dear son, Parham, thank you for your resilience and patience, for enduring the distance from your grandparents and the rest of your loving family, and for bringing light and joy to the most challenging days.

To my daughter, Hannah, thank you for being with me every step of this journey, which has filled me with hope and determination. You are truly part of this accomplishment.

To my cherished mom and dad, thank you for your unconditional love and endless sacrifices. Though you were far away, your prayers, encouragement, and strength were always with me and gave me courage in moments of doubt. To my beloved sisters, Mahnaz and Bahareh, my dear brother, Mahdi, and their families, thank you for your constant support, faith, and love. Your encouragement uplifted me in times of struggle, and your presence—near or far—reminded me that I was never alone.

To all who supported and inspired me along the way—thank you. This work would not have been possible without your contributions, care, and encouragement. This thesis is the result of collective effort, shared knowledge, and generous support from so many, and I am sincerely and humbly grateful to every one of you.

ABSTRACT

Direct air capture (DAC) of CO_2 [carbon dioxide] is a promising solution for reducing the carbon footprint through "negative emission" technology. However, the low CO_2 concentration and the dynamic nature of DAC processes present challenges in designing effective sorbent systems. Recent material design and structural engineering advancements have led to the development of high-performance solid sorbents. This thesis covers design principles, synthesis methodologies, and their impact on CO_2 chemisorption, comparing the advantages and limitations of each approach. The reaction pathways and interaction mechanisms of these sorbents with CO_2 are analyzed to guide future design. Additionally, the CO_2 chemisorption behaviors, including capacity, sorption kinetics, recyclability, and durability in the presence of gaseous impurities, will be evaluated and compared. The superbase ionic liquids (ILs)-modified carbon substrates were developed towards DAC of CO_2 by harnessing the strong CO_2 binding capability of IL and the ordered porous channels provided by the carbon supports. Detailed porosity analysis revealed that the IL with aromatic cation and oxygenate anion preferred to fill the micropores, and a thin layer was created on the surface of the mesopores. With the same IL coating amount, the DAC of CO_2 evaluation revealed that larger mesopore size and pore volume in the carbon/IL composite materials led to higher CO_2 uptake capacity by exposing more active sites to integrate CO_2 from diluted sources. To further probe the dynamics of CO_2 chemisorption within ILs, nuclear magnetic resonance (NMR) spectroscopy was employed, focusing on relaxation time measurements (T_1 and T_2) of CO_2-loaded ILs. These measurements revealed critical insights into CO_2 mobility and binding environments. A shorter T_2 relaxation time indicated stronger interactions and more restricted mobility of chemisorbed CO_2 species. In contrast, longer relaxation times correlated with weaker bound or physiosorbed CO_2. This dynamic profiling provided by NMR relaxometry enables a more comprehensive understanding of the CO_2 capture mechanisms and guides the optimization of sorbent structure for enhanced DAC performance.

TABLE OF CONTENTS

LIST OF TABLES

LIST OF FIGURES

CHAPTER 1 INTRODUCTION

THE CARBON CHALLENGE: DESIGN, SYNTHESIS, AND CHEMISORPTION BEHAVIOR OF SOLID SORBENTS IN DIRECT AIR CAPTURE OF CARBON DIOXIDE

A version of this chapter has been published in *Materials Today Energy* Journal:
Qiu, L., Mokhtarinori, N., Liu, H., Jiang, D. E., Yang, Z., & Dai, S. (2024). The carbon challenge: Design, synthesis, and chemisorption behavior of solid sorbents in direct air capture of carbon dioxide. *Materials Today Energy*, 101740.

1.1 Carbon Capture and Sequestration

The continuing carbon dioxide (CO_2) emission from the transportation, agriculture, industry, and energy sectors has been recognized as a major contribution to greenhouse gas accumulation, causing universal global warming and accompanying natural disasters [1], particularly from the combustion of fossil fuels in power plants. The implementation of a comprehensive set of carbon management technologies, such as capture, removal, conversion, transportation, and storage, is urgent and crucial to achieve the nations' climate goals such as a carbon-free economy by 2050, a carbon pollution free power sector by 2035, and a fifty percent reduction in economy-wide greenhouse gas emissions by 2030 compared to 2005 levels [2–4]. Carbon capture by the as-developed sorption procedures from large point sources such as power plants, refineries, and cement factories could alleviate the greenhouse effect, but has no contribution to the removal of currently existing CO_2 in the atmosphere [5].

Alternatively, direct carbon capture from ambient air could allow negative carbon emissions with less water and land being required compared with the nature-relying approaches [6–8]. Based on the Carbon Capture Program from the Department of Energy's Office of Fossil Energy and Carbon Management (DOE-FECM) in the US, advanced direct air capture (DAC) technologies are highly desired, relying on the discovery and optimization of new sorbent materials. The next-generation high-performance DAC materials will be evaluated by integrating with CO_2 separation equipment components to allow full leveraging of the unique characteristics of sorbents, maximizing CO_2 capture productivity, reducing pressure drop, maximizing CO_2 contact area, and minimizing heat and power requirements towards operation cost reduction. DAC was raised up by the Los Alamos National Laboratory towards atmospheric CO_2 level reduction in 1999 [9], but diverse technological and financial obstacles need to be addressed owing to the low CO_2 concentration and open nature of the DAC procedures

before making it a practical and viable solution to climate change [10]. For example, the extremely low atmospheric CO_2 concentration (~400 ppm) requires robust and highly selective CO_2 binding capability of the active sites in DAC sorbents in competition with other airborne components, such as water, which is 10–100 times more prevalent than CO_2 in the atmosphere [11]. In addition, to have a perceivable influence on the climate, the massive scale of DAC technology implementation should be considered in practical cost evaluation. The design and development of high-performance sorbents played critical roles in DAC technologies, in which both liquid [12–16] and solid [17,18] systems have been demonstrated. Leveraging the strong interaction strength of amine species with CO_2 molecules, aqueous amine solutions are state-of-the-art sorbents being deployed in practical carbon capture procedures, which still have limitations regarding the solvent/amine evaporation, equipment corrosion, decomposition, efficiency decline, and high energy input for CO_2 release. The development of liquid sorbents is further extended to aqueous alkaline hydroxide/carbonate solutions possessing even stronger chemical bond formation capability with CO_2 and lower cost, which, in turn, make the desorption and sorbent recycling more energy intensive [19]. Considering the solvent evaporation and extra energy supply to heat the solvent (with no contribution to uptake capacity) for chemical bond cleavage between CO_2 and the active sites, engineered solid sorbents capable of integrating the merits of strong interaction with CO_2 and having no economic/energy expense on solvents are extensively studied with the advances in the field of material design and structural engineering to tackle the carbon challenge via DAC of CO_2 and to provide solutions to the stability/safety/energy efficiency issues. Alkali or alkaline earth metals oxides are known for the capability to integrate CO_2 via chemical bonding formation via the reaction pathway of $M_xO + CO_2 \leftrightharpoons M_xCO_3$ (x = 1 and 2 for alkaline earth metals and alkaline metals, respectively) [20]. For example, solid alkali sorbents such as commercially available and cost-effective calcium oxide (CaO), also referred to as lime-type sorbents, have been deployed to capture low-concentration CO_2, generating carbonate or bicarbonate compounds under humid conditions [21]. The solid alkali sorbent-involved carbon capture approach was reversible via the carbonation-

calcination cycles, but the downside is the high energy input in calcination (e.g., 800–875 °C) to achieve complete decomposition of the carbonation products [22].

Currently, the amine-modified materials (e.g., porous silicas, zeolites, metal-organic frameworks (MOFs) [23–25], covalent organic frameworks (COFs) [26], carbons [27, 28], resins [29], and layered double hydroxides (LDHs)) [30] are the most widely developed types in low concentration carbon capture. Efforts have been made to improve the uptake capacities, stabilities, and sorption kinetics in CO_2 capture from ambient air via synthesis engineering, amine structure variation, CO_2 capture pathway control, surface/porosity modification of supports, and additive selection [31]. Notably, the intrinsic thermodynamic interaction between amines and CO_2 limited the tuning capability of amine-modified sorbents via carbamate, ammonium bicarbonate (in the presence of H_2O), or carbamic acid formation in a few cases [32], in terms of both carbon capture capacity and energy consumption for complete CO_2 release. Alternative solid sorbents have been generated to provide extra opportunities to control and enhance the performance in DAC of CO_2. The crystallization/precipitation procedure of iminoguanidine-derived molecules upon reacting with CO_2 accompanied by extensive hydrogen-bonded framework formation could be harnessed to provide extra driving force to integrate CO_2 molecules, and the desorption procedure could avoid the solvent involvement as the CO_2-saturated products could be isolated as solids via filtration [15, 33]. Ionic liquids (ILs)-engineered materials are also promising candidates to deliver tunable and enhanced performance in DAC of CO_2 with the unique properties of diverse cation/anion structure designability, favorable chemical/thermal stability, and large tuning capability in reaction enthalpy with CO_2 ranging from −17.1 to −116.8 kJ mol^{-1} [34–37]. The intensive studies in the chemisorption behavior of IL sorbents with pure CO_2 as the feeding source provide guidance on the design and selection of IL components in the construction of solid sorbents, leading to the successful development of IL-derived sorbents towards enhanced and reversible carbon capture behavior in DAC [38,39]. Besides, alkali ions or transition metal ions (e.g., Zn^{2+})-engineered zeolites displayed the capability to absorb low concentration CO_2 from air, in which the state, location, and

content of the as-introduced paired ions played critical roles to achieve high CO_2 capture capacity from air and selection of robust zeolite scaffolds was important to enable fast sorption kinetics and good recyclability particularly under humid conditions during long-term applications [40,41]. Therefore, a systematic summarization and comparison of the as-developed solid sorbents in DAC of CO_2 is highly desired for future material development and optimization beyond the amine-modified categories, particularly the design principles, synthesis techniques, advanced characterizations, reaction mechanism exploration, and carbon capture/releasing behavior control.

In the introduction section, recent progress in solid sorbent-based DAC of CO_2 will be systematically illustrated, with the materials related to amine-modified supports, hydrogen-bonded frameworks, ILs-engineered scaffolds, and metal ions-containing zeolites being involved **(Figure 1.1)**. We will focus on the design principles and the corresponding synthesis methodologies, considering the unique requirements of DAC procedures. Then, the advanced characterization techniques to confirm the solid sorbents' structures, the operando methods to study the structure evolution upon chemical bond formation/cleavage with CO_2, as well as the assistance from computational tools, will be summarized. Based on the successful production and characterization of the targeted sorbents, the reaction pathway and detailed interaction mechanism will be discussed, and then the as-delivered DAC of CO_2 performance, including capacity, recyclability, and sorption kinetics, will be illustrated and evaluated. Based on the conducted studies, the pros and cons of the sorbent systems, potential solutions to the existing issues, as well as opportunities to develop next-stage materials, will be provided to achieve enhanced DAC of CO_2 performance.

1.2 Design principles and synthesis methodologies of solid sorbents

Although solid sorbents in DAC of CO_2 via physisorption have been demonstrated, leveraging the combined functions of ultra-micropores and electrostatics from the anionic pillars in crystalline frameworks, inferior CO_2 capture capacity and poor CO_2/H_2O

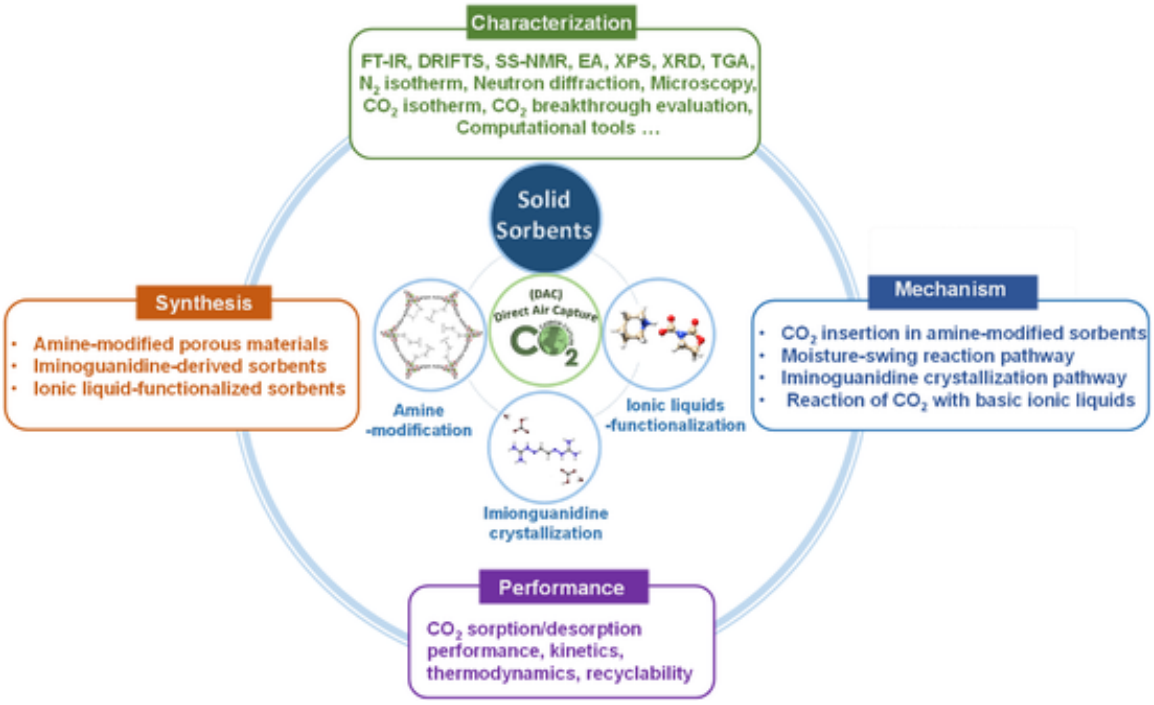

Figure 1.1 Schematic depiction of the design, synthesis, characterization, mechanism study, and DAC of CO_2 evaluation of solid sorbents

selectivity remained significant challenges compared with the chemisorption-involved procedures [42–44]. The scope of this review will be focused on the sorbents containing strong interaction sites with CO_2 and achieving high-performance DAC of CO_2 via N-C, O-C, and C-C chemical bonds formation. Generally, the reactive sites could be introduced into the scaffolds via physical impregnation/hybridization or anchoring via chemical connection, with the former being highlighted by the facile preparation procedure/controllable active sites concentration and the latter capable of providing improved stability and water-resistance. Besides the influence of the active site in DAC of CO_2, the supports should offer a robust nature upon integrating the strong basic modifiers, exceptional accessibility to the active sites, improved mass transfer, and enhanced diffusion capabilities. To ensure cost-effectiveness, supports should possess characteristics including prolonged thermal, hydrothermal, chemical, and mechanical durability over time, robust porous structure, superior wettability for the liquid modification, and high thermal conductivity [45].

1.2.1 Amine-modified porous materials

Mainly three categories of amine-modified sorbents have been demonstrated based on the material preparation methods being deployed **(Figure 1.2)**, including Class 1 sorbents being synthesized by integrating amines components into the porous supports via physical impregnation [46,47], Class 2 sorbents being synthesized by attaching the amine moieties on the support by covalent bond formation [48], and Class 3 sorbents being obtained via the polymerization and in situ chemical anchoring of amine-containing monomers on the support precursors [49]. The modification of porous supports, such as silicas, zeolites, MOFs, COFs, carbons, resins, and LDHs by amine moieties with primary, secondary, or tertiary types led to the production of highly CO_2-philic materials towards DAC of CO_2 application.

Physical Impregnation Method: The physical (wet) impregnation procedure represents a facile traditional method to afford Class 1 amine-based sorbents via direct adsorption of low-molecular-weight amine precursors by a high surface area substrate **(Figure 1.3A)**. In a typical synthesis procedure, a desired amount of liquid solution (e.g., in methanol) of

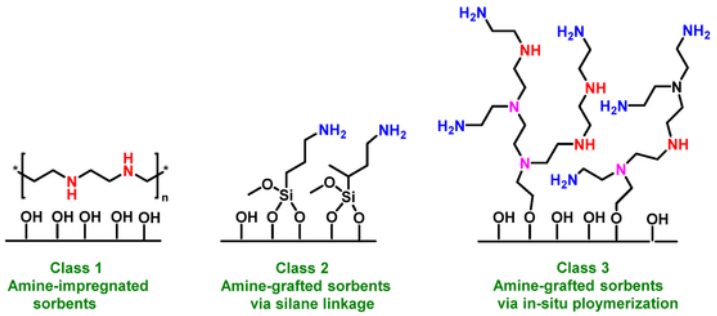

Figure 1.2 Amine-modified sorbents based on the materials preparation methods

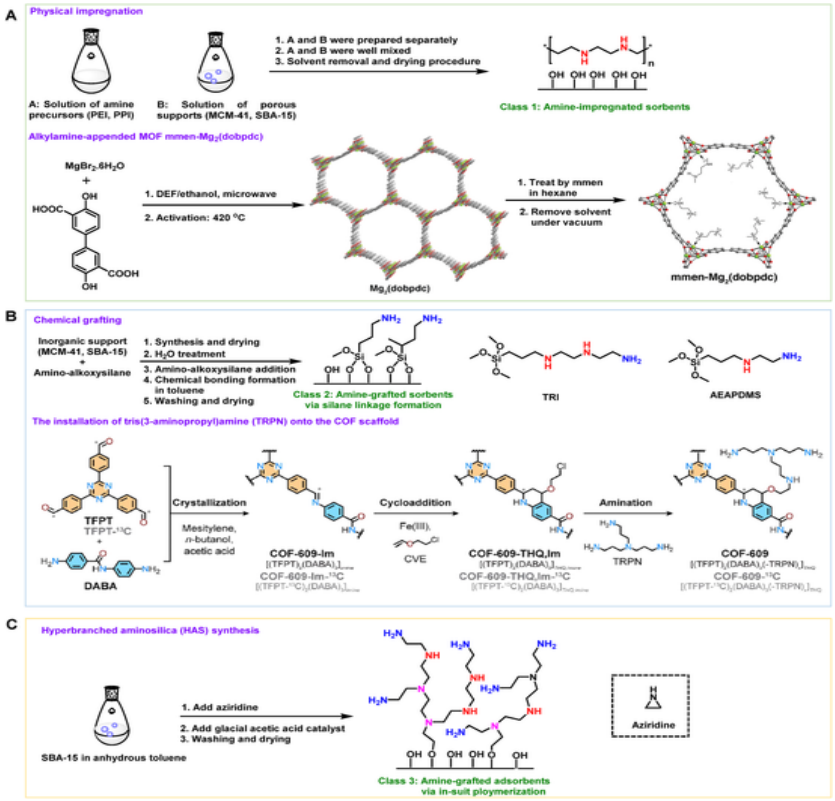

Figure 1.3 Synthesis methodologies of solid sorbents. (A) Representative procedure of physical impregnation to synthesize Class 1 amine-modified sorbents and mmen-Mg_2(dobpdc). (B) Synthesis of Class 2 amine-grafted sorbents via dehydration or amination reactions between the amine-bearing reagents and supports. (C) Synthesis of Class 3 polymeric amine-anchored sorbents via in situ polymerization of aziridine monomers.

amine precursor was mixed well with the highly dispersed porous supports, i.e., mesoporous molecular sieve (MCM-41) [50], silica [51], mesoporous silica (SBA-15) [52,53] or MOFs (MIL-101(Cr)) [54], which, after removing the organic solvents, led to the physically adsorbed amine moieties on the surface or within the porous channels of the supports. For example, when zeolite nanotubes possessing a quasi-one-dimensional (1D) hierarchical structure was deployed as the substrate for capturing CO_2 from dilute feeds after modification by poly(ethylenimine) (PEI) [55], the sorbent was prepared by mixing the methanol solution of the desired substrate with appropriate amount of 800 Mw branched PEI being dissolved in methanol via ultra-sonication and extra stirring. The targeted sorbent was obtained by removing the solvent under vacuum at elevated temperatures. MOFs with rigid porous structures and engineered surface structures are promising supports to synthesize solid sorbents in DAC applications. For example, the MOF scaffolds being constructed via the coordination of metal sites such as Mg, Mn, Fe, Co, Ni, and Zn with 4,4-dioxidobiphenyl-3,3′-dicarboxylate (dobpdc) ligand, being denoted as M_2(dobpdc) are deployed as supports to afford efficient low concentration CO_2 capture sorbents. They are featured by the involvement of 1D permanent hexagonal channels and abundant open metal sites for the anchoring of amines (e.g., alcoholamine, diamines, and polyamines) via wet impregnation [56–59]. In a typical procedure, Mg_2(dobpdc) precursor was synthesized via a microwave-assisted procedure from H_4dobpdc and $MgBr_2 \cdot 6H_2O$ in DEF: ethanol (volume ratio of 1:1) (DEF = N,N-diethylformamide), which was then activated at elevated temperature (420 °C) and modified by N,N′-dimethylethylenediamine (mmen) to generate the solid sorbent (mmen-Mg_2(dobpdc)) for carbon capture study **(Figure 1.3A)** [24,25]. Notably, to enable homogeneous amine loading, uniform dispersion of the substrates in amine solutions was required, assisted by ultrasonication or stirring. Solvents with relatively low boiling points, good solubility of the amine precursors, and no side reactions with the substrates/amines are preferred to allow complete solvent removal. For the drying procedure, thermal stability of the amine precursors should be considered to avoid decomposition or release under high vacuum and high temperature treatment.

Chemically Grafted Method: Compared with the wet-impregnation procedure, chemically bonded amines on the supports via the grafting technique exhibited improved chemical/thermal stability. Generally, the amine functionalities could be anchored via the reaction between amine-containing alkoxysilane reagents with the hydroxyl group on the surface of silicas, alumina materials, or cellulose, or the amination reaction between amine reagents with alkyl halide groups on the polymer or COFs scaffolds **(Figure 1.3B).** The amine functionality could be introduced to the MCM-41, MCM-41 silica with expanded pores (PE-MCM-41) [60] or SBA-15 [61] supports via the grafting technique in the presence of amino-alkoxysilane reagents (e.g., 3-(2-(2-aminoethylamino) ethylamino)propyltrimethoxysilane (TRI)) [60–63]. Typically, to enhance the surface coverage of amine-bearing species on the support material, water treatment was deployed to create a hydrated surface with increased hydroxyl group density. In addition, 3-aminopropyltriethoxysilane (APS) could be grafted onto porous alumina materials via a similar dehydration pathway [64]. Besides the hydroxyl group-bearing inorganic supports, amine-grafting on the nano fibrillated cellulose (NFC) with a high density of surface hydroxyl groups was conducted using N-(2-aminoethyl)-3-aminopropylmethyldimethoxysilane (AEAPDMS), and the as-produced sorbent (being denoted as AEAPDMS-NFC-FD) acted well in the subsequent carbon capture process [23,65,66]. The amination reaction pathways were harnessed to achieve amine-grafting on polymer scaffolds, such as porous polymer networks (PPN). PPN-6, possessing a covalently bonded structure, exhibits exceptional stability, a large internal pore surface, and a high surface area of 4023 m^2/g. These features make PPN-6 well-suited for functionalization with various chemical groups (e.g., sulfonic acid and amines) to accommodate diverse applications. Taking alkyl halide-containing PPN-6 as the precursor (denoted as PPN-6-CH_2Cl), diethylenetriamine (DETA) could be anchored via the amination reactions, and the as-produced sorbent (PPN-6-CH_2DETA) could be utilized in DAC of CO_2 [67,68]. The amine-grafting on highly crystalline COF scaffolds was achieved recently through a two-step modification procedure [26]. The imine bond connections in a COF-609-Im precursor were converted to a six-membered ring linkage

via cycloaddition reaction in the presence of anhydrous $FeCl_3$ and 2-chloroethyl vinyl ether. Then the alkyl chloride acted as the reactive sites to form a C-N bond with tris(3-aminopropyl)amine (TRPN) and afford amine-grafted COF for CO_2 chemisorption.

Polymer Amine Modification: Class 3 amine-modified sorbents are composed of polymeric amine moieties being grafted on selected porous supports, also being referred to as hyperbranched amino-support materials **(Figure 1.3C)** [69]. Typically, aziridine was used as the monomer, and the polymerization was initiated by a catalytic amount of glacial acetic acid in the slurry containing porous supports, producing the targeted sorbents with polymeric amine moieties chemically bonded on the surface of the scaffolds.

1.2.2 Iminoguanidine-Derived Sorbents

Iminoguanidine-derived sorbents could be used in DAC of CO_2 directly as solid sorbents or in the form of aqueous solution, and in the latter case, crystals could be precipitated from the mixtures upon reacting with CO_2 via the production of hydrogen-bonded glyoxal-bis(iminoguanidine) (GBIG) (bi)carbonate salts [33,70–72]. Typically, the chloride salt of GBIG was synthesized via the condensation reaction of iminoguanidine hydrochloride $GBIGH_2Cl_2$ with glyoxal in anhydrous ethanol **(Figure 1.4)** [73]. Then the basic iminogudanidine sorbents were synthesized as a crystalline dihydrate ($GBIG.2H_2O$) by neutralization of the chloride salt with NaOH. The imine bond formation between 2,6-pyridinedialdehyde and the aminoguanidinium chloride monomer led to the production of 2,6-pyridine-bis(iminoguanidine) (PyBIG) sorbents, after the neutralization treatment by aqueous NaOH [33].

1.2.3 Ionic Liquid-Modified Sorbents

Although state-of-the-art sorbents in DAC of CO_2 are still focused on amine-modified categories, the stability issues and limited tunability in interaction strength with CO_2 triggered the exploration of alternative functionalities beyond amino groups to form chemical bonding with CO_2, ideally, with improved stability and tunable reaction energy in a large region. ILs composed of organic cation and anion couples could meet the requirements in these two aspects, with attractive properties of high chemical/thermal

Figure 1.4 Representative procedures for the synthesis of iminoguanidine-derived sorbents

stability, negligible vapor pressure, structural diversity, and tunable interaction strength/reaction pathway to integrate CO_2 [74–76]. Taking a clue from the reaction of amines with CO_2, amino-functionalized ILs (AILs) [77–79] were developed, but the carbon capture performance was limited by the relatively high viscosity (extensive hydrogen bonding formation) and inferior CO_2 uptake capacity via carbamate product formation.

Then, superbase-derived ILs (SILs) exhibiting diminished viscosity (without active protons in the structures) were demonstrated, which possessed large tunability regarding the interaction strength with CO_2 via C-C, C-O, or C-N bond formation [80–84]. The SILs have exhibited great potential in DAC of CO_2 according to the extensive studies on their chemisorption behavior using pure CO_2 sources, and the development of SILs-derived sorbents in DAC of CO_2 will rely on the structure design of supports/SILs and synthesis approaches.

A straightforward and facile pathway is to modify the selected supports via wet impregnation by ILs. Notably, the wettability of the outer and inner surfaces of the supports should be considered to couple with the physical properties of the ILs. Compared with amine precursor, one strength of ILs lies in their large tunability via structure engineering, i.e., wettability could be altered by the alkyl chain length/structures on the cations coupled with the same anion [85,86]. In addition, the molecule size of the ILs could be designed to accommodate the porosity of the as-deployed supports. Notably, due to the requirement of active sites with relatively strong basicity to ensure efficient carbon capture under low-concentration conditions, supports are required to be robust under basic and highly ionic conditions, excluding some of the unstable MOFs and those containing abundant acidic moieties (e.g., -OH) on the surface.

For example, a wet impregnation method was deployed to fabricate SILs-engineered sorbents with mesoporous silica as the support and imidazolate ([Im])/triazolate anion ([Triz])-involved SILs as the active sites to react with CO_2, with the reaction enthalpy of -89.9 and -56.4 kJ mol^{-1} respectively **(Figure 1.5A)** [39,83]. To avoid the potential

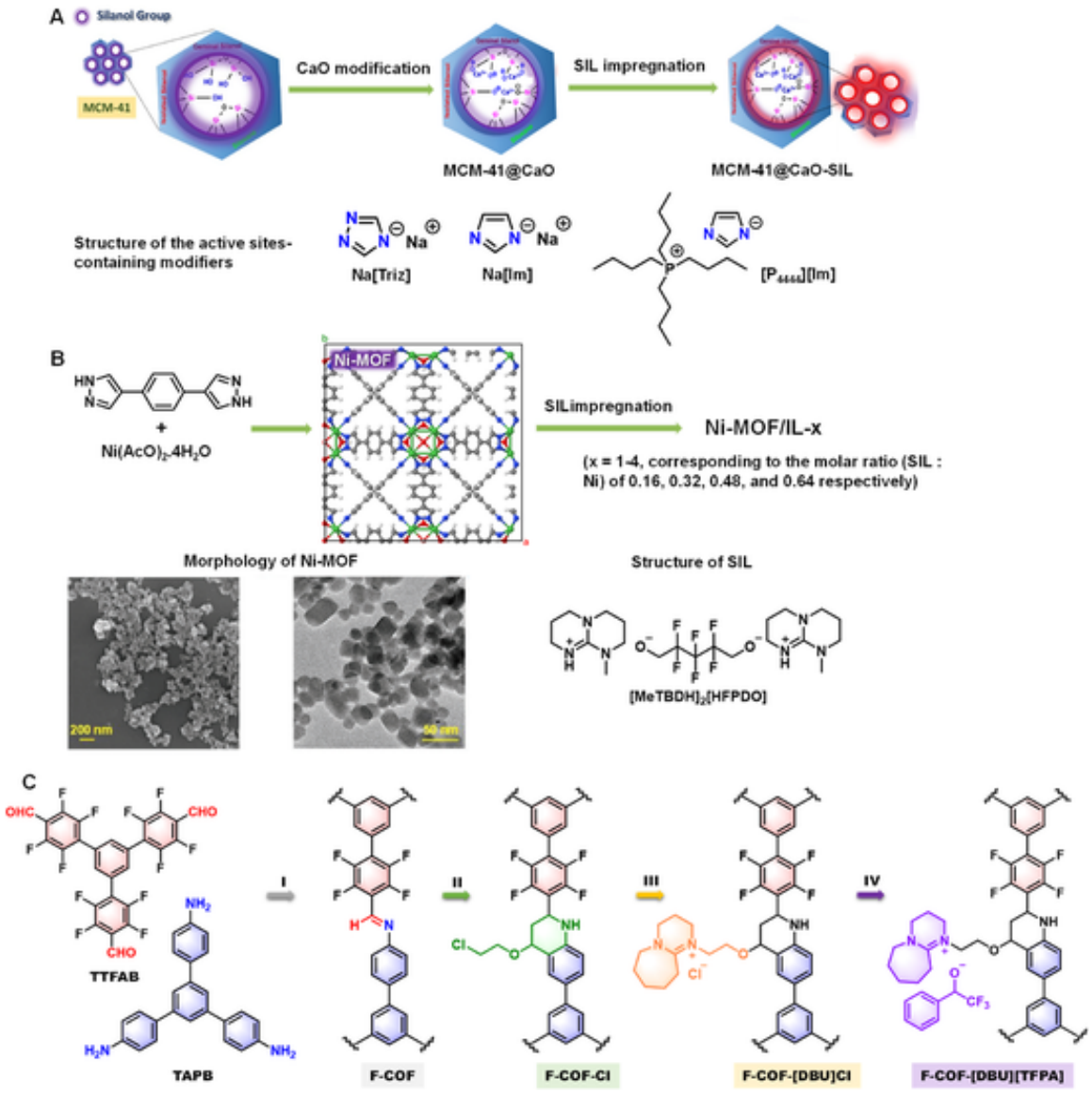

Figure 1.5 Representative wet impregnation procedures for the synthesis of superbase ionic liquid-engineered sorbents. (A) mesoporous silica or (B) Ni-MOF as the support. (C) Synthesis pathway of the ionic pairs-engineered F-COF-derived scaffolds.

deactivation of the basic sites in SILs by hydroxyl groups on the surface of silica, a thin layer of CaO was introduced via the $Ca(OAc)_2$-to-CaO transformation during the calcination process. The sodium salts (Na[Im] and Na[Triz]) were first introduced as modifier to simplify the system and study the influence of anions on the DAC of CO_2 performance via a wet impregnation approach. The corresponding SIL (tetrabutylphosphonium imidazolate, $[P_{4444}][Im]$) was then deployed to engineer the CaO-modified MCM41 support for DAC of CO_2 applications. The facile preparation procedures and large structure/property tuning capability of MOFs made them good candidates to be modified towards low-concentration carbon capture applications. In the case of using SILs as the modifier, the MOF scaffolds should be stable under basic and highly ionic conditions. A Ni-MOF being synthesized from the pyrazolate ligand and nickel acetate possessed isoreticular architecture, high surface area, microporosity, small nanoparticle size around 30 nm, and robust nature in the presence of SILs. **(Figure 1.5B)** [38]. The as-selected SIL $[MeTBDH]_2[HFPDO]$ was synthesized from the deprotonation reaction of a superbase (7-methyl-1,5,7-triazabicyclo[4.4.0]dec-5-ene, MeTBD) and fluorinated alcohol (2,2,3,3,4,4-hexafluoro-1,5-pentanediol, HFPDOH), which can capture CO_2 via the O-C bond formation and carbonate generation. A wet impregnation method was deployed to afford SIL/Ni-MOF composite sorbents with different loading amount of SIL for detailed DAC of CO_2 evaluation. In addition, the ionic pairs can be anchored on the porous scaffolds via covalent bond formation [87].

High stability of the supports was required to maintain the rigid structures under basic and highly ionic conditions. As shown in **Figure 1.5C**, a highly crystalline fluorinated COF (F-COF) was engineered step-by-step to improve the stability and introduce ionic pairs for CO_2 integration. Using imine-bond connected F-COF as the precursor, an imine-to-tetrahydroquinoline (THQ) ring transformation was performed to improve the stability and introduce the alkyl halide moieties.

The subsequent nucleophilic attack by organic base (1,8-diazabicyclo[5.4.0]undec-7-ene, DBU) introduces the ionic pairs with chloride anion, which was then treated by anion exchange to convert the chloride to fluorinated alcoholate anion possessing the capability

of to efficiently absorbing low concentration CO_2 source. Therefore, the design and synthesis procedures being developed in the production of amine-modified sorbents could provide guidance to afford IL-derived categories combining the unique features of diverse IL precursors being deployed towards improved DAC of CO_2 behavior via controllable chemisorption.

1.3 Characterization and Performance Evaluation Techniques

1.3.1 Experimental Characterization: Studying DAC of CO_2 by Solid Sorbents

Based on the sophisticated design and synthesis of targeted solid sorbents, it is crucial to detailly analyze and tune their physical and chemical properties via diverse characterization techniques, to provide information on but not limited to chemical structure of the scaffolds, porosity, thermal stability, active sites concentration and distribution, carbon capture/releasing behavior, and CO_2 binding form. However, accurate structure determination and evolution of the sorbents are challenging considering the complex pore structures, surface heterogeneities, influence of impurities, and the complicated kinetic and thermodynamic evolutions during the low-concentration carbon capture procedure. Therefore, it is critical to integrate diverse techniques and obtain comprehensive information via microscopy, spectroscopy, and operando analysis.

Fourier-transform infrared spectroscopy (FTIR): FTIR spectra could provide direct chemical bonding information according to the unique absorption frequency of specific functionalities. For example, upon Class 1 PEI/silica sorbent formation by physical impregnation, additional peaks were observed at 1570 cm^{-1} (secondary amine N-H bending) and 1650 cm^{-1} (primary amine N-H bending), indicating successful surface modification by PEI moieties [51]. For amine-grafting on highly crystalline COF scaffolds **(Figures 1.3B and 1.6A)**, the emerging imine stretch absorbance of COF-609-Im by the condensation of aldehyde and amine monomers was observed at 1622 cm^{-1}. Upon reacting with 2-chloroethyl vinyl ether to afford COF-609-THQIm, the imine bonds were transformed to tetrahydroquinoline (THQ), being confirmed by the broad

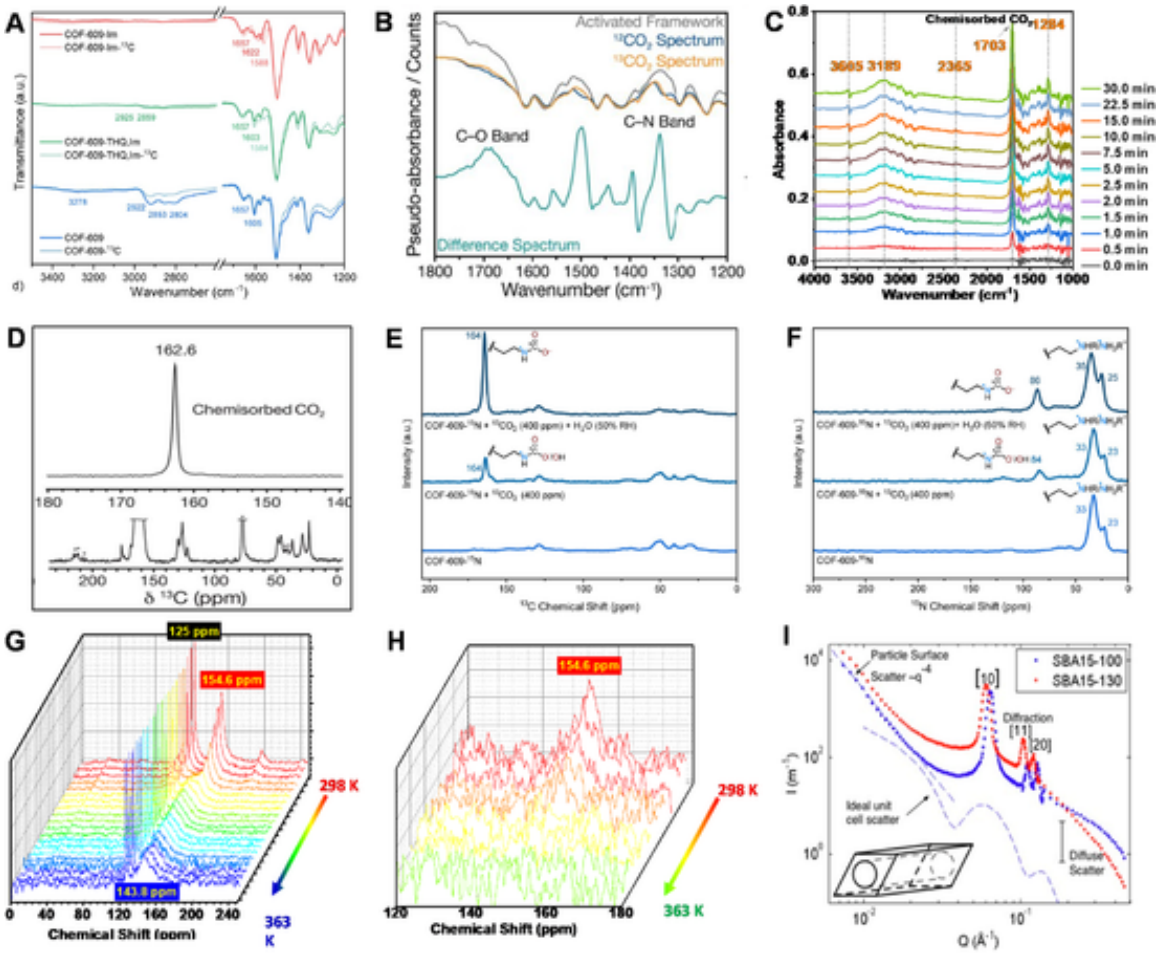

Figure 1.6 Characterization and performance evaluation techniques in DAC of CO_2. (A) FT-IR spectra of the COF scaffolds before and after amine modification. (B) DRIFTS spectra of CO_2 sorption by Mg_2(dobpdc)(3-4-3). (C) DRIFTS spectra of Ni-MOF/IL-3 under air atmosphere with 400 ppm CO_2 being involved. (D) MAS SS-^{13}C NMR spectrum of Mg_2(dobpdc)(3-4-3) exposing to 1038 mbar of $^{13}CO_2$. (E and F) ^{13}C and ^{15}N SS NMR spectra of COF-609-^{15}N under dry and humid conditions in the $^{13}CO_2$ dosing experiments. (G) NMR signal evolution of Ni-MOF/IL-3 + $^{13}CO_2$ with the temperature raising up from 298 to 363 K in a sealed NMR rotor. (H) NMR signal evolution with the temperature rising up to 363 K under open environment. (I) Small-angle neutron scattering (SANS) patterns of SBA15−100 and SBA15−130.

bands at 2925 (aliphatic C-H bonds) and 2859 cm^{-1} (2-chloroethoxyl side chain). Finally, nucleophilic substitution led to functionalization by the aliphatic amines (3278 cm^{-1}) [26]. For the iminoguanidine system, by bubbling a flue gas mixture in an aqueous solution containing GBIG, a fresh absorption peak at 1450 cm^{-1} emerges, confirming the formation of bicarbonate $GBIGH_2(HCO_3)_2(H_2O)_2$) [70–72].

Diffuse reflectance infrared Fourier transform spectroscopy (DRIFTS): It is a powerful tool to provide the real-time structure evolution of the sorbents upon exposure to an atmosphere containing CO_2. For example, the CO_2 sorption procedure of Mg_2(dobpdc)(3-4-3) (3-4-3 = N,N-bis(3-aminopropyl)-1,4-diaminobutane) could be illustrated by the carbamate formation with newly formed C-N stretch at 1339 cm^{-1} and a C-O stretch at 1689 cm^{-1} **(Figures 1.3A and 1.6B)**, providing critical information in CO_2chemisorption pathway with amine [88]. The structure evolution of the Ni-MOF/IL-3 **(Figure 1.5B)** upon exposure to 400 ppm CO_2 was monitored via DRIFTS [38]. Taking the IR spectrum of Ni-MOF/IL-3 as the background, new peaks were observed at 1284 and 1703 cm^{-1} within 0.5 min upon exposing to the air atmosphere at 298 K **(Figure 1.6C)**, corresponding to the newly formed C-O and C=O bond in the carbonate product respectively, the intensity of which were gradually increased and remained constant after 10 min, indicating the fast CO_2 sorption kinetics [38]. Rapid CO_2 release at 353 K under nitrogen atmosphere was demonstrated by the complete disappearance of these peaks within 2 min.

Solid-state nuclear magnetic resonance (SS-NMR): SS-NMR spectra could provide information on the local chemical environment of individual atoms identifying the types of chemical bonds and studying the dynamics of molecules in a confined space in solid sorbents, i.e., rotational and translational movements. For example, the cross-polarization magic-angle spinning (CP-MAS) ^{13}C SS-NMR spectra showed a signal at 158 ppm (imine bond) in COF-609-Im (**Figure 1.3B**), which diminished in COF-609, indicating the transformation of the imine bonds during the two-step post synthetic transformation process [70–72]. For the Mg_2(dobpdc)(3-4-3), a new peak showed up at 162.6 ppm after reacting with CO_2, being assigned to the carbamate product formation **(Figure 1.6D)**[88].

Operando SS-NMR: Combining the isotope-labeling techniques, in situ SS-NMR study could be an efficient technique to study the kinetics and reaction pathway in DAC of CO_2. The operando high-resolution MAS NMR could assist in exploring the mechanism of CO_2 absorption and desorption on the active sites (i.e., the nature of the active intermediates, the interaction between CO_2 and the active sites, and the product generation as a function of reaction time). Particularly, this technique will elucidate the time-evolution of the formation of carbamate, carbonate salt, or possible unidentified intermediates between the basic sites and CO_2. The characterization tool is well-suited for monitoring the heterogeneous systems, which include gas-liquid, gas-solid, and liquid-solid interfaces. For example, by feeding IL-modified sorbents and 400 ppm CO_2 within the operando MAS NMR rotor, the changes occurring in gas phase molecules, IL, the interface between gas and IL, and the surface between gas and IL-modified sorbents can be concurrently investigated. Analyzing chemical shifts allows us to discern differences in molecules across these phases, enabling to monitor the transition of CO_2 and even the role of H_2O within the sorbents. This monitoring is conducted continuously through operando ^{13}C and ^{1}H MAS NMR spectra, shedding light on the uptake and release of CO_2 and other substances by ILs or supported ILs [38,89,90]. For example, using $^{13}CO_2$ (^{13}C-labeled CO_2) as the feeding source could provide enhanced carbon signals in SS-NMR, and solid sorbents containing ^{15}N-label functionalities could obtain good signal variation in ^{15}N NMR spectra. Through in situ SS dynamic nuclear polarization-enhanced ^{13}C cross-polarization magic-angle spinning ^{13}C nuclear magnetic resonance (DNP-CP/MAS ^{13}C NMR) analysis, the reaction pathway of COF-609-^{15}N **(Figure 1.3B)** (being synthesized using ^{15}N-labeled aromatic amine monomer) with low concentration CO_2 using a gas stream containing 0.04 % $^{13}CO_2$ was monitored [26]. Upon exposing to the gas atmosphere, a new peak appeared at 164 ppm in the ^{13}C NMR spectrum, accompanied by a new signal in the ^{15}N NMR spectrum at 84 ppm **(Figure 1.6E and F),** indicating the carbamate species formation upon integration of CO_2 molecules [70–72]. As shown in **Figure 1.6G-H**, the use of Ni-MOF/IL-3 **(Figure 1.5B)** as sorbent resulted in the formation of a carbonate product when 15 psi $^{13}CO_2$ was charged [38]. The

captured $^{13}CO_2$ (peak located at 154.6 ppm) could be released by ramping up the temperature to 363 K, even in a sealed environment under a $^{13}CO_2$ atmosphere. Notably, an intermediate state of sorbed CO_2 appeared at 143.0 ppm as a broad peak within a wide range of temperatures **(Figure 1.6G).** Under an open environment, complete CO_2 release could be achieved immediately with the temperature rising up to 363 K **(Figure 1.6H),** demonstrating the fast CO_2 capture/release kinetics achieved by Ni-MOF/IL-3.

NMR relaxometry: This approach enables the assessment of the dynamic properties of sorbent systems toward CO_2 absorption kinetic in the DAC procedure. Recently, a fundamental study on the mobility of polyethylenimine (PEI) in a mesoporous γ-Al_2O_3 composite in response to CO_2 sorption across a wide range of temperatures and relative humidity (RH) was carried out to evaluate the performance of DAC [91]. The accessibility of amine sites directly correlates with amine distribution in the pores and overall pore filling as well as the dynamics of the amine chains, so the structure and mobility of amines impregnated in the pores of porous supports have a direct impact on gas sorption [92]. Dipolar coupling between spins is a significant factor that affects the complex phenomena of transverse spin-spin relaxation time (T_2). In materials with high molecular mobility, T_2 can be longer as the process is less effective, whereas strong dipolar coupling in solid samples promotes rapid decoherence. Shorter T_2 values are a sign of reduced mobility in polymeric systems due to stronger attachments and/or cross-linking density [93]. So far, this type of NMR has not been applied to the sorption kinetic assessment of CO_2 DAC, but it can be a promising procedure to evaluate the energy exchange and dynamic properties of solid sorbents utilized for carbon capture.

Elemental analysis (EA): It is an analytical technique to determine the exact chemical composition. For example, for solid sorbents derived from nitrogen-free supports, the concentration of amino groups could be determined by the N content via EA. For the preparation of alkyl halide-functionalized support intermediates, EA on the halide species could provide information on the halogenation degree.

X-ray photoelectron spectroscopy (XPS): XPS is a useful tool to determine the concentration of surface species as well as their chemical state as reflected by the binding

energies (BE). In addition, in situ XPS techniques could be used to monitor the electronic structure evolution of the active sites upon exposure to a CO_2-containing atmosphere, which holds great significance in determining the CO_2 chemisorption [94].

Textural structure analysis: Most of the solid sorbents being deployed in DAC of CO_2 possessed porous scaffolds to facilitate mass transfer and achieve good carbon capture kinetics. Therefore, it is critical to gain the porosity information (e.g., surface area, pore size, and pore volume) and study the influence on carbon capture behavior. The N_2 adsorption/desorption isotherms (77 K) could provide related textural structure information ranging from micro- to mesopores. For some porous materials containing ultra-micropores below 5 Å, gas molecules with smaller kinetic diameters are required. The CO_2 isotherms being collected at 195 K and Ar isotherms being collected at 273 K could provide porosity information in the ultra-micropore range [95]. For example, the analysis from N_2 sorption isotherms showed limited porosity in COF-609 **(Figure 1.3B).** Nevertheless, the CO_2 sorption isotherms (195 K) of COF-609 displayed a rapid CO_2 uptake in the very low-pressure region, indicating the presence of ultra-micropores within the architecture [70–72].

Thermogravimetric analysis (TGA): The thermal stability of solid sorbents under either inert or oxidative atmosphere is one of the most important indicators to evaluate the durability. In addition, for inorganic support-derived sorbents, the weight loss at high temperatures could correspond to the content of organic moieties being involved. For the Class 1 PEI/silica sorbent, MCM-41-PEI-50 exhibited a weight loss of approximately 10.5 % at 100 °C, and a total weight loss of approximately 56 % at 600 °C. The calculated PEI loading was about 50 wt%, consistent with the theoretical loading amount, indicating no PEI loss during the preparation process [50].

X-ray diffraction (XRD): XRD can be used to investigate the crystalline structure, crystallography, and phase composition of the sorbent materials. For crystalline MOF or COF-derived sorbents, XRD was deployed to study the structure evolution in the modification and the carbon capture procedure. For the iminoguanidine system, the

formation of crystalline bicarbonate product ($GBIGH_2(HCO_3)_2(H_2O)_2$) after CO_2 bubbling could be confirmed by XRD [70–72].

Small-angle X-ray scattering (SAXS): SAXS measurements can be applied to a wide range of materials, including liquids, solids, polymers, nanoparticles, and biological macromolecules. It is useful for studying the internal structures, shapes, and cavities of these materials. For example, in the composite materials composed of SIL and Ni-MOF, the confinement behavior of the SIL within the cavity of the MOF scaffolds was studied by SAXS [38]. For the pure SIL, the intermolecular correlations caused the appearance of an adjacency peak at about 1.15 $Å^{-1}$, which shifted to higher q values upon being trapped in the cavity of Ni-MOF, indicating the shorter intermolecular distances between the ions in SILs caused by the confinement effect.

Neutron diffraction: It is a valuable technique for studying the atomic and molecular structure of materials because neutrons are electrically neutral particles, which means they can penetrate deep into materials without being significantly affected by the electrons in the material. Unlike charged particles, which interact strongly with electrons and are therefore absorbed or scattered by the material, neutrons can pass through the material and provide information about the positions of atoms within the material. These techniques can provide detailed information about the arrangement of atoms within the crystal lattice, which can then be used to study the relationship between the structure and properties of the crystalline materials. For iminoguanidine system, the crystal-structure analysis by X-ray and neutron diffraction showed the presence of extended clusters containing carbonate and water molecules arranged in a one-dimensional pattern. Additionally, stacked $PyBIGH_2^{2+}$ cations were also observed within the crystal lattice [7]. For the PEI/silica composites, the small-angle neutron scattering (SANS) could be used to prob the spatial distribution of the supported PEI **(Figure 1.6I)** [96].

Microscopy: Combined analyses using scanning electron microscope (SEM), energy-dispersive X-ray spectroscopy (EDS), and transmission electron microscopy (TEM) could be used to evaluate their morphologies and monitor the variation during the carbon capture procedures.

CO_2 chemisorption behavior evaluation: Diverse techniques have been developed to evaluate the carbon capture/releasing and cycling behaviors of the solid sorbents in DAC procedure, including thermogravimetric analysis under low concentration CO_2 (e.g., ~400 ppm in He)/simulated air atmosphere, a combined calorimetric–volumetric adsorption apparatus consisting of a calorimeter, CO_2 isotherm being collected at low pressure region around 0.4 mbar at different temperatures (e.g., 273 and 298 K), and breakthrough curves collection using IR gas analyzer to monitor the outlet gas compositions. Temperature programmed desorption (TPD) method could provide information on the absorbed CO_2 quantity and the desorption temperature, in which the CO_2-saturated sorbents were thermally treated under inert gas flow, and the exhausted gas flow was monitored by a mass spectrometer (MS) [42]. The influence of humidity could be studied by feeding a determined humidity level into the inlet gas sources.

1.3.2 Computational Tools in Studying the DAC of CO_2 by Solid Sorbents

Computational tools, including but not limited to ab initio calculations, molecular simulations, and kinetic modeling, are among the powerful arsenals at researchers' disposal to tackle the tasks related to the effective and efficient application of engineered solid sorbents in DAC of CO_2, complemented with the diverse experimental techniques.

Mechanistic studies by DFT calculations. Complemented with spectroscopy and NMR measurements, DFT calculations provide an invaluable tool for mechanistic studies to unravel the nature of adsorbed species and elucidate the CO_2 reaction pathway in the presence and absence of moisture. CO_2 adsorption on supported amines generates carbamic acid and alkylammonium carbamate and/or bicarbonate, depending on amine species and adsorption conditions [97]. The formation of zwitterion intermediates seems to be crucial for the pathway of ammonium carbamate or carbamic acid. However, a recent DFT study suggests a unified six-membered mechanism to describe all possible interactions of CO_2 with amines and water, each playing the role of a nucleophile and/or Brønsted base, depending on the actual conditions **(Figure 1.7A).** The formation of zwitterion is energetically prohibitive, and the formation of ammonium bicarbonate/carbonate in protic amines does not proceed through the widely accepted

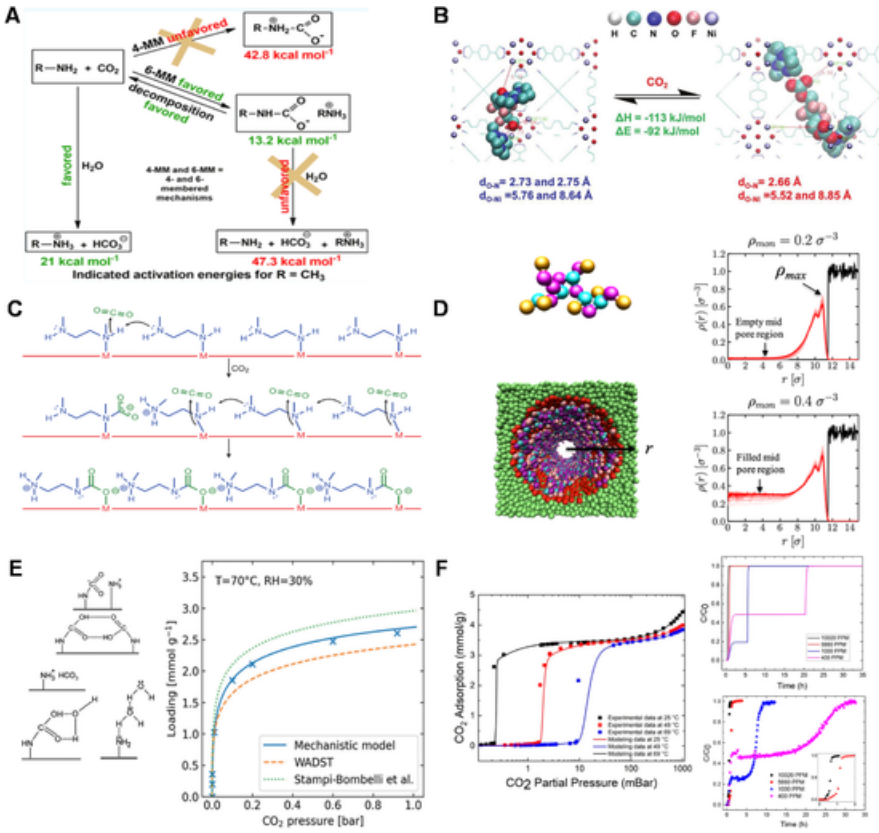

Figure 1.7 Computational tools in studying the DAC of CO_2. (A) An unified CO_2−amine reaction mechanism. (B) The optimized structure of SIL confined within the cavity of Ni-MOF and the corresponding reaction energy. (C) A cooperative insertion mechanism for CO_2 adsorption in mmen-M_2(dobpdc) [24]. (D) PEI (a bead-spring representation) dispersion in model cylindrical pore. A pore impregnated with PEI at a loading density of ρmon (ρmon = number of PEI beads/volume of cylinder) showing red attractive beads and green repulsive support beads. (E) Comparison of experimental co-adsorption CO_2 isotherms (markers) and predictions from an empirical co-adsorption model and the two mechanistic models based on three governing mechanisms: species of ammonium carbamate and paired carbamic acids at dry condition; additional species (ammonium bicarbonate and water-stabilized carbamic acid) with moisture; and hydrogen bonding between water and the supported amines. (F) CO_2 adsorption isotherms (left panel) of experiments (symbols) and model fit (solid curves) in mmen−Mg_2(dobpdc).

hydration of carbamate/carbamic acid. Instead, water behaves as a nucleophile that attacks CO_2 with catalytic assistance by amine groups, and carbamate/carbamic acid decomposes back to amine and CO_2 [98]. DFT calculations can also be used to probe the conformation of SIL within the Ni-MOF framework and variation of the CO_2-involved reaction thermodynamics between the liquid and confined form. The higher CO_2 reaction enthalpy in Ni-MOF indicated that the confinement effect of the Ni-MOF framework can enhance the interaction strength of the SIL with CO_2 in carbon capture **(Figure 1.7B)** [38]. The cooperative CO_2 adsorption mechanism in diamine-M_2(dobpdc) was investigated in DFT calculations [24,99].It was demonstrated that each metal atom of M_2(dobpdc) forms an M-N bond with one amine of the diamine, and the other amine acts as a Lewis base. CO_2 molecule attaches to the free amine and inserts into metal–amine bonds with the help of an adjacent diamine nucleophilic attack to form M-O bond and C–N bond, forming the chains of ion-paired ammonium carbamate along the framework channel **(Figure 1.7C)**. The selective absorption of CO_2 in diamine-M_2(dobpdc) under humid conditions was computationally verified, where CO_2 insertion to form an O-bound carbamate is much more energetically favorable than binding H_2O at the open metal site of the corresponding bare M_2(dobpdc) framework [100].

Molecular simulation method. Molecular simulation is an important computational tool to provide physical insights for understanding amine distribution inside porous supports. The amine loading and its distribution inside the pores greatly affect the performance of supported amines. The amine distribution essentially dictates CO_2 accessibility to active amine sites, subsequently amine efficiency. In the well-known plug model, SANS results indicate that poly(ethylenimine) first forms a thin conformal coating on the pore walls of mesoporous silica, and all additional PEI aggregates into plugs that grow along the pore axis [96]. Molecular dynamics (MD) simulations agree with the neutron scattering results in SBA-15, where PEI fills the pore beginning at the pore walls and grows concentrically but non-uniformly, thereby suggesting that at a certain polymer loading, plugs and voids inside the cylindrical pores are formed **(Figure 1.7D)** [101]. PEI dispersion can be altered by its interaction with porous substrate supports, which in turn impacts their CO_2 capture performance. Strong densification and plug formation were only found for PEI inside

mesoporous carbon, much less in nanoporous silica. This behavior was well reproduced in MD simulations through variation of the polymer–substrate interactions, where the PEI−carbon interactions are much more strongly attractive than the PEI−silica interactions [102]. The SIL loading limit within the Ni-MOF framework can be estimated by the canonical Monte Carlo simulations, which demonstrated the maximum loading amount of SIL pairs corresponding to a molar ratio of 0.4 (SIL:Ni sites). Notably, SIL/Ni-MOF sorbent with a SIL:Ni molar ratio of 0.48 displayed a good (400 ppm) CO_2 uptake capacity via both volumetric and fixed-bed breakthrough test [38].

Kinetic modeling of CO_2 sorption in fixed-bed absorber. Kinetic modeling using computational fluid dynamics method is an important tool for optimizing the DAC process and reducing energy consumption of sorbents. There are only a few kinetic modeling studies under realistic DAC conditions. Quantitative mathematical model of enhanced CO_2 co-sorption with moisture is a prerequisite for reliable modeling. Empirical enhancement factors to single CO_2 Toth isotherm were usually applied to take the enhanced co-adsorption with moisture in supported amines into account [103,104]. Two mechanistic co-adsorption isotherm models with consideration of three governing mechanisms were recently proposed to describe moisture effect on CO_2 adsorption and accurately reproduce the co-adsorption performance on the commercial Lewatit R VP OC 1065 sorbent **(Figure 1.7E)** [105]. The stepped CO_2 sorption isotherms in the packed bed of mmen-Mg_2(dobpdc) were modeled to determine the CO_2 uptake at different flow rates and concentrations. The results indicate that increasing the CO_2 concentration improves the CO_2 extraction rate. The sigmoidal CO_2 isotherm is a combination of the low-pressure Sips and the high-pressure Langmuir–Henry isotherms. The Avrami kinetic model was used to describe the CO_2 adsorption kinetics at 400 ppm, while the Michaelis–Menten expression is more successful at higher concentrations (**Figure 1.7F**) [106]. The CO_2 breakthrough behavior in a fixed-bed column of CaO- and SIL-engineered MCM-41 sorbents was kinetically modeled to characterize the CO_2 sorption kinetics. A heterogeneous kinetic model can properly capture the prolonged tails observed in experimental breakthrough curves [39].

1.4 Reaction Pathways and Mechanisms

1.4.1 CO_2 Insertion Pathways in Amine-Modified Sorbents

For amine-modified solid sorbents, the CO_2 integration pathways are related to the types of amino groups. For primary and secondary amines, nucleophilic attack of the amino groups on the carbon atom of CO_2 led to the formation of a zwitterion intermediate, which was then deprotonated by another amine molecule or extra base (as additives) to form the carbamate product coupled with the ammonium cation (or [base-H]$^+$cation) (**Figure 1.8A**). Comparatively, tertiary amines cannot directly react with CO_2 via N-C bond formation under dry conditions. However, in the presence of H_2O, the tertiary amine could act as a base to generate hydroxide anion (-OH) and quaternary cationic species via deprotonation. Then the reaction between the -OH and CO_2 led to the formation of bicarbonate products coupled with the as-formed ammonium cation. Notably, under humid conditions, sorbents with primary/ secondary amine moieties could capture CO_2 via a similar pathway. Detailed studies revealed that for the H_2O-involved CO_2 uptake procedure, the activation energy towards HCO_3^- formation is lower than the carbamate generation, but the rate constant of the former pathway is lower. That is, carbamates are produced as the initial products in primary/secondary amine-modified sorbents upon reacting with CO_2, which is gradually altered to carbonate and bicarbonate products. The reaction mechanism of different amine structures under diverse conditions could affect the CO_2 chemisorption behavior of the corresponding solid sorbents, particularly in the low-pressure region. For example, for Class 2 amine-modified silica sorbents with comparable amine loading amount but different types, under dry conditions [107], the CO_2 uptake behavior at low-pressure region revealed that primary amine-modified sorbents exhibited the highest uptake capacity, surpassing that obtained by secondary amine-involved materials, while the tertiary amine-functionalized silica showed no capability to absorb CO_2 molecules at low concentration [5]. Thermodynamic evaluation and calculation demonstrated that based on the CO_2 uptake isotherms being

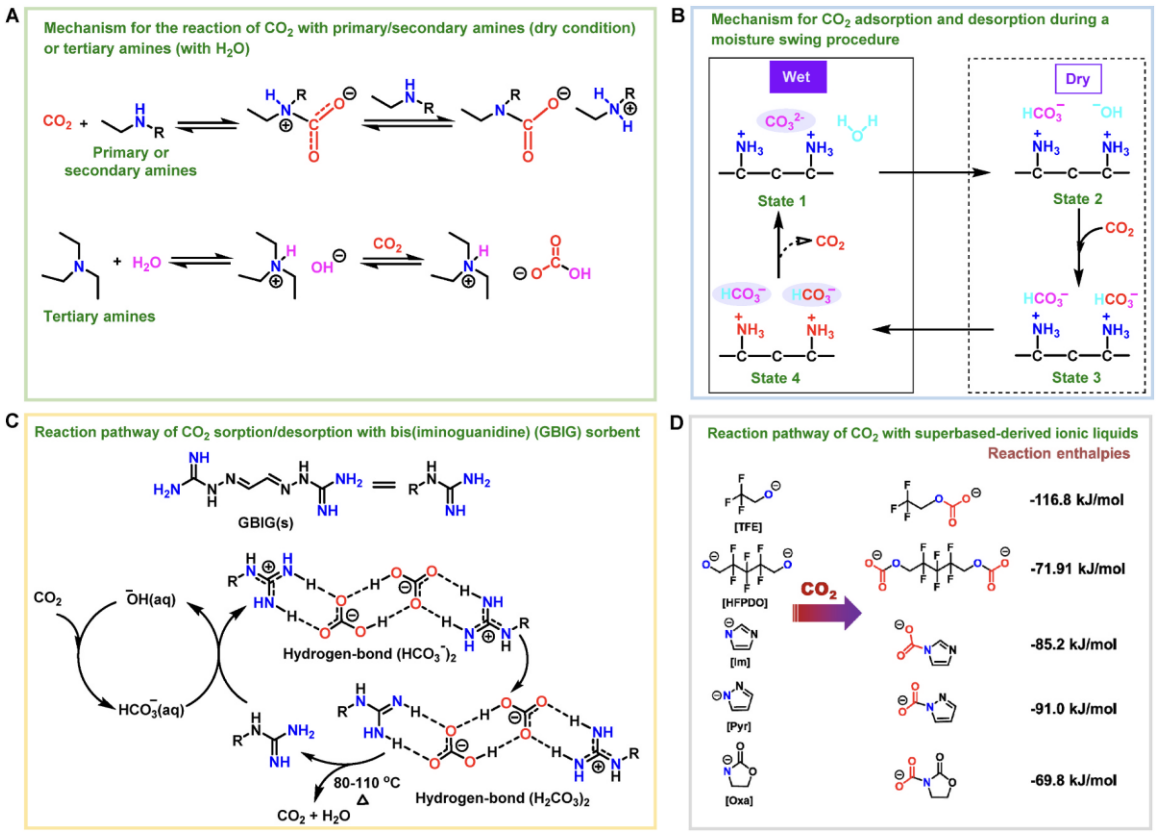

Figure 1.8 CO_2 insertion pathways in sorbents. (A) The reaction mechanism of CO_2 with primary/secondary amines (dry conditions) and tertiary amines (humid conditions). (B) Reaction pathway of CO_2 sorption and desorption during a moisture swing procedure. (C) The CO_2 capture/release procedure by iminoguanidine-derived sorbents. (D) Reaction pathway of selected SILs with CO_2 and the reaction enthalpy values.

collected at different temperatures [108], the isosteric heats of adsorption for primary and secondary amine-modified scaffolds were -112 and -84 kJ mol^{-1}, respectively, which was matched well with the steeper CO_2 uptake isotherms at the low-pressure region being obtained by primary amine-modified materials. In addition, the calorimetry study revealed that the aliphatic primary and secondary amines had comparable reaction enthalpies with CO_2 of about -90 kJ mol^{-1}, indicating that the preferred performance of primary amine-modified materials in DAC of CO_2 procedure was probably caused by the entropic variables rather than enthalpic contributions [109].

1.4.2 Moisture-Swing Reaction Pathway

Due to the relatively strong interaction strength between amino groups and CO_2, high energy consumption is required in the CO_2 releasing procedure, which is one of the issues hindering the wide application of amine-modified sorbents and could lead to decomposition of the amine moieties at elevated temperatures. To address this issue, moisture-swing sorbents were developed for capturing CO_2 from ambient air. Typically, these sorbents can bind CO_2 under dry conditions and release CO_2 upon exposure to moisture. The CO_2 chemisorption was driven by the carbonate-to-bicarbonate (and reverse) transformation triggered by water molecules (**Figure 1.8B**) [110]. A wet resin containing water-stabilized carbonate anion coupled with ammonium cations was deployed as the original sorbents (State 1). When the resin was treated under dry conditions and more and more water molecules were removed, the carbonate anion became unstable compared with the singly charged anions, leading to the formation of a bicarbonate anion and a hydroxide anion (State 2). The strong interaction strength between the hydroxide anion with CO_2 could be harnessed to achieve efficient carbon capture from a low concentration CO_2 source, generating another bicarbonate anion as the product (State 3). When the CO_2-saturated resin is re-moistened, the bicarbonate anions are fully hydrated (State 4) and prone to decompose to water-stabilized carbonate anion and release CO_2 molecules into the gaseous atmosphere (State 1), to close the cycle and achieve recycling.

1.4.3 Iminoguanidine Crystallization Pathway

For iminoguanidine-derived sorbents towards DAC of CO_2, the CO_2 integration could be achieved by solid-state crystallization formation or solution-based crystal precipitation, in both of which the hydrogen bonding network formation played a critical role. For example, when the glyoxal-bis(iminoguanidine) (GBIG) was deployed as sorbent in the form of aqueous solution, upon reacting with CO_2, bicarbonate crystals composed of hydrogen-bonded $(HCO3^-)_2$ dimers (anti-electrostatic) being stabilized by water and guanidinium cations are formed and precipitated from the solution phase (**Figure 1.7C**) [111]. Then CO_2 release could be conducted via the heating treatment to regenerate the GBIG sorbent and close the CO_2 sorption/desorption cycle. The rate-limiting step involves the proton transfer from the guanidinium cations to the bicarbonate anions, formation of carbonic acid dimers, and release of H_2O and CO_2, with a determined activation energy of about -102 kJ mol^{-1}. The total energy for regenerating the sorbents was -151.5 kJ mol^{-1} (CO_2), 24 % lower compared with that required by the monoethanolamine-derived sorbent systems.

1.4.4 Reaction Mechanism of CO_2 with SILs

As discussed above, SIL-derived structures with large tunability in interaction strength with CO_2 are promising candidates to be used as modifiers, affording sorbents capable of achieving high-performance DAC of CO_2. As an illustration, the enthalpy tuning in superbase-derived phenolic ILs ($[P_{66614}][SPhO]$) can be achieved through modifications in the substituents within the phenoxide anions, varying from -51.4 to -17.1 kJ mol^{-1} [112]. The fine tuning in reaction enthalpy could be achieved by the structure of the anions with aza-fused rings, i. e., $[P_{66614}]$[3-BrPyra] (-55.9 kJ mol^{-1}), $[P_{66614}][5\text{-}CH_3Im]$ (-57.8 kJ mol^{-1}) and $[P_{66614}]$[Im] (-59.8 kJ mol^{-1}) [113]. However, although the reaction enthalpy values can be regulated in the range of -19.1 to -91.0 kJ mol^{-1} (and beyond through structure design) depending on the basicity of the anions in SILs, the super diluted CO_2 in air atmosphere raised constraints in SILs selection, in which relatively strong chemical bond formation was preferred to allow efficient CO_2 capture. On the other hand, considering the energy consumption in CO_2 release, it is critical to search for

the ILs based on anions with multiple binding sites in the same chemical unit. The reaction pathways and enthalpy values of selected basic anions with CO2 are shown in **Figure 1.8D** CO_2 could be integrated via the C-O and C-N bond formation, leading to the carbonate or carbamate formation. For example, the hybridization of Ni-MOF and SIL[MeTBDH]$_2$[HFPDO] was used to capture CO_2 by O-C bond formation between $[HFPDO]_2^-$ and CO_2 molecules (e.g., reaction enthalpy of -71.91 kJ mol^{-1}), leading to the generation of carbonate [38]. The CaO- and SIL $[P_{4444}][Im]$-engineered sorbent showed good performance in carbon capture (400 ppm CO_2 in He) due to its strong interaction with CO_2 via N-C bond formation with a reaction enthalpy of -85.2 kJ mol^{-1} [39].

1.5 CO_2 Sorption/Desorption Performance Evaluation

1.5.1 DAC of CO_2 Performance of Amine-Modified Sorbent

With the solid sorbents being synthesized and well characterized, their DAC of CO_2 behavior was then evaluated to gain insights into the structure-performance relationship. The choice of solid support significantly influences the carbon capture efficiency of the amine-modified sorbents. The highly ordered mesoporous silica supports, such as SBA-15 and MCM-41, are widely deployed due to their high pore volume and ability to accommodate high amine loading. It is noteworthy that the CO_2 capture performance of these materials relies on factors including surface area, porosity, intrinsic pore volume, and structure of amine modifiers [114].

Among the numerous amine structures, PEI is the one that is most frequently utilized. Due to its high amine concentration, stability, easy customization, and availability, it is a valuable benchmark oligomeric amine for sorbent creation. By increasing the pore volume from 1.51 to 1.82 cm^3 g^{-1} at 75 ˚C and 0.15 bar, the sorption capacity of 50 wt% PEI- PEI-impregnated mesocellular silica foam (MCF) was increased from 2.51 to 4.04 mol CO_2 per gram of sorbent [116]. While three-dimensional hexagonal mesoporous silica with wormhole-like pore structure was utilized as support, after 60 wt% PEI loading, a sorption capacity of 4.18 mmol CO_2/g sorbent was achieved at 75 ˚C [119]. Furthermore, when the pore size was changed from 5.6 to 7.6 nm, the CO_2 sorption

capacity of TEPA-impregnated ordered mesoporous silica (OMS) increased from 2.31 to 3.1 CO_2/g sorbent [117].

The microporous materials (e.g., zeolites) are less deployed as supports for amine loading as the small pores are unfavorable for achieving high loading amounts. Recently, PEI-impregnated zeolite nanotubes (ZNs) were deployed for capturing CO_2 from the air. The ZN at 65 % PEI loading performed better CO_2 uptake of about 2.23 mmol CO_2/g sorbent than standard benchmark PEI impregnated MCM-41, with a CO_2 uptake capacity of 1.74 mmol CO_2/g sorbent. [50,51] and kept stability over several cycles. It also has good performance in moderate humidity levels up to 35 %. The uptake kinetics of the sorbent were roughly four times faster than a comparable sorbent made by impregnating PEI into SBA-15 (captured 1.8 mmol CO_2/g sorbent). The improved accessibility of mesopores, the zeolitic and microporous walls of the nanotube, and the short length of the nanotubes are preferred to achieve improved carbon capture capacity and kinetics in ZNs.

A growing number of studies have been conducted on developing other aminopolymers for sorbent fabrication. Regardless of amine loading, it was discovered that poly(propylene imine) (PPI)-based sorbents were superior to PEI-based adsorbents at capturing CO_2 [52,53]. Poly(allylamine) (PAA), as another sort of primary amine rich polymer, exhibits improved thermal and oxidative resilience, making it a suitable material for CO2 capture [120,121]. Since Poly-(glycidyl amine) (PGA) solely contains primary amines, it could be able to collect CO_2 more effectively than PEI. In simulated air, the SBA-15 treated with PGA displayed higher capacity of about 0.6 mmol CO_2/g sorbent compared with PEI [115]. Pentaethylenehexamine (PEHA), which includes one more amine group than tetraethylenepentamine (TEPA), has demonstrated favorable characteristics for DAC than TEPA [122]. Tris (2-aminoethyl)amine (TREN) impregnate MIL-101(Cr) displayed better CO_2 capacity than PEI, despite a large loss of amines during the cycling procedure [54]. Therefore, for smaller amines-modified sorbents, low diffusion resistance and high amine loading could be achieved, but lower regeneration temperatures are required to solve their thermal volatility issues.

Taking inspiration from amine-functionalized silicas, a series of amine-modified-MOFs (e.g., Mg_2(dobpdc)) sorbents was developed towards DAC of CO_2 applications. Notably, for the men-Mg_2 (dobpdc) sorbents, the as-obtained CO_2 isotherms exhibited a distinct step-shaped profile, with sudden increases in CO_2 uptake at certain pressures depending on the open metal sites in the MOF scaffolds (**Figure 1.9A**) [24, 56]. This phenomenon was caused by a cooperative mechanism in which CO_2 molecules were inserted into the metal-N bonds, producing ordered chains of oxygen-bound carbamate species (**Figure 1.7C**). This unique CO_2 sorption behavior provides the opportunity to improve the cycling capability of related sorbents with less pressure or temperature change, that is, with less energy input [24]. By adjusting the attached diamine structures, the CO_2 capture characteristics could be further modified, creating sorbents with the ability to capture CO_2 from different emission sources [123,124]. Then, a tetraamine precursor was used to modify the Mg_2(dobpdc) (**Figure 1.9B and C**) [88]. The CO_2 uptake isotherms of Mg_2(dobpdc)(3-4-3) exhibit step-shaped CO_2 capture between 90 and 120 ˚C at 4 mbar. The experiments conducted at 100 ˚C under the same humid conditions were aimed at the simulating a real fixed-bed adsorption process. The results revealed that Mg_2(dobpdc)(3-4-3) was able to capture CO_2 at a high rate of 90 %, with a breakthrough capacity of 2.0 ± 0.2 mmol/g (**Figure 1.9D**). Additionally, a thermogravimetric analyzer determined that tetraamine volatilization observed during 1000 CO_2 adsorption-desorption cycles was negligible (**Figure 1.9E**).

To further enhance processability and stability in humid conditions for amine-functionalized Mg_2(dobpdc) families, the N-ethyl-ethylenediamine (een)-Mg_2(dobpdc)/alumina/silane beads (een-MOF/Al-Si) coated with hydrophobic silanes and alkyl epoxides were synthesized [58]. The beads showed a high CO_2 capacity of 2.82 and 2.54 mmol CO_2/g sorbent at 40 and 80 ˚C, respectively, at a pressure of 150 mbar CO2 (**Figure 1.9F**).

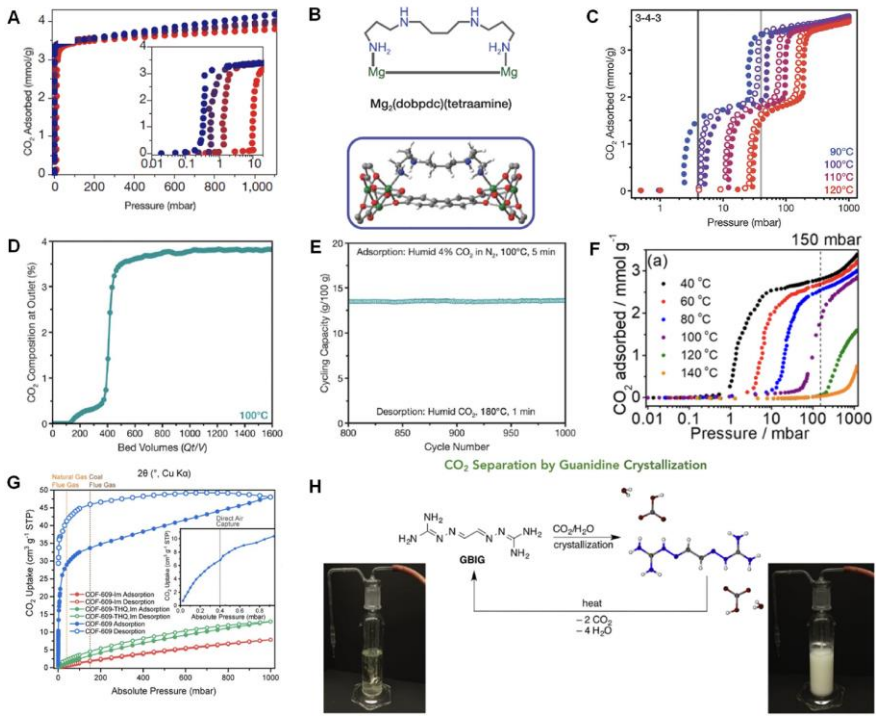

Figure 1.9 CO_2 sorption/desorption isotherm in sorbents. (A) CO_2 absorption isotherms at 25 (blue), 40 (blue-violet), 50 (red-violet), and 75 °C (red) for mmen-Mg_2(dobpdc). (B) Tetraamine-functionalized MOF material with the tetraamine coordinating to two Mg^{2+} sites. (C) CO_2 adsorption (filled circles) and desorption (open circles) isotherms at 90, 100, 110, and 120 °C for Mg_2(dobpdc)(3-4-3). (D) CO_2 breakthrough profile at 100 °C and atmospheric pressure for Mg_2(dobpdc)(3-4-3) under simulated humid (~2.6 % H_2O) natural gas (4 % CO_2 in N_2). (E) Mg_2(dobpdc)(3-4-3) was subjected to prolonged temperature-swing cycling using a thermogravimetric analyzer at air pressure. (F) CO_2 isotherms of een-Mg_2(dobpdc)/alumina/silane/epoxide composites (een-MOF/Al-Si-C_{17}; 17 =number of carbon atoms attached to epoxide; een =N-ethylethylenediamine) measured at various temperatures. (G) The CO_2 isotherm of COF-609 (Inset: the CO_2 isotherms of COF-609 at 0–1 mbar). (H) CO_2 capture via guanidine bicarbonate crystallization. (For interpretation of the references to color in this figure legend, the reader is referred to the Web version of this article.

The selective separation of CO_2 was confirmed through dynamic breakthrough experiments using wet CO_2. These results indicate that the modified adsorbent has potential for efficient CO_2 capture in industrial processes.

Class 2 amine-grafted sorbents have amine functional groups chemically bonded onto the support surface and high amine loadings, making them more stable during regeneration than Class 1 amine-impregnated sorbents. The triamine-grafted mesoporous silica (TRIPE-MCM-41) demonstrated remarkable selectivity for CO_2 with a capacity of 0.98 mmol CO_2/g sorbent at low CO_2 concentrations [60] In addition, alumina can be tailored to have significant acidity or basicity due to its amphoteric nature and might thus take part in the CO_2 sorption process. The CO_2 uptake capacity of the sorbent at 400 ppm CO2 in N_2 ranges from 0.15 to 0.75 mmol CO_2/g sorbent, depending on the APS amine loading of the alumina substrate [64]. The amine-based nano fibrillated cellulose (NFC) sorbent was able to absorb 1.39 mmol CO_2/g sorbent [23]. After conducting 20 successive 2h absorption and 1h desorption cycles to test its stability, the cyclic capacity of the sorbent was 0.695 mmol CO_2/g sorbent. The amine-grafted PPN has the benefit of porous three-dimensional scaffolds. The amine-grafted PPNs (PPN-6-CH_2DETA) showed a high CO_2 selectivity and capacity (1.04 mmol CO_2/g sorbent) [68].

The modified COF-609 framework can absorb CO_2 gas significantly, even at low pressure, which makes it a potential candidate for carbon capture technologies [26]. COF-609 can adsorb 6.8 cm^3/g STP (0.304 mmol/g) at 0.4 mbar CO_2 pressure, which is a 1360-fold increase compared to COF-609-THQ,Im without amine-grafting, which can only adsorb 0.005 cm^3/g STP (0.00022 mmol/g) at the same pressure (**Figure 1.9G**). Additionally, the uptake capacity is further enhanced by 29 % in the presence of humidity.

1.5.2 Low Concentration CO_2 Capture of Iminogunidine-Derived Sorbents

An alternative DAC of CO_2 procedure was demonstrated by adopting aqueous iminogunidine-type compounds as the sorbents. Different from the aqueous amine solutions, in which the CO_2-integrated products are still soluble in water, a white precipitation that was identified as the GBIGH2$(HCO_3)_2(H_2O)_2$ product was observed after the flue gas mixture was bubbled through the aqueous solution of GBIG (10 mM)

for 30 min, resulting in a CO_2 sorption capacity of 10.47 mmol CO_2/g GBIG (**Figure 1.9H**) [70].

1.5.3 Carbon Capture Behavior of SIL-Derived Sorbents in DAC of CO_2

The SIL-derived sorbents being synthesized via the wet impregnation procedures have been utilized in low-concentration carbon capture with diluted CO2 or air as the feeding gas. The CO_2 capture performance of CaO- and Na[Im]-modified MCM-41 (denoted as MSC-[Na] [Im]) was tested via fixed-bed breakthrough at 298 K with 400 ppm CO_2 (in He) as the feeding gas [39]. The pseudo-equilibrium capacity of CO_2 capture was found to be approximately 0.97 mmol/g, while the breakthrough capacity was calculated to be around 0.63 mmol/g (**Figure 1.10A and B**). While SIL [P_{4444}][Im] was deployed as the modifier, the corresponding MSC-[P_{4444}][Im] sorbent displayed an uptake capacity of 0.65 mmol/g via breakthrough measurement (**Figure 1.10C**).

These sorbents exhibited good cycling stability with CO_2 being released under inert atmosphere at 353 K. Both low-pressure (<1 mbar) volumetric CO_2 capture assessment and a fixed-bed breakthrough examination was conducted on the composite sorbents being fabricated from Ni-MOF and SIL, in which good performance in DAC of CO_2 was demonstrated (**Figure 1.10D–F**) [38]. For example, Ni-MOF/IL-3 with the molar ratio (SIL: Ni) of 0.48 led to an uptake capacity of 0.58 mmol/g from 400 ppm CO_2 in He at 298 K, which could be desorbed at 353 K under He flow, and the sorbent had good cycling stability over at least five runs. The CO_2 uptake capacity (0.57 mmol/g) almost had no change in the presence of water impurities at a RH level of 2.5 % via the breakthrough study. The stability of the composite sorbent was further illustrated by the well-maintained CO_2 uptake capacity under humid conditions, benefiting from the confinement effect of the Ni-MOF cavity to the SIL. In addition, the Ni-MOF/IL-3 exhibited a remarkable and highly selective interaction with CO_2 compared to N_2. The CO_2/N_2 selectivity was measured to be over 5000 based on the ideal adsorbed solution

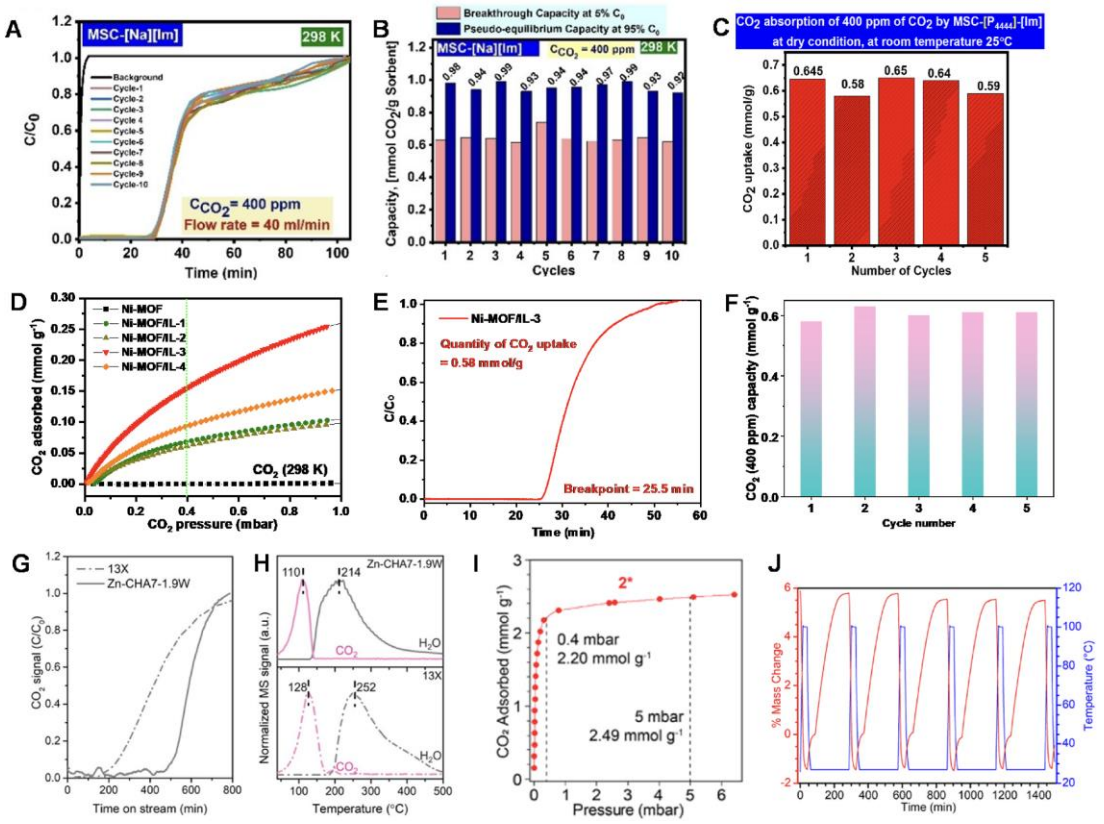

Figure 1.10 400 ppm CO_2 uptake behavior in sorbents. (A) Breakthrough curves for MSC-Na[Im], featuring ten cycles with 400 ppm CO_2 (B) Breakthrough (C/C0 =0.05) and pseudo equilibrium (C/C_0 =0.95) CO_2 capture capacities of MSC-Na[Im] for up to ten cycles. (C) Equilibrium CO_2 uptake capacities of MSC-[P_{4444}][Im] for up to five cycles (D) The CO_2 uptake isotherms of Ni-MOF and Ni-MOF/IL-x (x =1–4) under low-pressure region (<1 mbar) are being collected at 298 K. (E) The breakthrough curve of CO_2 (400 ppm) uptake by Ni-MOF/ IL-3 at 298 K. (F) Recyclability of Ni-MOF/IL-3 in CO_2 (400 ppm) capture via breakthrough evaluation (G) Column breakthrough profiles of 13X and Zn-CHA7-1.9W zeolites for the adsorption of dry CO_2. (H) Temperature programmed desorption profiles of CO_2 and H_2O from Zn-CHA7-1.9W and 13X zeolites after saturation with humid CO_2 (relative humidity =49%). (I) Low-pressure region of the CO_2 sorption isotherm of [$Zn(ZnO_2CCH_3)_4(bibta)_3$]. (J) Adsorption-desorption cycling of [$Zn(ZnO_2CCH_3)_4(bibta)_3$] under simulated air conditions (395 ppm of CO_2) showing changes in sample mass (red) and temperature swing (blue).

theory (IAST) with CO_2/N_2 (50:50, v/v), thus rendering it a valuable resource for effectively capturing CO_2 from the air atmosphere.

1.5.4 DAC of CO_2 Performance of Other Types of Sorbents

Although this review is mainly focused on the amine-modified, iminoguanidine-based, and SIL-functionalized sorbents, there are also other types of promising sorbents in DAC of CO_2. For example, chabazite (CHA) zeolites containing Zn have been demonstrated to absorb low concentrations of CO_2 [41]. They exhibit a higher capacity, faster kinetics, and lower desorption energy compared to standard low-silica zeolites. The positioning and state of Zn ions within the CHA cages are crucial for achieving high CO_2 adsorption capacity. When Zn^{2+} ions are located in zeolites with a Si/Al ratio of 7, the adsorption capacity increases by 17 times compared to the parent H-form. The Zn-CHA-type material exhibits faster adsorption kinetics than standard zeolite (Si/Al ratio of 1.1), as illustrated by the sharper breakthrough profile (**Figure 1.10G**). The Zn-CHA-type material has a lower desorption temperature for both CO_2 and H_2O compared to standard zeolite under the humid CO_2 condition (RH =49 %) profile (**Figure 1.10H**). Furthermore, reducing the Si/Al ratio further increases CO_2 capacity. The capacity of Zn ion-exchanged CHA can be further enhanced to about 0.67 mmol CO_2/g zeolite with a Si/Al ratio of 2.

Recently, a Zn-benzotriazolate MOF $[Zn(ZnO_2CCH_3)_4(bibta)_3]$ ($bibta^{2-}$=5,5′-bibenzotriazolate) was altered by ligand exchange and heat activation to produce nucleophilic Zn-OH groups similar to the active site of α-carbonic anhydrase [118]. This alteration produced a highly effective, mild-temperature regenerable MOF sorbent for trapping trace levels of CO_2. The volumetric CO_2 capture of $[Zn\ (ZnO_2CCH_3)_4(bibta)_3]$ at 0.4 mbar has a capacity of 2.20 mmol/g, equivalent to CO_2 concentration of 400 ppm (**Figure 1.10I**). Thermal swing adsorption (TSA) experiments were conducted to test the stability of Zn-benzotriazolate MOF during adsorption-desorption cycles and to determine its CO_2 uptake capacity from simulated air. The MOF showed a CO_2 uptake of 5.8 wt % after cycling with a simulated air mixture (395 ppm CO_2, 21 % O_2, N_2 balance). The adsorption capacity only slightly decreased after 5-10 adsorption-desorption cycles (**Figure 1.10J**). However, when exposed to a water-saturated gas stream, the MOF

showed immediate CO_2 breakthrough. This indicates that Zn-benzotriazolate MOF is not effective in humid conditions.

Adsorption and desorption kinetics, energy requirements for regeneration, chemical stability, CO_2 uptake over a wide range of temperatures and humidity levels, and economic and environmental viability in the life cycle assessment are the key metrics that can be used to assess the performance of DAC adsorbents. These factors are important in designing and developing effective and practical DAC technologies for capturing CO_2 from the atmosphere. For the as-developed sorbents being deployed in DAC of CO_2, they all have advantages and disadvantages, but it is difficult to meet all the requirements for large-scale direct air capture by one specific sorbent. The energy cost of thermal regeneration is still generally high, future research should focus on developing sorbents with energy-efficient cycling, improved stability, rapid sorption kinetics, and enhanced capacity and cost-effectiveness.

1.6 Conclusion and Overview of Thesis

In this introductory chapter, we have outlined the critical role of engineered solid sorbents in addressing the carbon challenge through direct air capture (DAC) of CO_2. While amine-modified materials have dominated the landscape of solid sorbents, alternative systems such as superbase-derived ionic liquids (SILs), iminoguanidine-based compounds, and IL-functionalized frameworks have emerged as promising candidates due to their tunable chemisorption behavior, enhanced stability, and potentially lower energy penalties during regeneration. The importance of rational sorbent design considering chemical reactivity, structural durability, porosity, and sorption kinetics has been emphasized as key to achieving viable DAC performance under ultra-dilute CO_2 conditions. In the following chapters, we will focus on a particular class of sorbents: carbonaceous solid materials modified by superbase-derived ionic liquids.

Specifically, Chapter 2 and Chapter 3 will investigate SIL-functionalized carbon fibers and porous carbon scaffolds, respectively, with attention to how the porosity and microstructure of these supports influence the efficiency and selectivity of CO_2 capture.

This includes tailoring pore environments to enhance IL dispersion, accessibility to active sites, and confinement effects.

Chapter 4 will then delve into the NMR relaxation study as a dynamic characterization approach to understand the molecular behavior of CO_2 within these sorbents. We will comparatively explore the CO_2 dynamics in chemically versus physically captured forms using different ionic liquids, thereby offering insight into the sorption mechanisms, kinetics, and the role of molecular mobility in determining sorbent performance.

Through this focused investigation, our objective is to provide a comprehensive understanding of the structure–property–performance relationship of SIL-modified carbonaceous sorbents. This study lays the foundation for future investigations into the scalability of the sorbents; however, comprehensive techno-economic analyses and evaluations of technology readiness levels are essential to determine their feasibility for real-world deployment.

References

[1] T.R. Karl, K.E. Trenberth, Science 302 (2003) 1719.

[2] H. Konishi, T. Ueda, T. Muto, K. Manabe, Org Lett, vol. 14, 2012, p. 4722, doi:10.1021/ol301850y.

[3] P.D.A. Kraaijenbrink, M.F.P. Bierkens, A.F. Lutz, W.W. Immerzeel, Nature 549 (2017) 257, doi:10.1038/nature23878.

[4] C.D. Koven, B. Ringeval, P. Friedlingstein, P. Ciais, P. Cadule, D. Khvorostyanov, G.Krinner, C. Tarnocai, Proc. Natl. Acad. Sci. U.S.A.108 (2011).

[5] S. Choi, J.H. Drese, C.W. Jones, ChemSusChem 2 (2009) 796

[6] X. Zhu, W. Xie, J. Wu, Y. Miao, C. Xiang, C. Chen, B. Ge, Z. Gan, F. Yang, M. Zhang, D. O'Hare, J. Li, T. Ge, R. Wang, Chem. Soc. Rev. 51 (2022) 6574, doi:10.1039/D1CS00970B.

[7] R. Custelcean, Chem.

[8] E.S. Sanz-Pérez, C.R. Murdock, S.A. Didas, C.W. Jones, Chem. Rev. 116 (2016) 11840, doi:10.1021/acs.chemrev.6b00173.

[9] K. Lackner, H.-J. Ziock, P. Grimes, 1999.

[10]K.S. Lackner, Energy 50(2013) 38, doi:10.1016/j.energy.2012.09.012.

[11]R. Custelcean, N.J. Williams, X. Wang, K.A. Garrabrant, H.J. Martin, M.K. Kidder, A.S.Ivanov, V.S. Bryantsev, ChemSusChem 13 (2020) 6381, doi:10.1002/cssc.202001114.

[12]J.M. Hanusch, I.P. Kerschgens, F. Huber, M. Neuburger, K. Gademann, Chem. Commun. 55 (2019) 949.

[13]Y.-H. Luo, C. Chen, D.-L. Hong, X.-T. He, J.-W. Wang, T. Ding, B.-J. Wang, B.-W. Sun, ACS Appl. Mater. Interfaces 10 (2018) 9495, doi:10.1021/acsami.8b01044.

[14]S. Zeng, X. Zhang, L. Bai, X. Zhang, H. Wang, J. Wang, D. Bao, M. Li, X. Liu, S.Zhang, Chem. Rev. 117 (2017) 9625, doi:10.1021/acs.chemrev.7b00072.

[15]F.M. Brethomé, N.J. Williams, C.A. Seipp, M.K. Kidder, R. Custelcean, Nat. Energy 3 (2018) 553, doi:10.1038/s41560-018-0150-z.

[16]J. Septavaux, C. Tosi, P. Jame, C. Nervi, R. Gobetto, J. Leclaire, Nat. Chem. 12 (2020) 202, doi:10.1038/s41557-019-0388-5.
[17]K.S. Lackner, Eur. Phys. J.: Spec. Top. 176(2009) 93, doi:10.1140/epjst/e2009-01150-3.
[18]Z. Zhang, Q. Ding, J. Cui, X. Cui, H. Xing, Sci. China Mater. 64 (2021) 691, doi:10.1007/s40843-020-1471-0.
[19]D.W. Keith, G. Holmes, D. St Angelo, K. Heidel, Joule 2 (2018) 1573, doi:10.1016/j.joule.2018.05.006.
[20]R. Chang, X. Wu, O. Cheung, W. Liu, J. Mater. Chem. A 10 (2022) 1682, doi:10.1039/D1TA07697C.
[21]C. Gunathilake, M. Jaroniec, J. Mater. Chem. A 4 (2016) 10914, doi:10.1039/C6TA03916B.
[22]V. Nikulshina, M.E. Gálvez, A. Steinfeld, J. Chem. Eng. 129 (2007) 75, doi:10.1016/j.cej.2006.11.003.
[23]C. Gebald, J.A. Wurzbacher, P. Tingaut, T. Zimmermann, A. Steinfeld, Environ. Sci. Technol.45 (2011) 9101, doi:10.1021/es202223p.
[24]T.M. McDonald, J.A. Mason, X. Kong, E.D. Bloch, D. Gygi, A. Dani, V. Crocellà, F.Giordanino, S.O. Odoh, W.S. Drisdell, B. Vlaisavljevich, A.L. Dzubak, R. Poloni, S.K.Schnell, N. Planas, K. Lee, T. Pascal, L.F. Wan, D. Prendergast, J.B. Neaton, B. Smit, J.B. Kortright, L. Gagliardi, S. Bordiga, J.A. Reimer, J.R. Long, Nature 519 (2015) 303, doi:10.1038/nature14327.
[25]V.Y. Mao, P.J. Milner, J.H. Lee, A.C. Forse, E.J. Kim, R.L. Siegelman, C.M. McGuirk, L.B. Zasada, J.B. Neaton, J.A. Reimer, J.R. Long, Angew. Chem. Int. Ed. 59 (2020) 19468.
[26]H. Lyu, H. Li, N. Hanikel, K. Wang, O.M. Yaghi, J. Am. Chem. Soc. 144 (2022) 12989, doi:10.1021/jacs.2c05382.
[27]S. Sircar, T.C. Golden, M.B. Rao, Carbon 34 (1996) 1.
[28]F. Rodríguez-Reinoso, M. Molina-Sabio, Carbon 30 (1992) 1111, doi:10.1016/0008-6223(92)90143-K.

[29]X. Shi, H. Xiao, K.S. Lackner, X. Chen, Angew. Chem. Int. Ed. 55 (2016) 4026.
[30]Z. Yong, A.r.E. Rodrigues, Energy Convers. Manag. 43 (2002) 1865.
[31]A.-H. Liu, R. Ma, C. Song, Z.-Z. Yang, A. Yu, Y. Cai, L.-N. He, Y.-N. Zhao, B. Yu, Q.-W. Song, Angew. Chem. Int. Ed. 51 (2012) 11306.
[32]M.W. Hahn, J. Jelic, E. Berger, K. Reuter, A. Jentys, J.A. Lercher, J. Phys. Chem. B 120 (2016) 1988.
[33]C.A. Seipp, N.J. Williams, M.K. Kidder, R. Custelcean, Angew. Chem. Int. Ed. 56 (2017) 1042.
[34]X. Zhang, X. Zhang, H. Dong, Z. Zhao, S. Zhang, Y. Huang, Energy Environ. Sci. 5 (2012) 6668.
[35]Y. Sun, H. Huang, H. Vardhan, B. Aguila, C. Zhong, J.A. Perman, A.M. Al-Enizi, A.Nafady, S. Ma, ACS Appl. Mater. Interfaces 10 (2018) 27124.
[36]Y. Wang, Y. Shao, H. Wang, J. Yuan, Acc. Mater. Res. 1(2020) 16.
[37]G. Cui, J. Wang, S. Zhang, Chem. Soc. Rev. 45 (2016) 4307.
[38]L. Qiu, L. Peng, D. Moitra, H. Liu, Y. Fu, Z. Dong, W. Hu, M. Lei, D.-e. Jiang, H. Lin, J.Hu, K.A. McGarry, I. Popovs, M. Li, A.S. Ivanov, Z. Yang, S. Dai, Small 19 (2023) 2302708.
[39]D. Moitra, N. MokhtariNori, K.M. Siniard, L. Qiu, J. Fan, Z. Dong, W. Hu, H. Liu, D.-e. Jiang, H. Lin, J. Hu, M. Li, Z. Yang, S. Dai, ChemSusChem 16 (2023) e202300808.
[40]J. Zhang, R. Singh, P.A. Webley, Microporous and Mesoporous Materials, vol. 111, 2008, p. 478.
[41]D. Fu, Y. Park, M.E. Davis, Angew. Chem. Int. Ed. 61 (2022) e202112916.
[42]A. Kumar, D.G. Madden, M. Lusi, K.-J. Chen, E.A. Daniels, T. Curtin, J.J. Perry Iv, M.J. Zaworotko, Angew. Chem. Int. Ed. 54 (2015) 14372.
[43]P. Nugent, Y. Belmabkhout, S.D. Burd, A.J. Cairns, R. Luebke, K. Forrest, T. Pham, S.Ma, B. Space, L. Wojtas, M. Eddaoudi, M.J. Zaworotko, Nature 495 (2013) 80.
[44]P.M. Bhatt, Y. Belmabkhout, A. Cadiau, K. Adil, O. Shekhah, A. Shkurenko, L.J.Barbour, M. Eddaoudi, J. Am. Chem. Soc. 138 (2016) 9301.

[45]Y. Liu, Y. Yang, Y. Qu, Y.-Q. Li, M. Zhao, W. Li, Nanoscale Adv, vol. 3, 2021, p. 1397.
[46]A. Goeppert, M. Czaun, G.K. Surya Prakash, G.A. Olah, Sci. 5 (2012) 7833.
[47]J. Tanthana, S.S.C. Chuang, ChemSusChem 3 (2010) 957.
[48]M.A. Sakwa-Novak, S. Tan, C.W. Jones, ACS Appl. Mater. Interfaces 7 (2015) 24748.
[49]J.H. Drese, S. Choi, R.P. Lively, W.J. Koros, D.J. Fauth, M.L. Gray, C.W. Jones, Adv. Funct. Mater. 19 (2009) 3821.
[50]X. Xu, C. Song, J.M. Andresen, B.G. Miller, A.W. Scaroni, Energy Fuels, vol. 16, 2002, p. 1463
[51]S. Choi, M.L. Gray, C.W. Jones, ChemSusChem4 (2011) 628.
[52]S.H. Pang, L.-C. Lee, M.A. Sakwa-Novak, R.P. Lively, C.W. Jones, J. Am. Chem. Soc. 139 (2017) 3627.
[53]S.H. Pang, R.P. Lively, C.W. Jones, ChemSusChem 11(2018) 2628.
[54]L.A. Darunte, A.D. Oetomo, K.S. Walton, D.S. Sholl, C.W. Jones, ACS Sustain. Chem. Eng. 4 (2016) 5761.
[55]G.N. Short, E. Burentugs, L. Proaño, H.J. Moon, G. Rim, I. Nezam, A. Korde, S. Nair, C.W. Jones, JACS Au, vol. 3, 2023, p. 62.
[56] T.M. McDonald, W.R. Lee, J.A. Mason, B.M. Wiers, C.S. Hong, J.R. Long, J. Am. Chem. Soc. 134 (2012) 7056.
[57] P.-Q. Liao, X.-W. Chen, S.-Y. Liu, X.-Y. Li, Y.-T. Xu, M. Tang, Z. Rui, H. Ji, J.-P.Zhang, X.-M. Chen, Chem Sci, vol. 7, 2016, p. 6528.
[58]J.H. Choe, H. Kim, M. Kang, H. Yun, S.Y. Kim, S.M. Lee, C.S. Hong, J. Am. Chem. Soc. 144 (2022) 10309.
[59]J.S. Yeon, W.R. Lee, N.W. Kim, H. Jo, H. Lee, J.H. Song, K.S. Lim, D.W. Kang, J.G.Seo, D. Moon, B. Wiers, C.S. Hong, J. Mater. Chem. A 3 (2015) 19177
[60]Y. Belmabkhout, R. Serna-Guerrero, A. Sayari, Chem. Eng. Sci. 65 (2010) 3695.
[61]M. Jahandar Lashaki, A. Sayari, Chem. Eng. J. 334 (2018) 1260.
[62]P.J.E. Harlick, A. Sayari, Ind. Eng. Chem. Res. 45 (2006) 3248.

[63]P.J.E. Harlick, A. Sayari, Ind. Eng. Chem. Res. 46 (2007) 446.
[64]M.E. Potter, K.M. Cho, J.J. Lee, C.W. Jones, ChemSusChem 10 (2017) 2192
[65]S.J. Eichhorn, C.A. Baillie, N. Zafeiropoulos, L.Y. Mwaikambo, M.P. Ansell, A.Dufresne, K.M. Entwistle, P.J. Herrera-Franco, G.C. Escamilla, L. Groom, M. Hughes, C. Hill, T.G. Rials, P.M. Wild, J. Mater. Sci. 36 (2001) 2107.
[66]D. Klemm, B. Heublein, H.-P. Fink, A. Bohn, Angew. Chem. Int. Ed. 44 (2005) 3358.
[67]W. Lu, J.P. Sculley, D. Yuan, R. Krishna, Z. Wei, H.-C. Zhou, Angew. Chem. Int. Ed. 51 (2012) 7480.
[68]W. Lu, J.P. Sculley, D. Yuan, R. Krishna, H.-C. Zhou, J. Phys. Chem. C 117 (2013) 4057.
[69]S. Choi, J.H. Drese, P.M. Eisenberger, C.W. Jones, Environ. Sci. Technol. 45 (2011) 2420.
[70]N.J. Williams, C.A. Seipp, F.M. Brethomé, Y.Z. Ma, A.S. Ivanov, V.S. Bryantsev, M.K.Kidder, H.J. Martin, E. Holguin, K.A. Garrabrant, R. Custelcean, Chem 5 (2019) 719.
[71]R. Custelcean, N.J. Williams, C.A. Seipp, Angew. Chem. Int. Ed. 54 (2015) 10525.
[72]R. Custelcean, N.J. Williams, C.A. Seipp, A.S. Ivanov, V.S. Bryantsev, Chem. Eur J. 22 (2016) 1997.
[73]M. Koskinen, I. Mutikainen, H. Elo, vol. 49, 1994, p. 556.
[74]M. Ramdin, T.W. de Loos, T.J.H. Vlugt, Ind. Eng. Chem. Res. 51 (2012) 8149.
[75]Z.-Z. Yang, Y.-N. Zhao, L.-N. He, RSC Adv. 1 (2011) 545.
[76]Z.-Z. Yang, L.-N. He, J. Gao, A.-H. Liu, B. Yu, Energy Environ Sci, vol. 5, 2012.
[77]F.-F. Chen, K. Huang, Y. Zhou, Z.-Q. Tian, X. Zhu, D.-J. Tao, D.-e. Jiang, S. Dai, Angew. Chem. Int. Ed. 55 (2016) 7166.
[78]B.E. Gurkan, J.C. de la Fuente, E.M. Mindrup, L.E. Ficke, B.F. Goodrich, E.A. Price, W.F. Schneider, J.F. Brennecke, J. Am. Chem. Soc. 132 (2010) 2116.
[79]E.D. Bates, R.D. Mayton, I. Ntai, J.H. Davis, J. Am. Chem. Soc. 124 (2002) 926.
[80]C. Wang, H. Luo, X. Luo, H. Li, S. Dai, Green Chem. 12 (2010) 2019.

[81]X. Suo, Y. Fu, C.-L. Do-Thanh, L.-Q. Qiu, D.-e. Jiang, S.M. Mahurin, Z. Yang, S. Dai, JACS, vol. 144, 202221658.
[82]X. Suo, Z. Yang, Y. Fu, C.-L. Do-Thanh, H. Chen, H. Luo, D.-e. Jiang, S.M. Mahurin, H. Xing, S. Dai, ChemSusChem 14 (2021) 2854.
[83]C. Wang, X. Luo, H. Luo, D.-e. Jiang, H. Li, S. Dai, Tuning the basicity of ionic liquids for equimolar CO2 capture, Angew. Chem. Int. Ed. 50 (2011) 4918.
[84]C. Wang, H. Luo, D.-e. Jiang, H. Li, S. Dai, Angew. Chem. Int. Ed. 49 (2010) 5978.
[85]H.F.D. Almeida, M.G. Freire, A.M. Fernandes, J.A. Lopes-da-Silva, P. Morgado, K.Shimizu, E.J.M. Filipe, J.N. Canongia Lopes, L.M.N.B.F. Santos, J.A.P. Coutinho, Langmuir 30 (2014) 6408.
[86]T. Liu, M.H. Rahman, P.L. Menezes, A. Martini, J. Phys. Chem. B 126 (2022) 4354.
[87]L. Qiu, M. Lei, C. Wang, J. Hu, L. He, A.S. Ivanov, D.e. Jiang, H. Lin, I. Popovs, Y.Song, J. Fan, M. Li, S.M. Mahurin, Z. Yang, S. Dai, Small (2024) 2401798.
[88]E.J. Kim, R.L. Siegelman, H.Z.H. Jiang, A.C. Forse, J.-H. Lee, J.D. Martell, P.J. Milner, J.M. Falkowski, J.B. Neaton, J.A. Reimer, S.C. Weston, J.R. Long, Science 369 (2020) 392.
[89]A. Vjunov, M.Y. Hu, J. Feng, D.M. Camaioni, D. Mei, J.Z. Hu, C. Zhao, J.A. Lercher, Angew. Chem. Int. Ed. 53 (2014) 479.
[90]N.R. Jaegers, K.T. Mueller, Y. Wang, J.Z. Hu, Acc. Chem. Res. 53(2020) 611.
[91]G.A. Russell Parks, N. Leick, M.A.T. Marple, N.A. Strange, B.G. Trewyn, S.H. Pang, W.A. Braunecker, J. Phys. Chem. C127 (2023) 15363.
[92]H.J. Moon, R.-S. Sekiya, C.W. Jones, J. Phys. Chem. C127 (2023) 11652.
[93]A.K. Whittaker, vol. 34, 1997, p. 105.
[94]X. Li, S. Wang, L. Li, Y. Sun, Y. Xie, J. Am. Chem. Soc. 142 (2020) 9567.
[95]S. Du, J. Huang, M.R. Ryder, L.L. Daemen, C. Yang, H. Zhang, P. Yin, Y. Lai, J. Xiao, S. Dai, B. Chen, Nat. Commun. 14 (2023) 1197.
[96]A. Holewinski, M.A. Sakwa-Novak, C.W. Jones, J. Am. Chem. Soc. 137 (2015) 11749.

[97]R. Afonso, M. Sardo, L. Mafra, J.R.B. Gomes, Environ. Sci. Technol. 53(2019) 2758.
[98]R.B. Said, J.M. Kolle, K. Essalah, B. Tangour, A. Sayari, ACS Omega, vol. 5, 2020 26125.
[99]H. Zhang, L.-M. Yang, E. Ganz, Langmuir 36 (2020) 14104.
[100]J.-H. Lee, R.L. Siegelman, L. Maserati, T. Rangel, B.A. Helms, J.R. Long, J.B. Neaton, Chem. Sci. 9 (2018) 5197.
[101]J.M.Y. Carrillo, M.A. SakwaNovak, A. Holewinski, M.E. Potter, G. Rother, C.W.Jones, B.G. Sumpter, Langmuir 32 (2016) 2617.
[102]G. Rother, U. Tumuluri, K. Huang, W.T. Heller, S. Dai, J.-M. Carrillo, B.G. Sumpter, Langmuir 37 (2021) 4622.
[103]V. Stampi-Bombelli, M. van der Spek, M. Mazzotti, Adsorption26 (2020) 1183.
[104]J.A. Wurzbacher, C. Gebald, S. Brunner, A. Steinfeld, J. Chem. Eng. 283(2016) 1329.
[105]J. Young, E. García-Díez, S. Garcia, M. van der Spek, Energy Environ. Sci. 14 (2021) 5377.
[106]L.A. Darunte, T. Sen, C. Bhawanani, K.S. Walton, D.S. Sholl, M.J. Realff, C.W. Jones, Ind. Eng. Chem. Res. 58 (2019) 366.
[107]P. Bollini, S.A. Didas, C.W. Jones, J. Mater. Chem. 21 (2011) 15100.
[108]S.A. Didas, S. Choi, W. Chaikittisilp, C.W. Jones, Acc. Chem. Res. 48 (2015) 2680.
[109]T.L. Donaldson, Y.N. Nguyen, Ind. Eng. Chem. Fundam. 19 (1980) 260.
[110]T. Wang, K.S. Lackner, A.B. Wright, Phys. Chem. Chem. Phys. 15(2013) 504.
[111]R. Custelcean, N.J. Williams, K.A. Garrabrant, P. Agullo, F.M. Brethomé, H.J. Martin, M.K. Kidder, Ind. Eng. Chem. Res. 58 (2019) 23338.
[112]C. Wang, H. Luo, H. Li, X. Zhu, B. Yu, S. Dai, Chem. Eur J. 18 (2012) 2153.
[113] D. Hospital-Benito, C. Moya, M. Gazzani, J. Palomar, J. Chem. Eng. 468 (2023) 143630.
[114]R. Kishor, A.K. Ghoshal, nd. Eng. Chem. Res. 56 (2017) 6078.

[115]A.R. Sujan, D.R. Kumar, M. Sakwa-Novak, E.W. Ping, B. Hu, S.J. Park, C.W. Jones, ACS Appl. Polym. Mater. 1 (2019) 3137.
[116]X. Yan, L. Zhang, Y. Zhang, K. Qiao, Z. Yan, S. Komarneni, Chem. Eng. J. 168 (2011) 918.
[117]L. Wang, M. Yao, X. Hu, G. Hu, J. Lu, M. Luo, M. Fan, Appl. Surf. Sci.324 (2015) 286.
[118]C.E. Bien, K.K. Chen, S.-C. Chien, B.R. Reiner, L.-C. Lin, C.R. Wade, W.S.W. Ho, J. Am. Chem. Soc. 140(2018) 12662.
[119]C. Chen, S.-T. Yang, W.-S. Ahn, R. Ryoo, Chem. Commun.3627 (2009).
[120]H. Zerze, A. Tipirneni, A.J. McHugh, Separ. Sci. Technol. 52(2017) 2513,
[121]S. Bali, T.T. Chen, W. Chaikittisilp, C.W. Jones, Energy Fuels, vol. 27, 2013, p. 1547.
[122]A. Goeppert, H. Zhang, R. Sen, H. Dang, G.K.S. Prakash, ChemSusChem 12 (2019) 1712.
[123]P.J. Milner, R.L. Siegelman, A.C. Forse, M.I. Gonzalez, T. Runčevski, J.D. Martell, J.A.Reimer, J.R. Long, J. Am. Chem. Soc. 139 (2017) 13541.
[124]R.L. Siegelman, T.M. McDonald, M.I. Gonzalez, J.D. Martell, P.J. Milner, J.A. Mason, A.H. Berger, A.S. Bhown, J.R. Long, J. Am. Chem. Soc. 139(2017) 10526.

CHAPTER 2 : ENHANCED CARBON CAPTURE BEHAVIOR OF CARBON FIBERS VIA IL MODIFICATION

A version of this chapter was originally published in ChemNanoMat Journal:
Mokhtari-Nori, Narges, Huimin Luo, Ryan Paul, Frederic Vautard, Yuqing Fu, Juntian Fan, De-en Jiang, Zhenzhen Yang, and Sheng Dai. "Enhanced carbon capture behavior of carbon fibers via ionic liquid modification." *ChemNanoMat* 9, no. 1 (2023): e202200480.

2.1. Abstract

Carbon-based materials are widely deployed in carbon capture but are limited to physisorption procedures. Further extending functionalized carbon materials to CO_2 chemisorption under low CO_2 concentration is highly desirable and yet challenging. Herein, a carbon fiber composed solely of ultra-micropores (~ 0.45 nm) was deployed as the precursor to avoid the pore blocking effect, which was modified by superbase-derived ionic liquids (ILs) containing strong interaction sites with CO_2. By forming a thin coating layer on the surface, the as-afforded surface functionalized fiber materials demonstrated enhanced CO_2 uptake capacity and improved CO_2 sorption kinetics, as evaluated by both the volumetric method and thermogravimetric analysis, as well as the calculated energy distribution curves. The achievements made in this work guide the functionalization of carbon-based materials towards enhanced CO_2 chemisorption by forming a thin layer of selected IL coating.

2.2. Introduction

To improve the CO_2 capture capacity of the carbon materials, extensive studies have been conducted via strategies such as heteroatoms-doping (e. g., O, N, F, or S), [1] inorganic base activation (e. g., NaOH, KOH, $NaNH_2$), [2] utilization of templates during the preparation process,[3–4] and anchoring CO_2-philic functionalities on the surface, aiming at increasing the surface areas, tuning the porosity distributions, and enhancing the interaction strength with CO_2. For example, the carbon spheres being obtained by the KOH activation pathway exhibited abundant small micropores (< 0.8 nm), high surface area (2400 $m^2\ g^{-1}$), and promising CO_2 uptake capacity up to 8.9 mmol g^{-1} at 273 K and CO_2 pressure of 1 bar.[5] Although such progress has been made, the utilization of state-of-the-art carbon materials is still limited to CO_2 physisorption due to a lack of strong chemical interaction sites with CO_2 being involved within the scaffolds. Solid sorbents for CO_2 chemisorption are mainly strong basic metal oxides (e.g., CaO and MgO) and

amine-functionalized (e.g., polyethyleneimine (PEI)) porous materials, and the former are deployed in high-temperature carbon capture procedures. Comparatively, amine modification is widely used to afford porous solid materials capable of absorbing low-concentration CO_2, particularly in direct air capture of CO_2 (~ 400 ppm).[6–9] Notably, besides the amine-based moieties, ionic liquids (ILs) are another promising candidate to functionalize the porous scaffolds towards enhanced CO_2 chemisorption considering their unique features of good thermal stability, negligible vapor pressure, structure diversity, and corresponding large tuning space in their physiochemical properties towards specific CO_2 sources.[10–11] In this aspect, the CO_2 chemisorption behavior, reaction pathways, and property variation of amino-functionalized ILs (AILs) [12–13] and superbase-derived ILs [14–15] have been extensively studied in the form of liquid sorbents. In addition, the utilization of selected ILs to modify the as-prepared nanoporous materials towards enhanced CO2 physi- and chemisorption was also explored, which could combine the advantages of these two categories of sorbents depending on the chemical/textural properties of the nanoporous supports and the ILs, as well as the modification methodology. For example, deploying mesoporous SBA-15 with different pore lengths as the scaffolds, systematic studies have been conducted to investigate the CO_2 sorption behavior of the hybrid materials after coating with basic SILs. [16] Using IL 1-butyl-3-methylimidazolium acetate for the modification, a hybrid material composed of carbon fiber with a microporous structure and IL has been prepared. The CO_2 capture behavior of those materials has been studied via a thermogravimetric method, and parameters including surface area and loading mass ratio were investigated, in which enhanced CO_2 capture was achieved, benefiting from the synergy between the IL and the support, together with promising cycling stability.[17]

2.3 Results and Discussion

Herein, a carbon fiber precursor was deployed as the support, which was composed of only ultra-micropores at around 0.45 nm. Correspondingly, ILs composed of a relatively big phosphonium cation and basic/neutral anion were introduced on the surface to form a thin coating layer without penetrating the pores. The CO_2 sorption behavior of the fiber

precursor, the pure ILs, and the IL-coated fibers was evaluated by the volumetric method and thermogravimetric analysis. Enhanced CO_2 uptake capacity from a low-pressure region to atmospheric CO_2 pressure and improved CO_2 sorption kinetics were achieved by forming a thin layer of IL coating on the fiber surface, particularly the ILs containing strong interaction sites with CO_2. The as-calculated energy distribution curves matched well with the reported CO_2 reaction enthalpy values. The methods and obtained results in this work demonstrated the promising function of ILs in modifying the properties of porous scaffolds towards enhanced carbon capture, particularly for low concentration CO_2 sorption, such as in direct air capture. It is demonstrated that for the post-modification of porous materials by anchoring organic moieties, diminished surface areas and pore sizes are observed, which makes it difficult to separate the influence of porosity and functionality on the carbon capture behavior. In the case of IL modification, it is preferred if the pore blocking could be avoided by the molecular sieve effect, that is, deploying ILs with a size larger than the pores of the carbon materials and providing insights on the sole influence of IL modification. As a preliminary test, carbon fiber was prepared using high softening point coal tar pitch as the precursor at a thermal treatment temperature of 600°C, and the product was denoted as fiber600 and used as the support to coat ILs layer for the carbon capture study (**Figure 2.1A**). The textural structure of fiber600 was first analyzed by N_2 (kinetic diameter of 3.64 Å) adsorption/desorption isotherms being collected at 77 K, but the results demonstrated that there were no pores existing in the scaffolds. Comparatively, when CO_2 molecules with a smaller kinetic diameter (3.30 Å) were deployed as the probe molecules, the CO_2 adsorption/desorption isotherms collected at 195 K showed significantly increased CO_2 uptake capacity, indicating the presence of narrowly distributed ultra-micropores within the scaffolds. The Brunauer–Emmett–Teller (BET) surface area and Langmuir surface area were calculated to be 164 and 246 m^2g^{-1}, respectively (**Figure 2.1B**), together with a total pore volume of 0.10 $cm^3\,g^{-1}$.

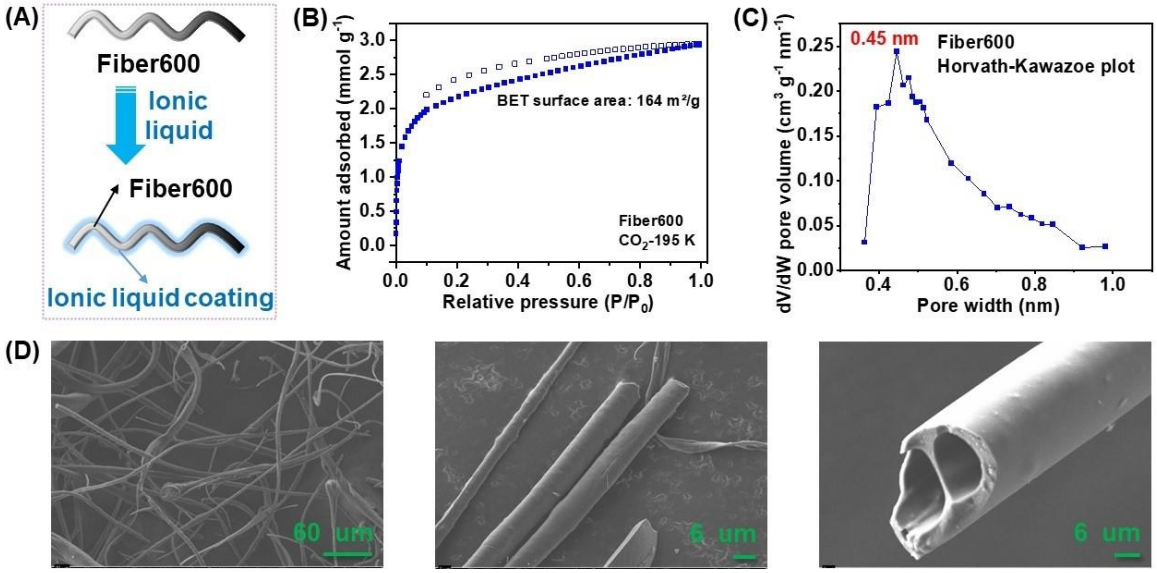

Figure 2.1(A) Schematic illustration of the surface modification of carbon fiber by ionic liquids. (B) CO_2 adsorption/desorption isotherms of fiber600 being collected at 195 K. (C) Pore size distribution curve of fiber600 being calculated using the Horvath-Kawazoe method. (D) SEM images of fiber600 being used in this work with different magnification scales.

Scanning electron microscope (SEM) images of fiber600 displayed the fiber morphology with a smooth surface, an outer diameter ranging from 5 to 20 μm, and a hollow structure (**Figure 2.1D**). Two ILs were selected to modify the fiber surface, including trihexyl(tetradecyl)phosphonium bis(trifluoromethylsulfonyl) imide ($[P_{66614}][NTf_2]$) and trihexyl(tetradecyl)phosphonium 1,2,4-triazolate ($[P_{66614}][Triz]$) (**Figure 2.2A**). The former is a widely used IL in CO_2 physisorption, and the latter was a SIL for CO_2 chemisorption being developed by our group, which had a CO_2 uptake capacity of 0.95 mol mol^{-1} and CO_2 reaction enthalpy of -56.4 kJ mol^{-1}.[15] Taking advantage of diverse spectroscopy and characterization methods, as well as the combined theoretical modeling, the transition between physisorption and chemisorption of CO_2 by a series of triazolate-derived SILs has been demonstrated, during which physisorption dominated the initial process and chemisorption was the major contribution in the later process.[18] Notably, the big size of the cations and strong electrostatic interaction between the cations/anions in these ILs could avoid the penetration of the ILs into the pores of the fiber600 and block the pores (**Figure 2.2B and Figure 2.3**).

Notably, the ILs had high thermal stability. For example, the thermogravimetric analysis (TGA) result of $[P_{66614}][Triz]$ under nitrogen atmosphere with a ramping rate of 1 °C min^{-1} exhibited an onset decomposition temperature of 297 °C, much higher than that of the amine-containing species. The high thermal stability of ILs, together with the good electrical conductivity, also brings opportunities to deploy the IL-modified carbon materials in the electric swing-involved carbon capture procedures. [16] The IL coating was performed by homogeneously dispersing the fiber600 in a methanol solution of the IL for 24 h, with a total IL amount of 5 wt% relative to the fiber600 being added, and then the solvent was completely removed by evaporation and drying procedure. The residual fiber600-IL materials were collected for further carbon capture evaluation. SEM image of fiber600-$[P_{66614}][Triz]$ and the corresponding elemental mapping results displayed a homogenous distribution of the thin IL layer on the surface of the fibers (**Figures 2.4 and 2.5**). Then, the carbon capture behavior was evaluated by a volumetric method with the CO_2 pressure up to 1 bar.

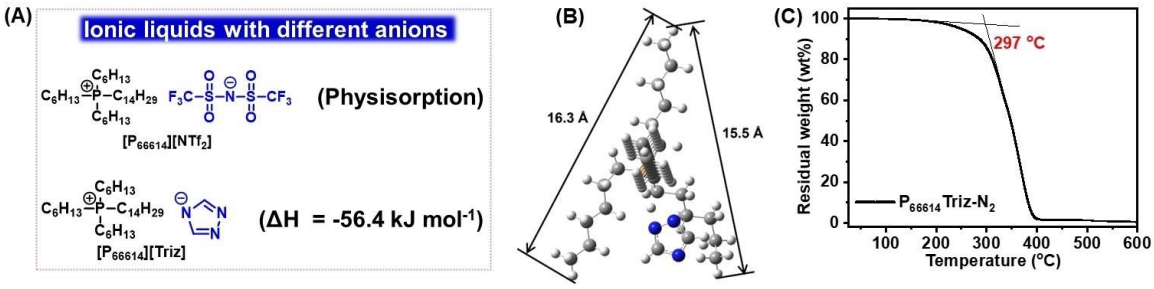

Figure 2.2 (A) Structures of the ionic liquids being used in this work. (B) Optimized structure of [P_{66614}][Triz] ionic liquid and the corresponding dimension sizes. (C) TGA result of [P_{66614}][Triz] being obtained under nitrogen atmosphere with a ramping rate of 1 °C min^{-1} from 25 to 600 °C.

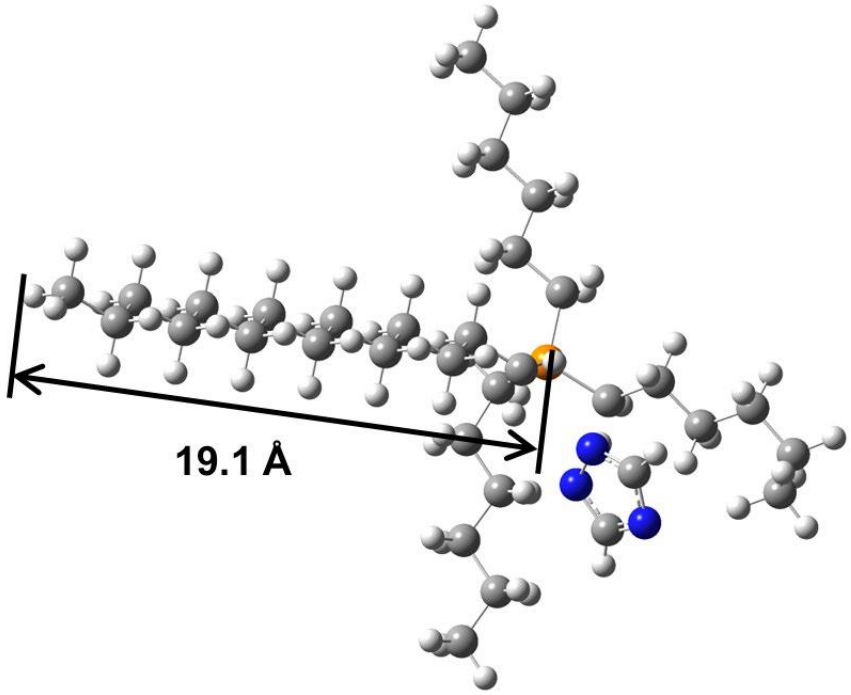

Figure 2.3 Optimized structure of [P_{66614}][Triz] ionic liquid and the corresponding dimension sizes.

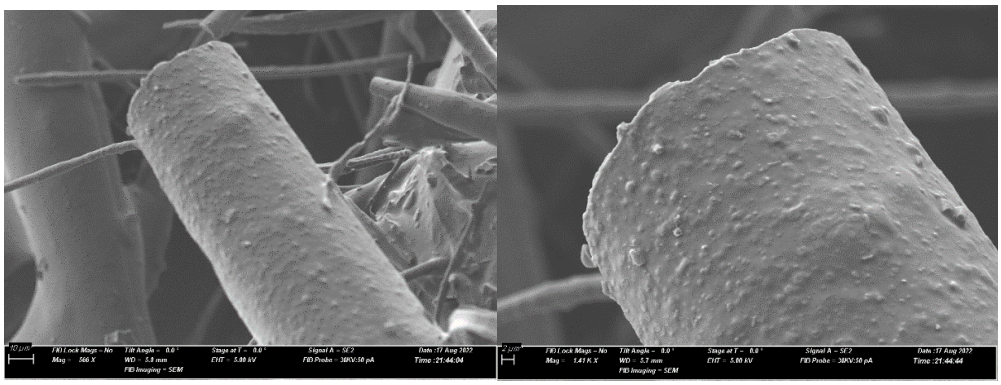

Figure 2.4 SEM images of the [P_{66614}][Triz]-coated fiber600

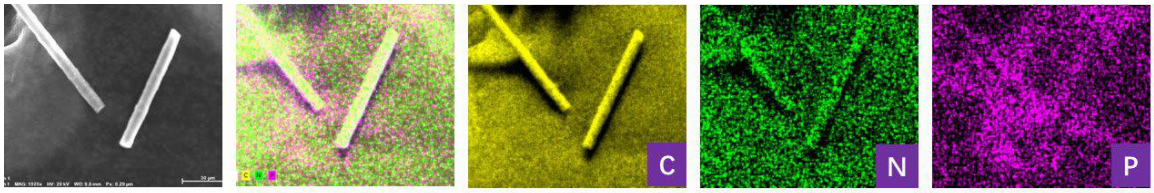

Figure 2.5 Elemental mapping of the [P_{66614}][Triz]-coated fiber600

The CO_2 uptake isotherms of the following three samples were collected at 273 and 298 K for comparison: the fiber600 precursor, fiber600-coated by 5 wt% $[P_{66614}][Triz]$, and physical mixture of fiber600 and 5 wt% $[P_{66614}][Triz]$ without the coating procedure by adding determined amount of fiber600 and $[P_{66614}][Triz]$ successively into the testing tube (as separate phase) (**Figure 2.3A and 2.3B**). At 298 K, a CO_2 uptake capacity of 0.85 mmol g^{-1} was achieved by fiber600 at 1 bar CO_2 pressure. Comparatively, the CO_2 uptake capacity increased to 0.87 mmol g^{-1} for fiber600-coated by 5 wt% $[P_{66614}][Triz]$, and the CO_2 sorption enhancement induced by $[P_{66614}][Triz]$ was more prominent in the low CO_2 pressure region. Notably, the CO_2 uptake isotherms of the pure$[P_{66614}][Triz]$ IL being collected by the volumetric method exhibited an unsmooth increasing trend, probably owing to the relatively high viscosity and the nonporous nature of the dense liquid phase, leading to sluggish CO_2 sorption kinetics, particularly at 273 K (**Figure 2.6A**). The CO_2 uptake capacity of the fiber600 coated by 5 wt% $[P_{66614}][Triz]$ surpassed not only that obtained by fiber600 but also that obtained by the pure IL$[P_{66614}][Triz]$ at the low-pressure region (<0.65 bar) (**Figure 2.6B**). This was probably caused by the formation of a thin IL layer on the surface of the fiber, which possessed improved CO_2 sorption kinetics. A control experiment was conducted using a physical mixture of fiber600 and 5 wt% $[P_{66614}][Triz]$ without the coating procedure, in which the two parts stayed separately in the testing tube, and inferior CO_2 sorption in the whole pressure region up to 1 bar was observed, indicating the critical role of the thin IL layer formation towards enhanced CO_2 uptake. Notably, the enhancement of CO_2 sorption by forming a thin layer of $[P_{66614}][Triz]$ on fiber600 was also demonstrated by the CO_2 uptake isotherms being collected at 273 K (**Figure 2.7B**), with the CO_2 uptake capacity, increased in the order of: a physical mixture of fiber600 + IL < fiber600 < fiber600-coated by IL. The recyclability of the material composed of fiber600 coated by 5 wt% $[P_{66614}][Triz]$ was evaluated for five cycles (**Figure 2.8**). CO_2 desorption was performed at 60 °C under vacuum for 12 h, and then the CO_2 isotherm of the material was collected at 298 K with CO_2 pressure up to 1 bar. The result displayed well-maintained CO_2 uptake capacity over the five runs, illustrating the promising stability of the SIL coating on

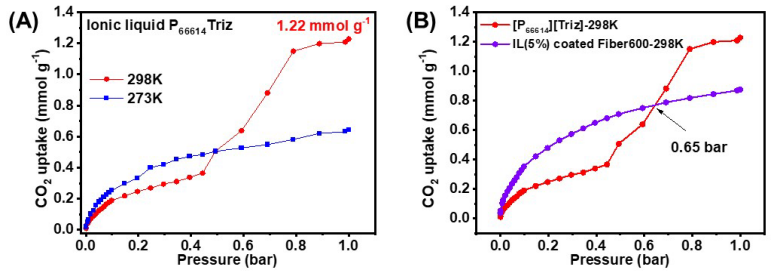

Figure 2.6 (A) CO_2 uptake isotherms of the pure $[P_{66614}][Triz]$ ionic liquid being collected at 273 and 298 K. (B) Comparison of the CO_2 isotherms of pure IL $[P_{66614}][Triz]$ and IL(5%)-coated fiber600.

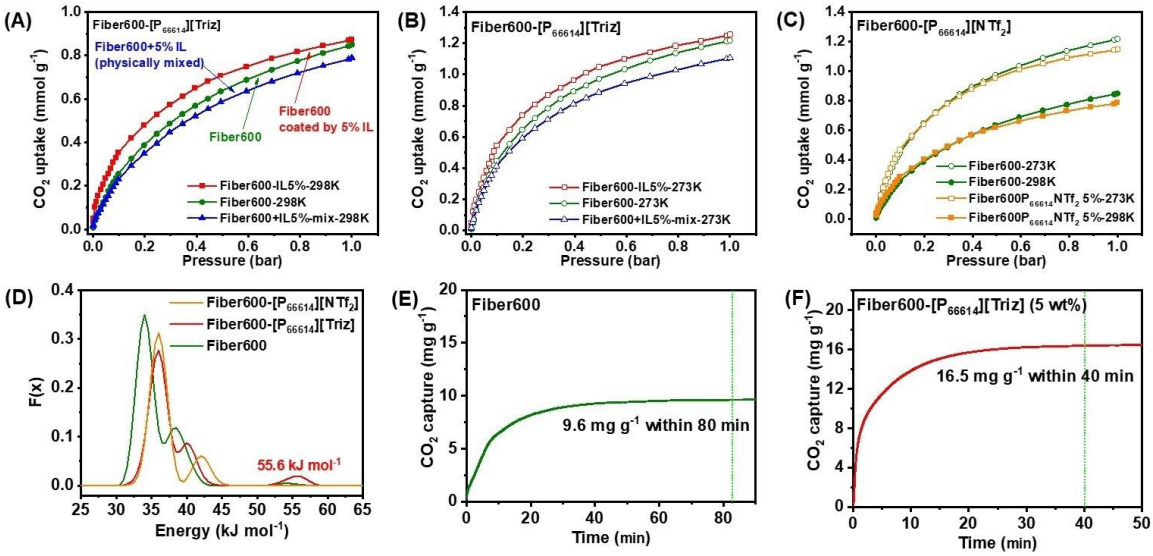

Figure 2.7 (A) CO_2 uptake isotherms of the fiber600, fiber600 modified by 5 wt% $[P_{66614}][Triz]$ via surface coating, and physical mixture of fiber600 and 5 wt% $[P_{66614}][Triz]$ and (B) 273 K. (C) fiber600 and fiber600 modified by 5 wt% $[P_{66614}][NTf_2]$ via surface coating at 298 K and 273 K. (D) The adsorption energy distribution calculated for adsorption of CO_2 (E) The CO_2 uptake capacity is being measured by the TGA method under a CO_2 atmosphere with a flow rate of 90 mL min^{-1} at 298 K.

fiber600. The fiber600-coated by 5 wt% $[P_{66614}][NTf_2]$ was further prepared using a similar coating procedure for comparison and illustration of the critical role of CO_2 reactive sites (triazolate anion in [P66614][Triz]) (**Figure 3C**). As shown by the CO_2 uptake isotherms of fiber600 and fiber600-coated by 5 wt%$[P_{66614}][NTf_2]$ at 273 and 298 K, inferior CO_2 uptake behavior, particularly at relatively high CO_2 pressure region, was demonstrated, indicating that without the CO_2 reactive sites within the IL structure, the IL coating cannot concentrate, trap, and transfer the CO_2 molecules within the pores of the fiber architecture. The adsorption energy distribution curves between CO_2 and different fiber materials were calculated using the CAESAR(computed adsorption energies, singular value decomposition(SVD) analysis result) algorithm based on the CO_2 uptake isotherms (298 K) via MatLab (**Figure 2.3D**).[13-14] The fiber600 precursor displayed a major peak at the adsorption energy of 34.0 kJ mol^{-1} and a minor one located at 38.4 kJ mol^{-1}, corresponding to the physisorption of CO_2. Comparatively, both peaks shifted to higher values in fiber600-coated by$[P_{66614}][NTf_2]$, 36.0 and 42.0 kJ mol^{-1}, respectively. Notably, the enhanced CO_2 sorption in fiber600-coated by $[P_{66614}]$[Triz] was well illustrated by the presence of two physisorption energy distribution peaks at 36.0 and 40.3 kJ mol^{-1}, together with one additional peak in the chemisorption region of 55.6 kJ mol^{-1},which was close to the reaction enthalpy from theoretical calculation. To further demonstrate the influence of basic IL coating. The SIL, trihexyl(tetradecyl)phosphonium imidazolate ($[P_{66614}]$[Im]), which had higher interaction strength with CO_2 via N-C bond formation (reaction enthalpy of -89.9 kJ mol^{-1})[15] was deployed to modify the surface of fiber600 via a similar coating procedure (**Figure 2.9A**). CO_2 isotherm of the as-prepared fiber600-coated by 5 wt%$[P_{66614}]$[Im] was collected at 298 K (**Figure 2.9B**), which was then used to calculate the energy distribution curves. The result exhibited the major peak with CO_2 adsorption energy of 35.4 kJ mol^{-1}, and an additional small peak at 95.8 kJ mol^{-1}, which was close to the as-calculated CO_2 reaction enthalpy related to the imidazolate anion (**Figure 2.9C and Figure 2.10**). This guides how to determine the distribution and ratio of adsorption and absorption sites possessing different interaction energies with CO_2 within

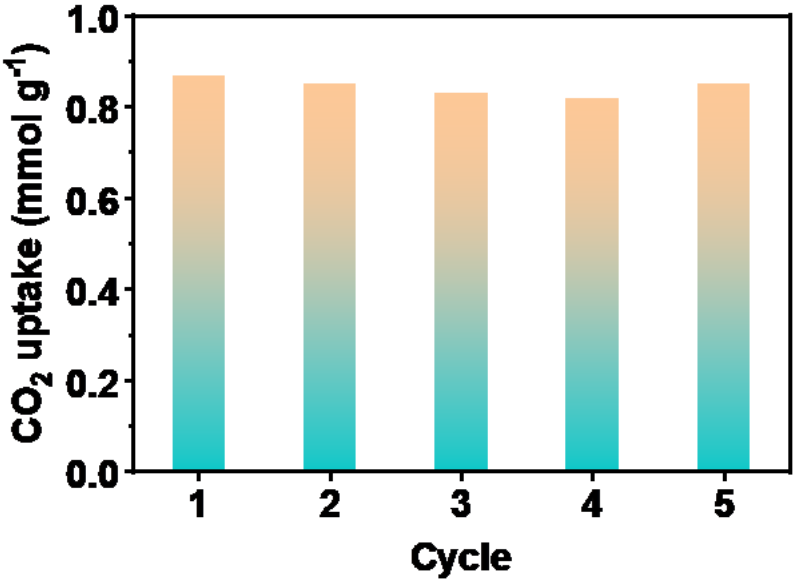

Figure 2.8 Recyclability of the material composed of fiber600 coated by 5 wt% $[P_{66614}][Triz]$. CO_2 desorption was performed at 60 °C under vacuum for 12 h, and The CO_2 isotherm of the material was collected at 298 K with CO_2 pressure up to 1 bar

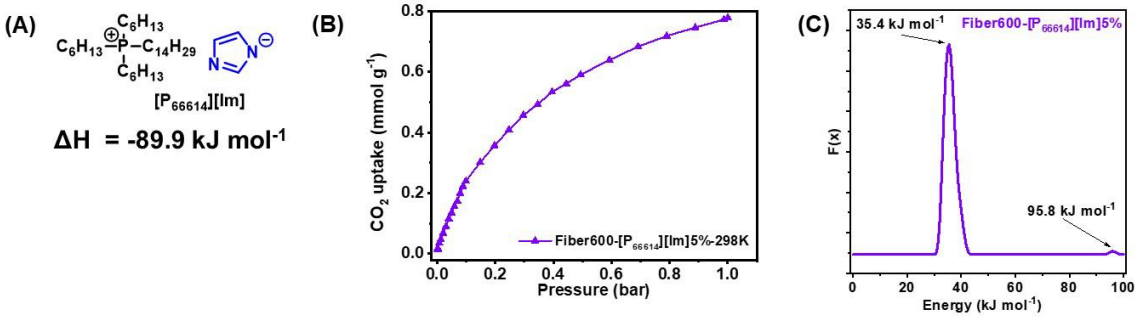

Figure 2.9 (A) Structure of the SIL $[P_{66614}][Im]$ and the CO_2 reaction enthalpy of imidazolate anion. (B) The CO_2 isotherm of Fiber600 coated by 5 wt% $[P_{66614}][Im]$ being collected at 298 K. (C) The adsorption energy distribution calculated for adsorption of CO_2 on Fiber600 coated by 5 wt% $[P_{66614}][Im]$.

the porous architectures, and those containing the strong chemisorption CO_2 sites have the potential to absorb low concentration CO_2. The influence of IL coating on carbon capture was further evaluated using a TGA method under CO_2 atmosphere with a flow rate of 90 mL min^{-1}. For the fiber600 precursor (**Figure 2.3E**),an absorption time of ~90 min was required to achieve CO_2 sorption equilibrium, delivering a saturated CO_2 uptake of 9.6 mg g^{-1}. For the pure IL $[P_{66614}][Triz]$, low CO_2 uptake of only 7.3 mg g^{-1} was obtained after 350 min (not saturated) due to the relatively high viscosity and slow sorption kinetics. Comparatively, using fiber600-coated by 5 wt% [P66614][Triz] as the sorbent, the CO_2 sorption equilibrium was achieved within 40 min with much higher uptake capacity (16.5 mg g^{-1}) under the same conditions (**Figure 2.3F**). This further demonstrated the positive effect generated by surface modification of fiber600 by a thin SILs layer with chemisorption reactive sites with CO_2, leading to improved CO_2 uptake capacity and enhanced CO_2 sorption kinetics compared with the fiber600 precursor and the pure IL phase.

2.4. Experimental

2.4.1. Synthesis of IL-Carbon Fibers

The carbon fiber was prepared by carbonization of coal tar pitches. High softening point coal tar pitch was melt-blown into fibers using a horizontal extruder and a single-hole die connected to heated air. The last zone of the extruder was at 300°C, and the hot air was at 330 °C. The airflow rate was 40 SCFH. Fibers were oxidized-stabilized in a forced air oven, ramping at 0.25 °C/min to 225°C, with a 5-hour hold. The mass gain after oxidation-stabilization was 2.9 wt%. Fibers were then carbonized in a horizontal tube furnace to 600 °C in nitrogen, ramping at 10°C/min with a 30-minute hold. The overall carbon yield was 86% for carbon fibers prepared at 600°C. The fiber600 precursor obtained after carbonization was dispersed in the solution of various ILs in methanol. First, 5 mL of methanol was mixed with the corresponding amount of IL (5 wt% based on the weight of fiber600). Then, 100 mg of fiber 600 was added to the above solution. The suspension was sonicated for 30 min and allowed to stand. After 24 h, the solvent was removed by vacuum heating at 60°C for over 12 h.

2.4.2. Instrumentation and Characterization

CO_2 Uptake Measurement using Thermogravimetric Analysis

The CO_2 uptake capacity of the IL-coated fiber600 compared to the fiber600 precursor and neat ionic liquids was assessed using a thermogravimetric analyzer (TGA) (STA300, Thermal Analysis System, Hitachi).To remove the trapped moisture and impurities, a crucible containing ~10 mg of sample was heated to 60°C and held therefor 70 min under a nitrogen atmosphere. The CO_2 capture measurement was performed using a 90 mL/min CO_2 gas flow rate until no weight variation was observed.

CO_2 Uptake measurement using the volumetric method

The CO_2 uptake isotherms were collected using a Gemini VII (Micromeritics)instrument. Before the measurement, the fiber600, the IL-modified fiber600 samples were pre-treated at 150°C for 16 h under a nitrogen atmosphere. For the CO_2 isotherms of the physical mixture, the corresponding IL and the fiber600 were added into the sample tubes successively without the pre-modification procedure. The isotherms were collected at 273 K (ice-water bath) and 298 K (water bath), respectively, with the CO_2 pressure gradually increasing up to 1 bar.

Adsorption Energy Distribution Calculated for Adsorption of CO_2

To calculate the adsorption energy distributions for the three samples of carbon fiber600, and carbon fiber600 modified by [P_{66614}][Triz] and [P_{66614}][NTf_2] ionic liquid, we used MatLab® software for the local CO_2 adsorption isotherms collected at 298 K using the CAESAR(Computed Adsorption Energies, SVD Analysis Result) algorithm. The heats of adsorption were initially obtained by fitting the individual CO_2 adsorption isotherms acquired at 0 °C and 25 °C to the Toth model.

$$q = \frac{q_{sat} bP}{(1 + (bP)^t)^{\frac{1}{t}}}$$

where qsat is the capacity at saturation at pressure, P, and b is the affinity parameter, and when t is at unity. Though other models like Freundlich, Langmuir, and Sips were also used to fit the isotherms, the Toth model provided the best fit to the experimental data.

Results from the Toth model fitting were then incorporated into the Clausius–Clapeyron equation to calculate the isosteric heats of adsorption (ΔH). The isosteric heat can be found at constant loading by plotting lnP vs. (1/T) at a range of temperatures, where the slope represents the isosteric heat and the intercept is a constant. Using two temperatures, the Clausius–Clapeyron equation can be rearranged to yield:

$$ln\left(\frac{P_1}{P_2}\right) = \Delta H_{ads} \times \frac{T_2 - T_1}{R \times T_1 \times T_2}$$

where P1 and P2 are the pressures from the corresponding isotherms with temperatures T1 and T2, respectively, R=8.315 J·K-1 mol-1. Due to instrument limitations, it is necessary to fit adsorption isotherms to obtain accurate pressures at the specified loading.

2.5. Conclusions

To further extend the application of carbon materials in carbon capture and to enhance their performance, a surface modification methodology was developed in this work. By deploying a fiber precursor with only ultra-micropores to avoid the influence of pore occupation and forming a thin layer of IL coating on the surface of fiber materials, the enhancement of introducing strong CO_2 reactive sites was demonstrated by the volumetric and TGA-based CO_2 sorption procedure. The calculated energy distribution curves were consistent with the theoretically calculated reaction enthalpy between CO_2 and the SILs. The achievements in this work provide guidance and opportunities to extend the application of carbon-based materials in carbon capture with low CO_2 concentrations, such as direct air capture.

References

[1] H. Wang, Y. Shao, S. Mei, Y. Lu, M. Zhang, J.-k. Sun, K. Matyjaszewski, M. Antonietti, J. Yuan, Chem. Rev. 2020, 120, 9363–9419.

[2] J. Wang, S. Kaskel, J. Mater. Chem. 2012, 22, 23710–23725.

[3] P. Zhang, J. Zhang, S. Dai, Chem. Eur. J. 2017, 23, 1986–1998.

[4] P. Zhang, L. Wang, S. Yang, J. A. Schott, X. Liu, S. M. Mahurin, C. Huang, Y. Zhang, P. F. Fulvio, M. F. Chisholm, S. Dai, Nat. Commun. 2017, 8, 15020.

[5] N. P. Wickramaratne, M. Jaroniec, J. Mater. Chem. A 2013, 1, 112–116.

[6] H. Lyu, H. Li, N. Hanikel, K. Wang, O. M. Yaghi, J. Am. Chem. Soc. 2022, 144, 12989–12995.

[7] T. M. McDonald, J. A. Mason, X. Kong, E. D. Bloch, D. Gygi, A. Dani, V. Crocellà, F. Giordanino, S. O. Odoh, W. S. Drisdell, B. Vlaisavljevich, A. L. Dzubak, R. Poloni, S. K. Schnell, N. Planas, K. Lee, T. Pascal, L. F. Wan, D. Prendergast, J. B. Neaton, B. Smit, J. B. Kortright, L. Gagliardi, S. Bordiga, J. A. Reimer, J. R. Long, Nature 2015, 519, 303–308.

[8] X. Shi, H. Xiao, H. Azarabadi, J. Song, X. Wu, X. Chen, K. S. Lackner, Angew. Chem. Int. Ed. 2020, 59, 6984–7006; Angew. Chem. 2020, 132, 7048–7072.

[9] E. J. Kim, R. L. Siegelman, H. Z. H. Jiang, A. C. Forse, J.-H. Lee, J. D. Martell, P. J. Milner, J. M. Falkowski, J. B. Neaton, J. A. Reimer, S. C. Weston, J. R. Long, Science 2020, 369, 392–396.

[10] S. Zeng, X. Zhang, L. Bai, X. Zhang, H. Wang, J. Wang, D. Bao, M. Li, X. Liu, S. Zhang, Chem. Rev. 2017, 117, 9625–9673.

[11] G. Cui, J. Wang, S. Zhang, Chem. Soc. Rev. 2016, 45, 4307–4339.

[12] E. D. Bates, R. D. Mayton, I. Ntai, J. H. Davis, J. Am. Chem. Soc. 2002, 124, 926–927.

[13] B. E. Gurkan, J. C. de la Fuente, E. M. Mindrup, L. E. Ficke, B. F. Goodrich, E. A. Price, W. F. Schneider, J. F. Brennecke, J. Am. Chem. Soc. 2010, 132,

2116–2117.
[14] C. Wang, H. Luo, D.-e. Jiang, H. Li, S. Dai, Angew. Chem. Int. Ed. 2010, 49, 5978–5981; Angew. Chem. 2010, 122, 6114–6117.
[15] C. Wang, X. Luo, H. Luo, D.-e. Jiang, H. Li, S. Dai, Angew. Chem. Int. Ed. 2011, 50, 4918–4922; Angew. Chem. 2011, 123, 5020–5024.
[16] J. Cheng, Y. Li, L. Hu, J. Liu, J. Zhou, K. Cen, Fuel Process. Technol. 2018, 172, 216–224.
[17] E. D. Isaacs-Páez, A. J. García-Pérez, C. Nieto-Delgado, L. F. Chazaro-Ruiz, J. R. Rangel-Mendez, J. Mol. Liq. 2022, 350.
[18] X. Hu, X. Yang, L. Chen, M. Mei, Z. Song, Z. Fei, P. J. Dyson, Z. Qi, Chem. Eng. J. 2022, 435.
[19] R. P. P. L. Ribeiro, C. A. Grande, A. E. Rodrigues, Sep. Sci. Technol. 2014, 49, 1985–2002.
[20] K. M. Nelson, S. M. Mahurin, R. T. Mayes, B. Williamson, C. M. Teague, A. J. Binder, L. Baggetto, G. M. Veith, S. Dai, Microporous Mesoporous Mater. 2016, 222, 94–103.
[21] P. J. Dauenhauer, O. A. Abdelrahman, ACS Cent. Sci. 2018, 4, 1235–1243.

CHAPTER 3 : THE POROSITY EFFECT OF SUPERBASE IONIC LIQUID-MODIFIED CARBON SORBENTS IN DAC

A version of this chapter was originally published in *Materials Today Energy* Journal:

Mokhtari-Nori, Narges, Liqi Qiu, Yanpei Song, Lilin He, Arvind Ganesan, Alexander S. Ivanov, Qingju Wang, Tao Wang, Zhenzhen Yang, and Sheng Dai. "Unveiling the porosity effect of superbase ionic liquid-modified carbon sorbents in CO2 capture from air." *Materials Today Energy* 45 (2024): 101693.

3.1. Abstract

Direct air capture (DAC) of CO_2 represents one of the most promising technologies to achieve negative carbon emissions. Herein, the superbase ionic liquids (ILs)-modified carbon substrates were developed towards DAC of CO_2 by harnessing the strong CO_2 binding capability of IL and the ordered porous channels provided by the carbon supports. Detailed porosity analysis revealed that the IL with aromatic cation and oxygenate anion preferred to fill the micropores, and a thin layer was created on the surface of the mesopores. Strong π-π interaction between the IL layer and the carbon surface was disclosed by wide-angle X-ray scattering (WAXS) analysis, leading to enhanced thermal stability of the IL phase. With the same lL coating amount, the DAC of CO_2 evaluation revealed that larger mesopore size and pore volume in the carbon/IL composite materials led to higher CO_2 uptake capacity by exposing more active sites to integrate CO_2 from diluted sources. The thermodynamic analysis confirmed the critical role of IL coating in providing strong chemisorption sites and significantly improved selectivity to enrich the diluted CO_2 from the air atmosphere. This work provides guidance on leveraging the scaffolds' surface properties and porosities of the scaffolds to tune the DAC of CO_2 behavior.

3.2. Introduction

Carbon dioxide (CO_2) is a major factor driving global climate change.[1, 2] Fossil fuels are the primary source of energy across the world, resulting in an annual release of nearly 40 Gt of CO_2 from these sources.[3, 4] To alleviate the environmental impact of CO_2 emissions, techniques of carbon capture and sequestration (CCS) are highly desired, including carbon mineralization, coastal blue carbon, terrestrial and geological

sequestration, bioenergy CCS, and direct air capture (DAC).[5-8] Particularly, DAC systems are designed to capture CO_2 from any sources at ultra-low CO_2 concentrations (~400 ppm), and it has been recognized as the most promising "negative carbon emission" approach, with no requirements on hectares of arable lands or to be located close to a coastal zone. Subsequently, the captured CO_2 is then released and stored through temperature or pressure swing procedures or integrated with the catalytic CO_2 transformation to produce value-added chemicals.[5, 6, 9-13]

The current DAC technologies mainly rely on sorbents with strong interaction with CO_2.[1, 4] The inorganic base-derived sorbents composed of aqueous alkali metal hydroxide such as KOH, NaOH, etc., or alkali metal oxide such as CaO have high CO_2 uptake capacity but with inferior features of high corrosivity and energy-intensive sorbent regeneration (> 250 °C).[10] The amine-derived sorbents, either aqueous solutions, solvent-lean amines, or amine-modified porous scaffolds, have exhibited diminished energy input for CO_2 releasing (about 120 °C),[12, 14] which still faced unsolved issues such as volatility, thermal/oxidative degradation, and performance fading caused by water accumulation-induced pore blocking.[15-17] Alternatively, ionic liquids (ILs)-derived sorbents have been developed, which can take advantage of the merits of ILs and porous scaffolds and provide alternative approaches to provide sorbents with improved durability and less energy input for regeneration. Compared to the amine moieties, ILs have nonvolatility and improved thermal/chemical stability.[18-20] In addition, their physical/chemical properties can be tuned by the structure of the cations and anions, leading to variable wettability, hydrophobicity, and interaction strength with CO_2.[21-24] Adaptability plays a critical role in providing high-quality IL-modified porous organic scaffolds when different substrates are deployed. Not only the structures of ILs but also the properties of supports can be harnessed to enhance the DAC performance of the sorbents. For example, by introducing a CaO thin layer on the surface of mesoporous silica and further coating superbase-derived ILs (ILs), the as-derived sorbents performed well in DAC of CO_2 in terms of high uptake capacity, easy CO_2 releasing, and good long-term durability.[25] The Ni-based metal-organic framework (Ni-MOF) could provide a

confinement effect over the as-introduced IL sites to facilitate diluted CO_2 sorption.[26] The stability of the ionic pairs can be further improved by covalently attached to the porous scaffolds towards DAC of CO_2 application.[27]

Porous carbons are the most extensively examined adsorbents in carbon capture, mainly via physisorption, which have demonstrated unique features of high surface area (over 4000 $m^2 g^{-1}$), tunable porosity ranging from micro- to mesopores, high thermal stability, and versatile surface modification.[28-31] Therefore, carbon-based scaffolds are promising supports to maximize the performance of IL in DAC of CO_2, offering exceptional accessibility, improved mass transfer, and enhanced diffusion capabilities.[28, 32] Besides, the surface properties of the carbon substrates can be modified via bottom-up synthesis control or post-treatment procedures (e.g., heteroatoms doping), leading to controllable wettability to accommodate the IL coating and the interaction between the IL and the carbon surface could be leveraged to affect the CO_2 insertion behavior. In addition, carbon substrates with ordered and regular porosity were preferred to allow uniform distribution and spreading of the coating layers involving strong CO_2 binding sites and build up the porosity-performance relationship. A fundamental understanding of these factors could help build the structure-performance relationship and guide the sorbent's design.[33]

In this work, the IL-modified carbon sorbents were developed towards the DAC of CO_2 application. Two carbon substrates with various surface areas (543 and 1895 $m^2 g^{-1}$) and porosities were deployed as the supports to study the porosity effect on CO_2 sorption after IL modification. Detailed porosity analysis revealed that the coated IL preferred filling the micropores and forming a thin layer on the mesopore surface. The mesoporous structures are still well maintained after IL modification, providing the channels for CO_2 penetration and interaction with the oxygenate sites in the IL layer. The breakthrough test using 400 ppm CO_2 in He as the feeding gas derived the CO_2 adsorption capacity up to 0.65 mmol g^{-1}, which can be tuned via the porosity of sorbents and the loading amount of IL. Strong π-π interaction between the carbon substrates and the IL phase was demonstrated by x-ray- and neutron-based analysis, leading to improved stability of the

IL. In addition, the thermodynamic study indicated that the interaction between the IL and the surface of the carbon substrates with π-conjugated structures could be harnessed to tune the reaction enthalpy for CO_2 insertion. The accomplishments of this study demonstrated the promising performance of ionic pair-modified sorbents in DAC of CO_2 by harnessing the hybridization of IL to afford strong CO_2 binding sites and carbon substrates to facilitate mass transport.

3.3. Experimental

3.3.1. Synthesis of Porous Carbon Materials

Ordered mesoporous carbon (OMC) materials (**Figure 3.1**) are fabricated through the carbonization of nano-polymeric composites. These composites are formed through the self-assembly of Pluronic F127 copolymer and phloroglucinol-formaldehyde resin in an acidic moiety using the soft-template procedure. As a typical procedure, a round-bottom flask was charged with 13.0 g of phloroglucinol, 26.2 g of F127, and 5.0 g of HCl (37 wt% aqueous) in 500 mL of ethanol for a conventional synthesis. Reflux was achieved by heating the mixture while stirring. This solution received 13.0 g of formaldehyde (37 wt% aqueous). Precipitates began to form several minutes after formaldehyde was added, suggesting the development of composite materials made of F127 and phenolic resin. The polymer particles were filtered and cleaned with ethanol before being dried in a 120°C oven for three hours. The polymer particles were heated to 850 °C with a heating rate of 2 °C min^{-1}, resulting in carbonization and sustained at this temperature for 2 h under flowing N_2.[28, 34]

To achieve a higher surface area, the OMC materials are activated by potassium hydroxide (KOH) to afford OMC-A products. This activation process involves heating the mixture of KOH and the prepared OMC particles (8:1 ratio) in a horizontal furnace with the flow of nitrogen gas at 800 °C for 1 h with a heating rate of 20 °C min^{-1}. The sample was subsequently leached in 500 mL of a 0.2 M HCl solution. The mixture was heated to 80 °C while being stirred for 30 min to completely remove the residual base, then rinsed and leached again in water until the pH of the liquid phase became neutral.

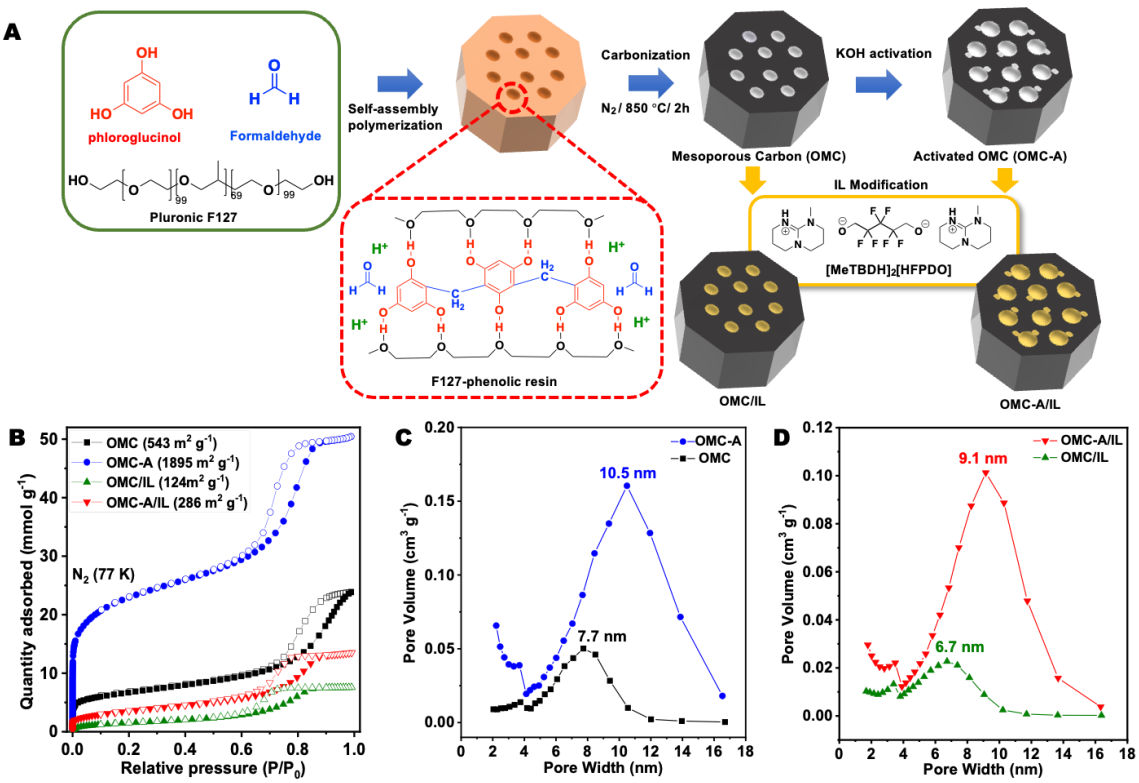

Figure 3.1 (A) Synthesis procedure of the OMC and OMC-A support used in this work, as well as the structure of the adopted IL. (B) N_2 adsorption and desorption isotherms of OMC, OMC-A, OMC/IL, and OMC-A/IL were collected at 77 K. (C) Pore size distribution curves of OMC and OMC-A being calculated using BJH method. (D) Pore size distribution curves of OMC/IL and OMC-A/IL were calculated using BJH method

3.3.2. Synthesis of SIL [MeTBDH]2[HFPDO]

In a typical synthesis, 7-Methyl-1,5,7-triazabicyclo[4.4.0]dec-5-ene (MeTBD) (5 mmol) and 2,2,3,3,4,4-hexafluoro-1,5-pentanediol (HFPDOH) (2.5 mmol) were introduced to acetonitrile (5 mL). Then, the solution was vigorously stirred at room temperature under N_2 atmosphere for 12 h, which can generate $[MeTBDH]_2[HFPDO]$ after removing the solvent by rotary evaporation. $[MeTBDH]_2[HFPDO]$ IL was further dried under vacuum at 65 °C for 12 h.

3.3.3. Synthesis of IL-modified carbon sorbents

In a typical procedure, OMC or OMC-A (100 mg) was added into the acetonitrile (10 mL) solution of a determined amount of IL $[MeTBDH]_2[HFPDO]$, which was stirred at room temperature under N_2 atmosphere for 12 h. Then, the solvent was evaporated by rotary evaporation to generate the OMC-A/IL-x (x = 10-50 wt%) composites, which were further dried under vacuum at 65 °C for 24 h to form a dry powder.

The $Na_2[HFPDO]$-modified OMC-A was synthesized through introducing hexafluoro-1,5-pentanediol (HFPDOH) (1.1 mmol) to 1g of OMC-A in acetonitrile (10 mL) under N_2 gas flow. After 12h, Sodium hydride (2.2 mmol) was added to the solution to deprotonate HFPDOH and make the $Na_2[HFPDO]$ salt in situ supported on the OMC-A. Subsequently, the solvent was removed by rotary evaporation and the product denoted as OMC-A/$Na_2[HFPDO]$.

3.4. Instrumentation and Characterization

The N_2 adsorption/desorption isotherms were measured at 77 K under a 3Flex Micromeritics surface area analyzer with a cryo-station for temperature control. The samples were outgassed at 80 °C for 24 h before the measurements. Surface areas were calculated from the adsorption data using Brunauer-Emmett-Teller (BET) methods. Pore size distribution curves were calculated via the nonlocal density functional theory (NL-DFT) or Barrett-Joyner-Halenda (BJH) method. The CO_2 and N_2 uptake isotherms were evaluated at 298 K with the pressure up to 1 bar.

Field emission scanning electron microscopy (SEM) observations and elemental maps were performed on a Hitachi S-4800 microscope operated at an accelerating voltage of 15.0 kV.

Thermogravimetric analysis (TGA) measurements were taken under a nitrogen atmosphere with a ramping rate of 5 °C min^{-1} from 25 °C to 800 °C using a TGA Q50 thermogravimetric analyzer.

Wide angle X-ray scattering (WAXS) experiments were carried out in the collaborator's laboratory using a Cu anode X-ray generator (Xenocs Xeuss 3.0) equipped with a Dectris Pilatus 2D detector. The data was then radially averaged to 1D. Analysis of the scattering scans was done after careful background correction.

The small angle neutron scattering (SANS) data were collected by our collaborator at the GP-SANS instrument, HFIR at Oak Ridge National Lab. The instrument configurations were set to cover a q-range of $0.004 < q < 0.5$ $Å^{-1}$. The raw data is azimuthally averaged to get 1D curve. The scattering profiles of three samples follow a combined model with power law decay in low q regime, an interacting polydisperse sphere in middle q regime, and a correlation length model at high q regime.

$$I(q) = \frac{A}{q^n} + \frac{B}{1 + (q\xi)^m} + C + I_{inc}$$

where A, B are the prefactors, n is the exponent of the power law decay, ξ is the correlation length describing the average size of the material inhomogeneity. C is the term from interacting polydisperse spheres. For the full analytical function of interacting polydisperse sphere model, please refer to (https://www.sasview.org/docs/old_docs/3.1.2/user/models/model_functions.html#sphere model)

I_{inc} is the incoherent scattering constant.

Fixed-bed breakthrough experiment

A custom-built fixed-bed reactor was used to perform CO_2 breakthrough experiments at 298 K. A certain amount of the sample was packed into the quartz column with an inner diameter of 6 mm. After sample activation at 80 °C under a dry He flow for 3 h, the packed bed column was cooled down with a set temperature of 298 K. The inlet gas stream was then switched to 400 ppm of CO_2 (40 mL/min) gas balanced in He through a three-way valve for the CO_2 capture test. During the breakthrough experiments, the CO_2

and H_2O concentrations of the outlet gas stream were continuously measured every second by an infrared gas analyzer (LI-840/LI-COR).

Calculation of energy distribution curves based on the CO_2 isotherms collected at 298k

To calculate the adsorption energy distributions were calculated in MatLab® software using the local CO_2 adsorption isotherms collected at 298 K via the CAESAR (Computed Adsorption Energies, SVD Analysis Result) algorithm, with an established fitting procedure and program.[1, 2]

Isotherms were initially fit using the non-temperature-dependent Langmuir equation:

$$q = \frac{q_{st} bP}{1+bP} \qquad (1)$$

$$b = b_o \exp\left(\frac{Q}{RT}\right) \qquad (2)$$

where q_{sat} is the capacity at saturation at pressure, P, and b is the affinity parameter. The temperature-dependent parameter b is further expressed by the temperature-independent pre-exponential factor, b_o, and the isosteric heat of adsorption, Q. The Langmuir model assumes adsorption on a homogeneous surface, which is certainly not the case in terms of porous carbons and other porous materials. In the Sips equation, the parameter n is introduced to compensate for the heterogeneity of the surface, where greater deviation from unity indicates increased heterogeneity of adsorption sites.

$$q = \frac{q_{sat}(bP)^{1/n}}{1+(bP)^{1/n}} \qquad (3)$$

$$\frac{1}{n} = \frac{1}{n_0} + \alpha\left(1 - \frac{T_0}{T}\right) \qquad (4)$$

The temperature dependence is then taken through the b from the Langmuir equation (eqn. 2) and to obtain the sticking parameter, α, using 273 K as a reference temperature for n and T_0.

Similarly, the Toth equation for fitting adsorption isotherms presents a similar advantage over the Langmuir equation and reduces to the Langmuir equation when t is at unity.

$$q = \frac{q_{sat} bP}{(1+(bP)^t)^{1/t}} \qquad (5)$$

$$t = t_0 + \alpha\left(1 - \frac{T_0}{T}\right) \qquad (6)$$

Furthermore, the distribution functions were calculated in Matlab® using the Langmuir local isotherm to solve the integral adsorption integral equation (IAE)[3]:

$$\theta_t(p) = \int_0^\infty \theta_l(p,x) f(x) dx \qquad (7)$$

where p is pressure, x is adsorption energy, Θ(p,x) is the local adsorption isotherm and f(x) is a distribution function characterizing the heterogeneities in the adsorption energy. The solution of the adsorption integral equation using splines (SAIEUS) algorithm is meant to give a stable solution to the integral adsorption equation. In this case, the distribution function is represented as follows:

$$f(x) = \sum_{j=1}^{m} b_j \varphi_j(x) \qquad (8)$$

where b_j are coefficients to be established later and φ are cubic b (basis)-splines with equally spaced knots over the interval a to b (the range of integration). It should be noted that b-splines are piecewise polynomial functions with well-defined first and second derivatives.

3.5. Results and Discussion

In this study, two kinds of carbon support with different surface areas and pore sizes were synthesized to study their effect on the DAC procedure after IL coating. One of the ordered mesoporous carbon supports was synthesized through the carbonization of nano-polymeric composites derived from soft templating synthesis via a reported procedure (denoted as OMC).[28, 30, 31, 34] The composite was formed through the self-assembly of Pluronic F127 as a block copolymer and phenolic resin through the polymerization of phloroglucinol and formaldehyde in the presence of hydrochloric acid, utilizing the soft-template process (**Figure 3.1A**).[35, 36] During the carbonization procedure, the soft template and the heteroatoms were gradually decomposed and removed from the carbon matrix. The five- and six-membered ring structures were generated to construct the carbon skeleton. The gasification and decomposition of the low molecular weight oligomers created ordered porous channels.[37] The porosity of the as-prepared OMC was analyzed by N_2 adsorption/desorption isotherms at 77 K (**Figure 3.1B**), in which the isotherms with the feature of type IV were observed, including a clear hysteresis loop in the high-pressure region (0.7-0.9 bar). The Brunauer–Emmett–Teller (BET) [38] surface

area was calculated to be 543 m^2 g^{-1} (**Figure 3.2 and Table 3.1**).[39] The pore size distribution calculated by the Barrett-Joyner-Halenda (BJH)[39] method indicated a broad peak center at 7.7 nm (**Figure 3.1C**). The total pore volume of OMC was calculated to be 0.44 cm^3 g^{-1}, with only 0.05 cm^3 g^{-1} being attributed to micropores (**Table 3.1**). The scanning electron microscopic (SEM) image of OMC clearly showed the ordered mesoporous architecture (**Figure 3.3**). Furthermore, to examine the impact of porosity and surface area on the CO_2 capture procedure, the OMC material was subjected to potassium hydroxide (KOH) activation, which was demonstrated as an efficient approach to create micropores within the carbon scaffolds and enhance the surface area and pore volume.[35, 40] The activation process was performed by heating up the OMC/KOH mixture up to 800 °C for 1 h under nitrogen atmosphere (**Figure 3.1A**). The as-collected KOH-activated carbon material after the washing and drying procedure was denoted as OMC-A. The N_2 isotherms of OMC-A maintained type IV features, with much higher N_2 adsorption capacity at the low-pressure region (< 0.1 bar), indicating the creation of more micropores (**Figure 3.1B**). A much higher BET surface area of 1895 m^2 g^{-1} was obtained, which was almost 3.5 times that of OMC (**Table 3.1**). The BJH pore size distribution curves revealed the existence of ordered mesopores around 10.5 nm, slightly increasing compared with OMC [35, 41] (**Figure 3.1C**). Correspondingly, an increased total pore volume of 1.79 cm^3 g^{-1} was obtained, of which 0.27 cm^3 g^{-1} was contributed by micropores (**Table 3.1**). The SEM image of OMC-A confirmed the well-maintained mesoporous morphology (**Figure 3.3**). To evaluate the effect of calcination temperature on porosity and surface area, OMC was activated at 600°C in the presence of KOH. In this way, the activation process was performed by heating up the KOH/OMC 8:1 mixture up to 600°C for 1 h under nitrogen atmosphere and the product was denoted

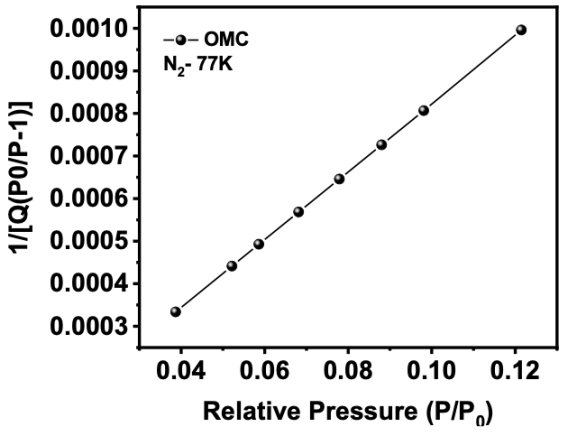

BET surface area: 543.3427 ± 0.9063 m^2/g
Slope: 0.007986 ±0.000013 g/cm^3 STP
Y-intercept: 0.000024 ± 0.000001 g/cm^3 STP
C: 329.353706
Qm: 124.8324 cm^3/g STP
Correlation coefficient: 0.9999917

Figure 3.2 BET plot and information of OMC

Table 3.1 Summary of the porosity parameters of OMC, OMC-A, OMC/IL, and OMC-A/IL.

Sample	Surface area ($m^2 g^{-1}$)	Micropore surface area ($m^2 g^{-1}$)	Total pore volume ($cm^3 g^{-1}$)	Micropore volume ($cm^3 g^{-1}$)	Pore size (BJH method) (nm)	Pore size (H-K method) (nm)
OMC	543	197	0.44	0.05	7.7	N/A
OMC/IL	124	0	0.28	0	6.7	0.63
OMC-A	1895	884	1.79	0.27	10.5	N/A
OMC-A-600	637	201	0.72	0.09	10.5	N/A
OMC-A/IL	286	9.4	0.91	0.03	9.1	0.47

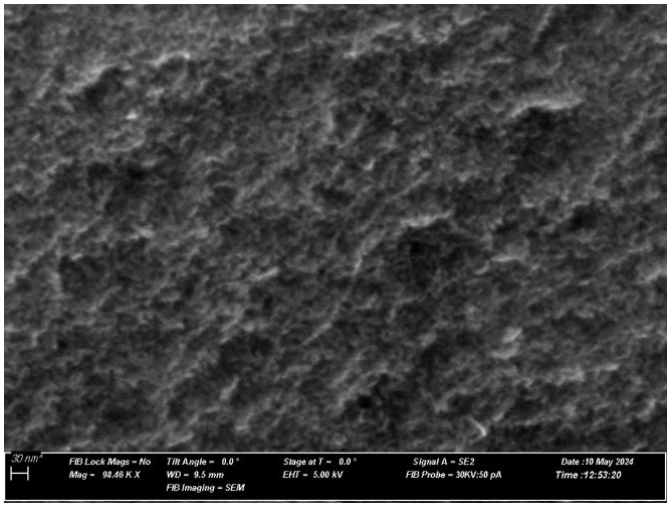

Figure 3.3 SEM images of OMC.

as OMC-A-600. N_2 adsorption/desorption isotherms at 77 K revealed that BET surface area of 637 m^2 g^{-1}. Pore size distribution curve calculated by BJH method indicates the activation process at 600°C creates the pore width centered at 10.5 nm which is similar to the pore width of OMC-A prepared at 800°C. Total pore volume of OMC-A-600 increased to 0.72 cm^3 g^1 with only 0.09 cm^3 g^{-1} being attributed by micropores compared to OMC, but still lower than OMC-A. (**Table 3.1**). The IL being synthesized via the deprotonation of 2,2,3,3,4,4-hexafluoro-1,5-pentanediol (HFPDOH) by 7-methyl-1,5,7-triazabicyclo[4.4.0]dec-5-ene (MeTBD), denoted as $[MeTBDH]_2[HFPDO]$ (**Figure 3.1A**), was deployed as modifier to engineer the surface of the porous channels and provide binding sites to integrate CO_2.[42] The oxygenate sites have shown the capability to capture CO_2 from a diluted source via O-C bond formation.[21, 26] The IL coating was performed via a wet impregnation method using acetonitrile as the solvent. The IL coating amount of 30 wt% was adopted for each OMC and OMC-A support, and the as-obtained sorbents were denoted as OMC/IL and OMC-A/IL.

First, the porosity analysis of OMC/IL and OMC-A/IL was performed to study the textural structure variation upon IL introduction within the porous channels. Notably, the type IV feature of the N_2 uptake isotherms was maintained for both sorbents (**Figure 3.1B**). After introducing IL coatings, diminished surface area was revealed for both sorbents, with 124 m^2 g^{-1} for OMC/IL and 286 m^2 g^{-1} for OMC-A/IL. Compared with the porosity of the original substrates, the IL layer preferred to fill the micropores, leading to significantly decreased microporous surface areas and pore volumes (**Table 3.1**). For OMC/IL, all the surface area and total pore volume (0.28 m^2 g^{-1}) correspond to mesopores (**Figure 3.1D**). This indicated the location of the IL was inside micropores as well as on the surface of mesopore walls. In addition, for OMC-A/IL, although the surface area was largely decreased, ordered mesopores around 9.1 nm still existed (**Figure 3.1D**). However, the micropores only contributed 9.4 m^2 g^{-1} to the surface area and 0.03 cm^3 g^{-1} to the total pore volume (0.91 cm^3 g^{-1}), and the residual of which was contributed by mesopores. The SEM images of OMC/IL and OMC-A/IL confirmed the well-reserved porous structures after IL coating (**Figures 3.4 and 3.5**). The preservation and retention of the porosity indicated a conformal coating of ILs on the surface of

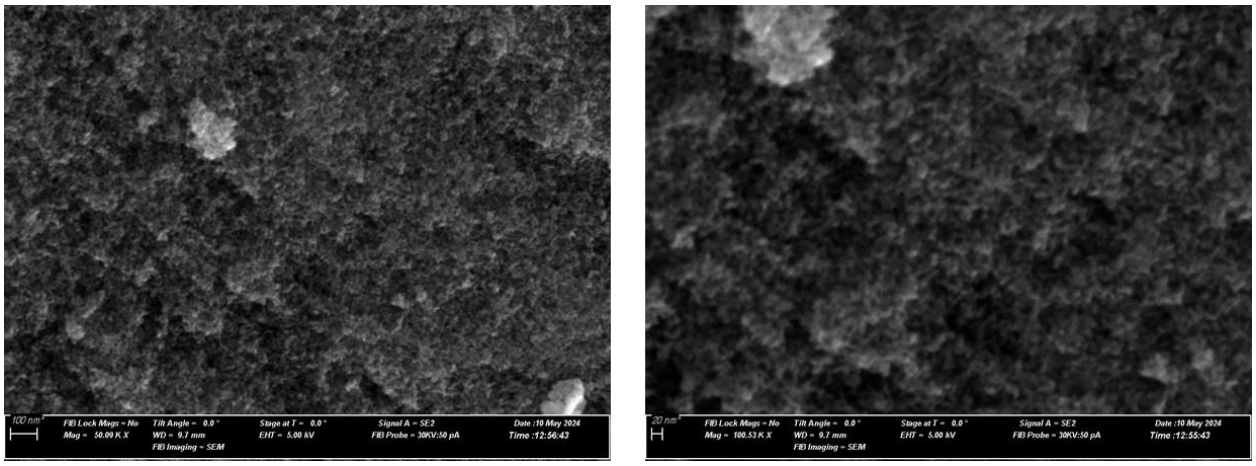

Figure 3.4 The SEM images of OMC/IL.

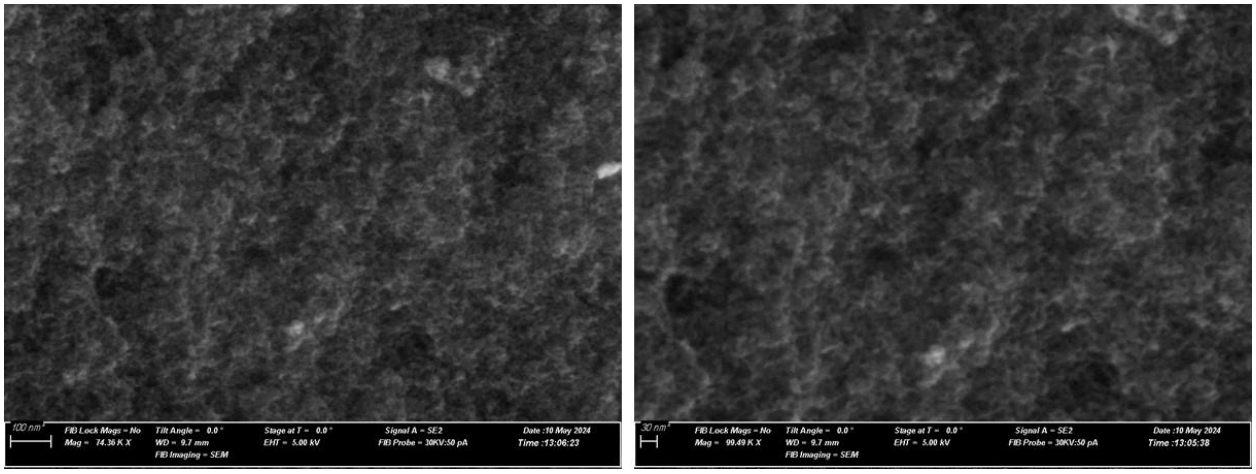

Figure 3.5 The SEM images of OMC-A/IL.

carbon materials, which are still accessible and not fully obstructed by the IL. The thermal stability of IL and carbon-IL samples was examined using thermogravimetric analysis (TGA) under an N_2 flow with a ramping rate of 5 °C min^{-1} in a range of 25-800 °C (**Figure 3.6**). The result illustrated the onset decomposition temperature of 182 °C for OMC-A/IL derived from the loss of IL at this temperature. TGA analysis revealed that after incorporating IL in the porous channels, the composite's thermal stability is improved compared with the pure IL, benefiting from the confinement effect and interaction with the carbon substrates.[25, 26]

The location and interaction of IL with the carbon substrate were then investigated via x-ray- and neutron-based methods. Wide-angle X-ray scattering (WAXS) patterns of IL, OMC-A/IL, and OMC/IL are presented in **Figure 3.7A**. The absence of strong/sharp diffraction peaks in all three samples can be attributed to the absence of crystalline features in both IL and the carbon substrates. Notably, broad peaks in the range of 0.5-3.0 $Å^{-1}$ were observed in these samples. A broad peak around 0.92 $Å^{-1}$ present in IL can be attributed to anion-anion nearest neighbor distances in the IL phase.[20, 43] These peaks are shifted to 1.09 and 1.21 $Å^{-1}$ for OMC-A/IL and OMC/IL, respectively, which can be attributed to the tighter ordering of IL due to enhanced interactions of IL with OMC-A and OMC. A broad peak around 2.02 $Å^{-1}$ in IL can be attributed to adjacent F-F distances in the fluorinated anion. Additionally, this peak became more concentrated, and the position shifted to 2.50 $Å^{-1}$ for OMC-A/IL and OMC/IL, which can be attributed to the perturbations after interacting with the carbon support.[20] The small angle neutron scattering (SANS) data were collected to provide the structure evolution information upon IL coating, taking OMC-A as an example (**Figure 3.7B**). The data fitting of the OMC-A material reveals that the low q power law decay is steeper than q^{-4} (porod exponent), which suggests a fuzzy surface of the structural feature with this length scale. The hierarchical pore structure with two pore populations agrees with the result from the gas adsorption measurements (**Figure 3.7B**). The correlation length of 3.60 Å reflects the average distance between the micropores and the solid wall.

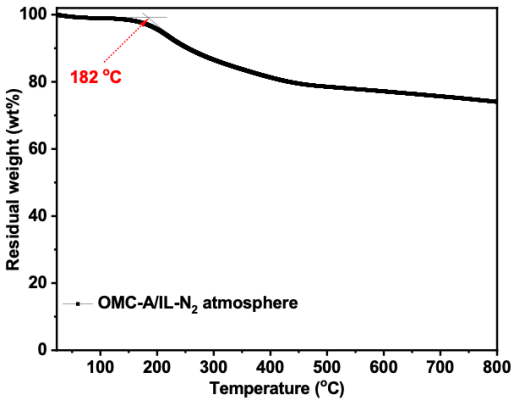

Figure 3.6 The TGA analysis of OMC-A/IL, being collected under N_2 atmosphere with a ramping rate of 5 °C min^{-1}.

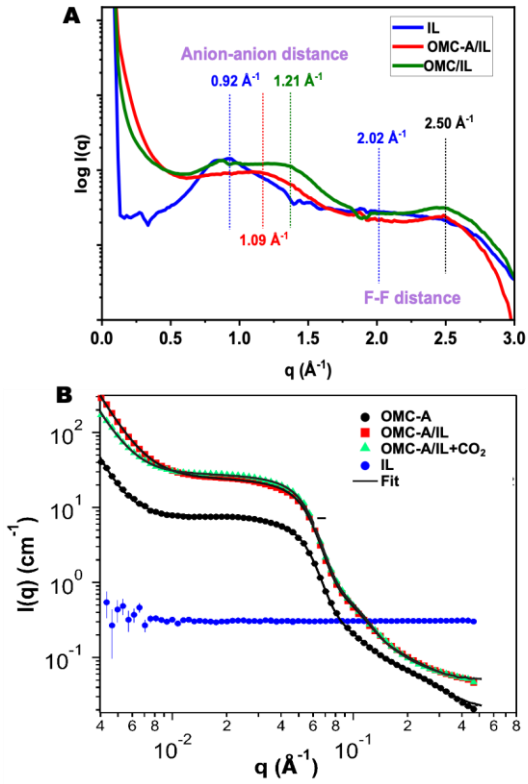

Figure 3.7 (A) Wide-angle X-ray scattering (WAXS) curves of IL, OMC/IL, and OMC-A/IL. (B) Small angle neutron scattering (SANS) patterns of OMC-A, OMC-A/IL before and after reacting with CO_2, the IL and fitting curves.

Upon filling with the IL in OMC-A/IL, both micro-sized and meso-sized pores were maintained well. Interestingly, the size distribution of meso-sized pores becomes narrower, which leads to a noticeable hump at ~0.1 $Å^{-1}$. That hump arises from the form factor of the spherical model. The performance of the IL-engineered carbon sorbents in direct air capture of CO_2 was evaluated via breakthrough analysis using 400 ppm CO_2 in He as the feeding gas. The OMC and OMC-A support both exhibited low CO_2 adsorption capacities of 0.09 and 0.12 mmol g^{-1}, respectively, due to the lack of active sites with relatively strong interaction strength with CO_2 (**Figure 3.8**). Comparatively, after 30 wt% IL coating, significantly increased CO_2 uptake capacity was revealed, with 0.49 mmol g^{-1} achieved by OMC/IL (**Figure 3.9A**), benefiting from the strong oxygenate sites in the anion of IL. Notably, with the same IL coating amount, a higher CO_2 adsorption capacity (0.65 mmol g^{-1}) was obtained by OMC-A/IL (**Figure 3.9B**). The comparison between OMC/IL and OMC-A/IL revealed that although the majority of the micropores in OMC-A was blocked after IL coating, the larger mesopore size and pore volume in OMC-A/IL could benefit the low-concentration CO_2 capture, providing higher uptake capacity in DAC of CO_2 study and capable of exposing more active sites to bind CO_2 from diluted sources. Comparatively, the uptake capacity of IL-modified OMC-A-600 sorbent has shown no significant improvement compared to OMC/IL, indicating the high surface area and pore volume of OMC-A do benefit the diluted CO_2 capture after IL coating (**Figure 3.10**). Taking OMC-A-derived sorbents as an example, the effect of IL coating amount was studied systematically via breakthrough test (**Figure 3.9C** and **Figure 3.11**). Even with a low IL loading amount of 10 wt%, a CO_2 adsorption capacity of 0.33 mmol g^{-1} was achieved.

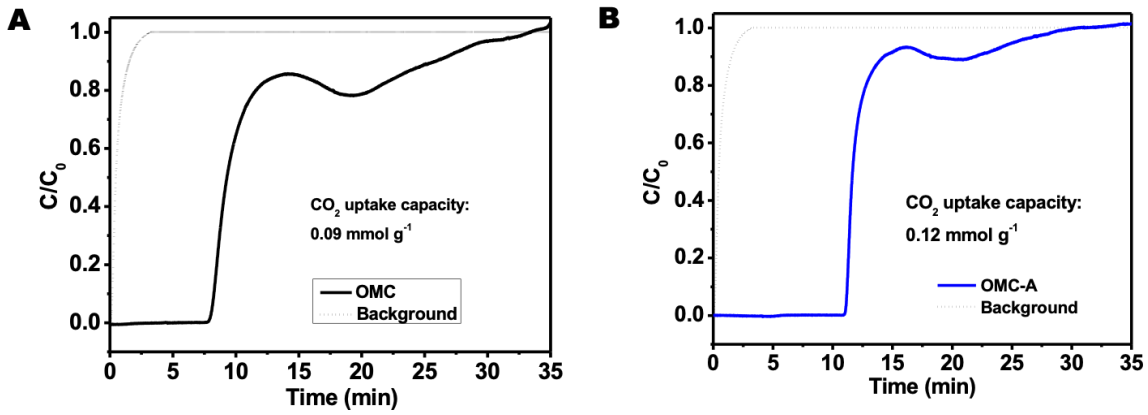

Figure 3.8 (A) The CO_2 uptake capacity of OMC and (B) OMC-A being obtained via breakthrough test at 298 K with 400 ppm CO_2 in He as the feeding gas.

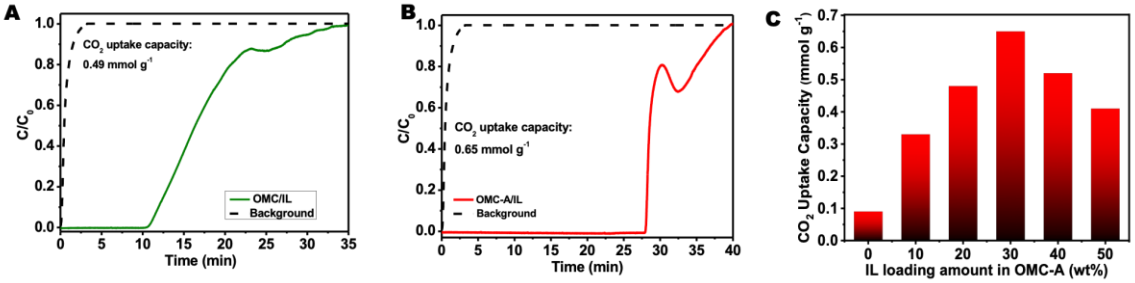

Figure 3.9 (A) The breakthrough test curve, being collected at 298 K using 400 ppm in He as the feeding gas of OMC/IL and (B) OMC-A/IL. (C) Influence of IL loading amount on the (400 ppm) CO_2 uptake capacity of IL-modified OMC-A sorbents

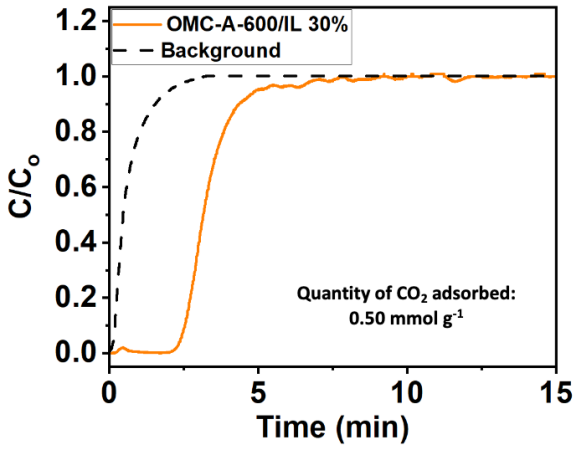

Figure 3.10 The CO_2 uptake capacity of OMC-A-600/IL being obtained via breakthrough test at 298 K with 400 ppm CO_2 in He as the feeding gas

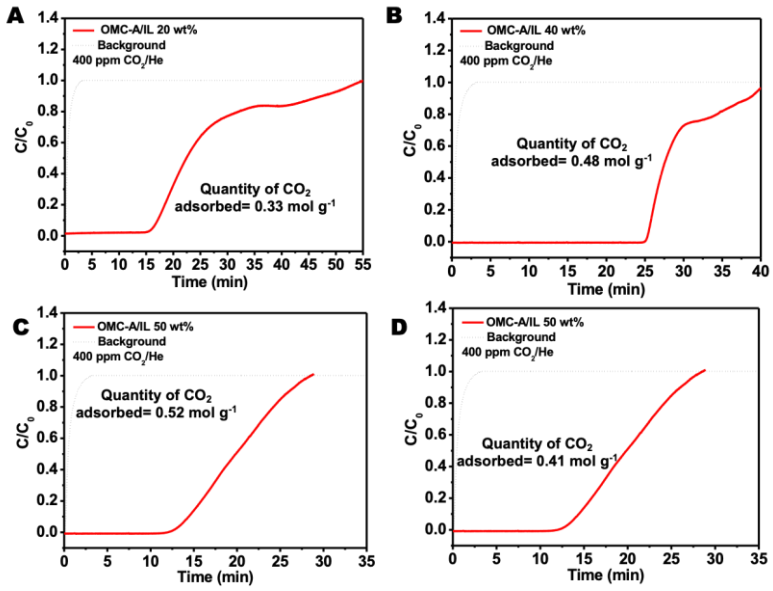

Figure 3.11 The CO_2 uptake capacity of OMC-A/IL with different IL loading amount, being obtained via breakthrough test at 298 K with 400 ppm CO_2 in He as the feeding gas

The highest CO_2 adsorption capacity (0.65 mmol g^{-1}) was obtained with an IL loading of 30 wt% on OMC-A. Further increasing the IL loading amount led to diminished CO_2 adsorption capacity using 400 ppm CO_2 in He as the feeding gas, probably owing to the blocking of the pores and the inaccessible active sites close to the carbon-IL interface. Notably, in the SANS spectrum of CO_2-saturated OMC-A/IL, with the sorption of CO_2, the micropores exhibit negligible changes (**Figure 3.7B**). The contrast between the pore space and the pore wall of meso-sized pores becomes slightly larger while the average size retains. Interestingly, the power law decays slower at low q, which may suggest a smoother surface and more ordered packing of the IL phase after interacting with CO_2 molecules.

The carbon capture thermodynamics of the IL-modified OMC and OMC-A sorbents were then studied via pressure-swing CO_2 uptake isotherms. First, the CO_2 adsorption isotherms of the carbon substrates and the IL-modified sorbents were collected at 298 K through a pressure swing procedure (CO_2 pressure up to 1 bar) (**Figure 3.12A**) and used to calculate the reaction enthalpy and gas uptake selectivity. Although higher capacity was achieved by OMC and OMC-A at high CO_2 pressure (1 bar) benefiting from the higher pore volume, IL coating greatly improved the CO_2 uptake behavior of the sorbents at low pressure region. For example, with a low CO_2 pressure of 0.1 bar, the CO_2 adsorption capacity enhanced in the order of OMC and OMC-A (0.48 mmol g^{-1}) < OMC-A/IL (0.60 mmol g^{-1}) < OMC/IL (0.79 mmol g^{-1}). Notably, higher capacity of OMC-A/IL over OMC-A was maintained within CO_2 pressure of 0.15 bar, and the capture capacity of OMC/IL surpassed OMC within CO_2 pressure of 0.59 bar. The absorption enthalpy is crucial for evaluating the interaction between gases and the sorbent, holding significant importance when opting for energy-efficient absorbents for CO_2 capture.[23] Using the CO_2 isotherms being collected at 298 K, the energy distribution curves were calculated by the CAESAR (Computed Adsorption Energies, SVD Analysis Result) algorithm.[44] For the pristine OMC and OMC-A, only physisorption sites were shown up, with the peak located at 22 kJ mol^{-1} (**Figure 3.12B**). The lack of chemisorption peaks in the curve corresponding to OMC and OMC-A indicates that there is no active site on the scaffolds to chemically react with CO_2, particularly at low pressure region. Comparatively, after IL

loading, three peaks were observed for both OMC/IL and OMC-A/IL at 40, 52, and 64 KJ.mol^{-1}, indicating the existence of moderate to strong chemisorption sites. Notably, the reaction energy obtained in the carbon-IL sorbents was much weaker than the pure IL (-71.9 kJ mol^{-1}) and the IL being confined in the cavity of MOF scaffolds (-113 kJ mol^{-1}).[26] This indicated the strong interaction of the IL cations/anions with the carbon scaffolds, leading to decreased electron density of the oxygenate sites for CO_2 integration. The strong interaction was induced by the π-conjugated structure of the carbon surface and the aromatic structure of the IL species, which was consistent with the TGA analysis, with enhanced thermal stability of the IL being observed (**Figure 3.13**). To evaluate the effect of alternative cation, the OMC-A substrate was modified by Na_2[HFPDO] with the equimolar $HFPDO^{2-}$ anion amount (0.65 mmol g^{-1}) as that in OMC-A/IL. The DAC of the CO_2 performance test was performed via breakthrough test and the as-prepared OMC-A/Na_2[HFPDO] resulted in a capture capacity of 0.32 mmol g^{-1}, which is lower than the [MeTBDH]$_2$[HFPDO] IL loaded sorbent. The control experiment indicated the critical role of the π-conjugated cation to interact with the carbon substrate, allowing uniform distribution and spreading of the active sites on the carbon surface. The influence of IL coating on the selectivity of CO_2/N_2 was evaluated and calculated via the Ideal Adsorbed Solution Theory (IAST) method using CO_2 and N_2 uptake isotherms being collected at 298 K (**Figure 3.12C, Figure 3.11, and Table 3.1**). With the CO_2 to N_2 ratio of 15:85, the calculated CO_2/N_2 selectivity was 9 to 20 for the OMC and OMC-A substrates. Comparatively, after IL coating, the CO_2/N_2 selectivity was significantly improved, with 68 to 390 for OMC/IL and 51 to 215 for OMC-A/IL being obtained, respectively, benefiting the DAC of CO_2 applications, particularly at the low-pressure region.

3.6. Conclusions

The DAC of CO_2 technologies holds great promise to achieve the negative carbon emission goal and solve the environmental issues caused by greenhouse gas emissions. The grand challenge lies in developing efficient sorbents capable of binding CO_2 from diluted sources (400 ppm) and releasing CO_2 with low energy input.

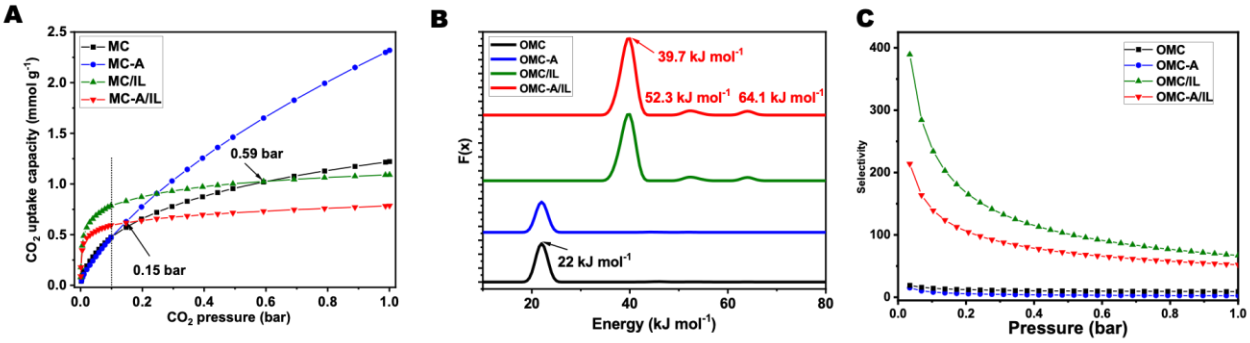

Figure 3.12 (A) CO_2 uptake isotherms of OMC, OMC-A, OMC/IL, and OMC-A/IL being collected at 298 K. (B) Energy distribution curves of the carbon support and IL-modified carbon sorbents being calculated based on the CO_2 uptake isotherms at 298 K. (C) The CO_2/N_2 selectivity being calculated using the IAST method based on CO_2 to N_2 molar ratio of 15:85.

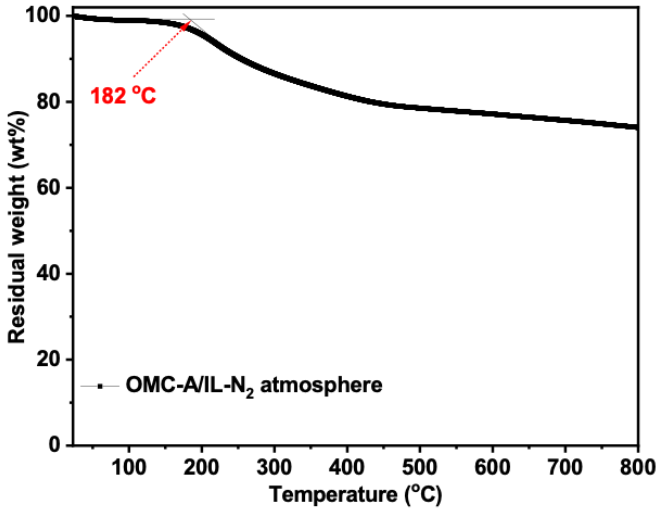

Figure 3.13 The TGA analysis of OMC-A/IL, being collected under N_2 atmosphere with a ramping rate of 5 °C min^{-1}.

The fundamental study revealed that the IL preferred filling the micropores in the carbon substrates and also created a thin layer on the surface of mesopores. The intense interaction between the IL and the carbon surface could be leveraged to tune the interaction strength with CO_2 molecules and improve the thermal stability of the active sites. With the same IL loading amount, larger mesopore size and pore volume delivered higher CO_2 uptake capacity from diluted source (400 ppm CO_2 in He or air). The findings in this work guide how to leverage the porosity and surface properties of the substrates to maximize the utilization efficiency of the active sites for CO_2 integration.

References

[1] M. Zeeshan, M.K. Kidder, E. Pentzer, R.B. Getman, B. Gurkan, Front. Sustain., 4 (2023).

[2] R. Monastersky, Nature, 497 (2013) 13.

[3] J. Rogelj, G. Luderer, R.C. Pietzcker, E. Kriegler, M. Schaeffer, V. Krey, K. Riahi, Nat. Clim. Change, 5 (2015) 519-527.

[4] Y. Shi, R. Ni, Y. Zhao, 37 (2023) 6365-6381.

[5] X. Zhu, W. Xie, J. Wu, Y. Miao, C. Xiang, C. Chen, B. Ge, Z. Gan, F. Yang, M. Zhang, D. O'Hare, J. Li, T. Ge, R. Wang, Chem. Soc. Rev., 51 (2022) 6574-6651.

[6] E.S. Sanz-Pérez, C.R. Murdock, S.A. Didas, C.W. Jones, Chem Rev, 116 (2016) 11840-11876.

[7] J.G. Vitillo, Chem Rev, 117 (2017) 9521-9523.

[8] J. Wang, L. Huang, R. Yang, Z. Zhang, J. Wu, Y. Gao, Q. Wang, D. O'Hare, Z. Zhong, Energy Environ. Sci., 7 (2014) 3478-3518.

[9] A. Goeppert, M. Czaun, R.B. May, G.K.S. Prakash, G.A. Olah, S.R. Narayanan, J Am Chem Soc, 133 (2011) 20164-20167.

[10] X. Shi, H. Xiao, H. Azarabadi, J. Song, X. Wu, X. Chen, K.S. Lackner, Angew Chem Int Ed, 59 (2020) 6984-7006.

[11] R. Custelcean, Chem Sci, 12 (2021) 12518-12528.

[12] D.J. Heldebrant, P.K. Koech, V.-A. Glezakou, R. Rousseau, D. Malhotra, D.C. Cantu, Chem. Rev., 117 (2017) 9594-9624.

[13] W.H. Lee, X. Zhang, S. Banerjee, C.W. Jones, M.J. Realff, R. Lively, Joule, 7 (2023) 1241-1259.

[14] J. Leclaire, D.J. Heldebrant, K. Grubel, J. Septavaux, M. Hennebelle, E. Walter, Y. Chen, J.L. Banuelos, D. Zhang, M.T. Nguyen, D. Ray, S.I. Allec, D. Malhotra, W. Joo, J. King, Nat Chem, (2024).

[15] M.A. Alkhabbaz, P. Bollini, G.S. Foo, C. Sievers, C.W. Jones, J. Am. Chem. Soc., 136 (2014) 13170-13173.

[16] S.A. Didas, S. Choi, W. Chaikittisilp, C.W. Jones, Acc. chem. res., 48 (2015) 2680-2687.
[17] A. Goeppert, M. Czaun, R.B. May, G.S. Prakash, G.A. Olah, S. Narayanan, J. Am. Chem. Soc., 133 (2011) 20164-20167.
[18] S. Zeng, X. Zhang, L. Bai, X. Zhang, H. Wang, J. Wang, D. Bao, M. Li, X. Liu, S. Zhang, Chem. Rev., 117 (2017) 9625-9673.
[19] M. Watanabe, M.L. Thomas, S. Zhang, K. Ueno, T. Yasuda, K. Dokko, Chem Rev, 117 (2017) 7190-7239.
[20] R. Hayes, G.G. Warr, R. Atkin, Chem. Rev., 115 (2015) 6357-6426.
[21] C. Wang, H. Luo, D.-e. Jiang, H. Li, S. Dai, Angew Chem Int Ed, 49 (2010) 5978-5981.
[22] C. Wang, X. Luo, H. Luo, D.-e. Jiang, H. Li, S. Dai, Angew Chem Int Ed, 50 (2011) 4918-4922.
[23] K. Huang, Y.-T. Wu, S. Dai, Ind. & Eng. Chem. Res., 54 (2015) 10126-10133.
[24] G. Cui, J. Wang, S. Zhang, Chem Soc Rev, 45 (2016) 4307-4339.
[25] D. Moitra, N. Mokhtari-Nori, K.M. Siniard, L. Qiu, J. Fan, Z. Dong, W. Hu, H. Liu, D.E. Jiang, H. Lin, J. Hu, M. Li, Z. Yang, S. Dai, ChemSusChem, 16 (2023) e202300808.
[26] L. Qiu, L. Peng, D. Moitra, H. Liu, Y. Fu, Z. Dong, W. Hu, M. Lei, D.E. Jiang, H. Lin, J. Hu, K.A. McGarry, I. Popovs, M. Li, A.S. Ivanov, Z. Yang, S. Dai, Small, 19 (2023) e2302708.
[27] L. Qiu, M. Lei, C. Wang, J. Hu, L. He, A.S. Ivanov, D.E. Jiang, H. Lin, I. Popovs, Y. Song, J. Fan, M. Li, S.M. Mahurin, Z. Yang, S. Dai, Small, n/a (2024) e2401798.
[28] C. Liang, Z. Li, S. Dai, Angew. Chem. Inter. Ed., 47 (2008) 3696-3717.
[29] P. Zhang, L. Wang, S. Yang, J.A. Schott, X. Liu, S.M. Mahurin, C. Huang, Y. Zhang, P.F. Fulvio, M.F. Chisholm, S. Dai, Nat. Commun., 8 (2017) 15020.
[30] J. Zhang, Z.-A. Qiao, S.M. Mahurin, X. Jiang, S.-H. Chai, H. Lu, K. Nelson, S. Dai, Angew. Chem. Int. Ed., 54 (2015) 4582-4586.

[31] Y. Fang, Y. Lv, J. Tang, H. Wu, D. Jia, D. Feng, B. Kong, Y. Wang, A.A. Elzatahry, D. Al-Dahyan, Q. Zhang, G. Zheng, D. Zhao, Angew. Chem. Int. Ed., 54 (2015) 8425-8429.
[32] Y. Meng, D. Gu, F. Zhang, Y. Shi, H. Yang, Z. Li, C. Yu, B. Tu, D. Zhao, Angew. Chem. Int. Ed., 44 (2005) 7053-7059.
[33] M.R. Benzigar, S.N. Talapaneni, S. Joseph, K. Ramadass, G. Singh, J. Scaranto, U. Ravon, K. Al-Bahily, A. Vinu, Chem. Soc. Rev., 47 (2018) 2680-2721.
[34] C. Liang, S. Dai, J. Am. Chem. Soc., 128 (2006) 5316-5317.
[35] X. Wang, J.S. Lee, C. Tsouris, D.W. DePaoli, S. Dai, J. Mater. Chem., 20 (2010) 4602-4608.
[36] Y. Fang, Y. Lv, J. Tang, H. Wu, D. Jia, D. Feng, B. Kong, Y. Wang, A.A. Elzatahry, D. Al-Dahyan, Angew. Chem., 127 (2015) 8545-8549.
[37] M.S. Shafeeyan, W.M.A.W. Daud, A. Houshmand, A. Shamiri, J. Anal. Appl. Pyrol., 89 (2010) 143-151.
[38] J. Tóth, , J Colloid Interf. Sci., 225 (2000) 378-383.
[39] R. Bardestani, G.S. Patience, S. Kaliaguine, , Can. J Chem. Eng., 97 (2019) 2781-2791.
[40] H. Khalil, M. Jawaid, P. Firoozian, U. Rashid, A. Islam, H.M. Akil, J Biobased Mater. Bioenergy, 7 (2013) 708-714.
[41] J. Zhang, Z.A. Qiao, S.M. Mahurin, X. Jiang, S.H. Chai, H. Lu, K. Nelson, S. Dai, Angew. Chem. Inter. Ed., 54 (2015) 4582-4586.
[42] M.J. Lashaki, S. Khiavi, A. Sayari, Chem. Soc. Rev., 48 (2019) 3320-3405.
[43] C.S. Santos, N.S. Murthy, G.A. Baker, E.W. Castner, Jr., J Chem Phys, 134 (2011) 121101.
[44] K.M. Nelson, S.M. Mahurin, R.T. Mayes, B. Williamson, C.M. Teague, A.J. Binder, L. Baggetto, G.M. Veith, S. Dai, Microporous and Mesoporous Mater., 222 (2016) 94-103.

CHAPTER 4 : CARBON DIOXIDE DYNAMICS IN IONIC LIQUIDS

4.1 Introduction

While macroscopic structure−performance relationships relating to the ionic liquid structure have been developed, dynamic information about the ionic liquid's interaction with CO_2 is less plentiful. Factors affecting the CO_2 uptake capacity of the supported amines include the nature of the ionic liquid compounds in terms of active sites, and the mobility of the confined CO_2, which is related to the viscosity of the ionic liquids. Here, we prepared a family of Bmim ionic liquids refers to a group of different ionic liquids where the cation is always 1-butyl-3-methylimidazolium ($[Bmim]^+$). The only variation within the family lies in the type of anion attached to this cation, allowing for diverse properties depending on the chosen anion. ^{13}C T_1−T_2 relaxation correlation Nuclear-magnetic resonance (NMR) experiments are utilized to characterize the structural and dynamic properties of the confined CO_2 in ILs [1]. Relaxation correlation of ^{13}C of CO_2, especially the T_1−T_2 correlation, can be used to discern unique relaxation times related to CO_2 hopping within different ionic liquids. Shorter T_2 sign of reduced mobility due to stronger attachment. In other words, T_2 can be longer in materials with higher mobility due to rapid decoherence [2-7]. $[Bmim][NTf_2]$ shows faster mobilities than $[Bmim][CTf_3]$ and $[Bmim][CHTf_2]$ because of its weaker attachment to CO_2, resulting in larger T_2 values. CO_2 appears to more easily transfer between domains within the structure of $[Bmim][CHTf_2]$, leading to generally faster CO_2 uptake rates with higher sorption capacities (0.108 mol_{CO2}/mol_{IL}), while $[Bmim][CTf_3]$ remained much less mobile and is thus less engaged in CO_2 capture due to stereochemistry hindrance of three trifluoromethane sulfonyl groups. Electrowithdrawing groups (EWGs) crowd also withdraw nucleophilic species and provide the opportunity for CO_2 to hop between the sites. This regard caused the smaller T_2 values of relaxation for $[Bmim][CTf_3]$ compared to $[Bmim][CHTf_2]$, although $[Bmim][CHTf_2]$ has lower viscosity.

4.2 Experimental and Characterization

In this study, we used one commercially available ionic liquid ($[Bmim][NTf_2]$), and two synthesized novel ionic liquids ($[Bmim][CHTf_2]$ and $[Bmim][CTf_3]$). The molecular structures of the SILs used in this work are provided in **Figure 4.1**, and their synthesis procedures are as follows:

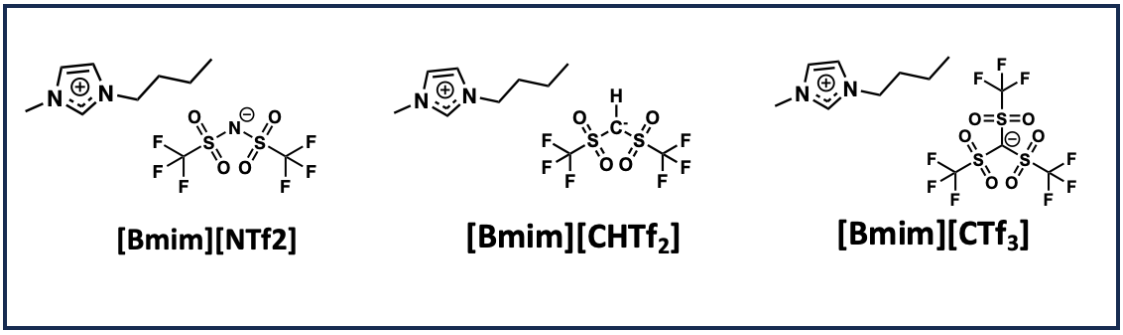

Figure 4.1 (A) Structures of Bmim NTf2, BmimCTf_2, and Bmim CTf_3.

4.2.1 Synthesis of 1-Butyl-3-methylimidazolium bis(trifluoromethylsulfonyl)methanide ([Bmim][$CHTf_2$])

1-Butyl-3-methylimidazolium chloride [Bmim]Cl was synthesized, purified, and dried through the published procedure. [1] The synthesis of [Bmim][$CHTf_2$] was carried out through an anion exchange reaction of 1-butyl-3-methylimidazolium chloride ([Bmim]Cl) and the sodium salt of Bis((trifluoromethyl)sulfonyl)methane (Na[$CHTf_2$]): Sodium hydride (NaH) was added to a three-necked round-bottom flask dispersed in Tetrahydrofuran (THF). An equimolar solution of Bis((trifluoromethyl)sulfonyl)methane (CH_2Tf_2) in THF was added under an inert atmosphere. The reaction mixture was stirred overnight at room temperature until the formation of the Na[$CHTf_2$] salt was complete. The solvent was then removed under reduced pressure to isolate the dry Na[$CHTf_2$] salt. The obtained salt was dissolved in methanol, followed by the addition of an equimolar amount of [Bmim]Cl in acetonitrile under continuous stirring. The mixture was allowed to react at room temperature to ensure complete anion exchange. After completion of the reaction, acetonitrile was removed under vacuum; Otherwise, the elimination of sodium chloride (NaCl) salt, which is soluble in methanol, is not possible. The remaining crude ionic liquid was dispersed in THF, where the NaCl byproduct formed as a precipitate due to its low solubility in THF. To enhance NaCl precipitation and facilitate its removal, the reaction concentration was adjusted by reducing the solvent volume. The precipitated NaCl was then separated by multiple rounds of centrifugation and filtration. The purified [Bmim][$CHTf_2$] was obtained after removing THF under vacuum and was further dried under reduced pressure at 60°C. The final ionic liquid was characterized by NMR spectroscopy **(Figure 4.2).** Liquid NMR spectra of ^{1}H, ^{13}C, and ^{19}F were recorded at ambient temperature on a JEOL 400YH spectrometer in deuterated DMSO.

4.2.2 Synthesis of 1-Butyl-3-methylimidazolium Tris (trifluoromethylsulfonyl) methanide ([Bmim][CTf_3])

This ionic liquid is also prepared through the anion exchange reaction, starting from commercially available Potassium tris(trifluoromethanesulfonyl)methanide (K[CTf_3]). K[CTf_3]) was added in an equimolar ratio to a solution of 1-butyl-3-methylimidazolium chloride ([Bmim]Cl) in acetonitrile. The reaction mixture was stirred at room temperature overnight to ensure complete anion exchange. After completion of the reaction, the solvent was removed under reduced pressure to obtain the crude ionic liquid containing precipitated KCl. The crude product was redispersed in tetrahydrofuran (THF) to facilitate the precipitation of KCl, which has low solubility in THF. To enhance purification, the mixture was subjected to multiple rounds of centrifugation and/or filtration to separate the KCl byproduct. The purified ionic liquid ([Bmim][CTf_3]) was obtained by removing THF under vacuum and drying under reduced pressure at 60°C to remove residual solvents. NMR characterized the final product to confirm purity and structural integrity. Liquid NMR spectra of ^{1}H, ^{13}C, and ^{19}F were recorded at ambient temperature on a JEOL 400YH spectrometer in deuterated DMSO (**Figure 4.3**). **Figure 4.4** indicates thermogravimetric analysis (TGA) results to measure the thermal stability of the synthesized ionic liquids. Viscosity measurements were carried out to relate the viscosity to NMR relaxation behavior, providing insight into the correlation between molecular mobility and CO_2 transport dynamics in ionic liquids. The measurements were conducted at various temperatures to evaluate the temperature dependence of viscosity and its impact on CO_2 transport. The viscosities of [Bmim][$CHTf_2$] (η = 248.1 cP) and [Bmim][CTf_3] (η = 161.5 cP) at 25 °C are higher than [Bmim][NTf_2] (η = 52.8 cP). The viscosity in higher temperatures decreses relatively.

4.2.3. ^{13}C NMR spectra for T_1 and T_2 relaxometry measurements

T_1 and T_2 NMR relaxometry measurements were carried out with a Varian VNMRS 500 NMR, operating at a frequency of 126 MHz for ^{13}C. [8] Approximately 700 mg of IL was used for the NMR experiments and was charged into tubes. ^{13}C-enriched CO_2, 99% gas was introduced to the samples for adsorption. T_1 or longitudinal

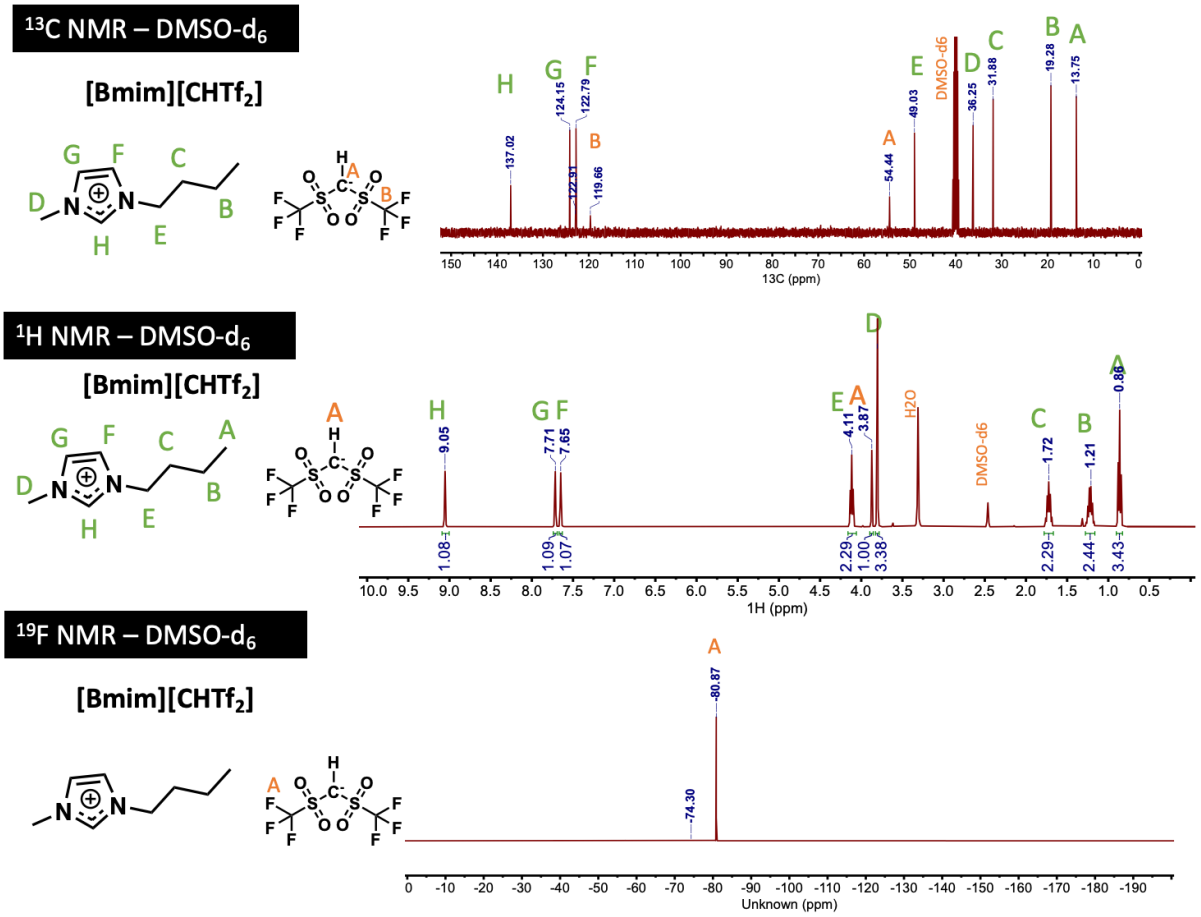

Figure 4.2 ^{13}C NMR Spectroscopy of [Bmim][CHTf$_2$] IL in DMSO-*d*$_6$

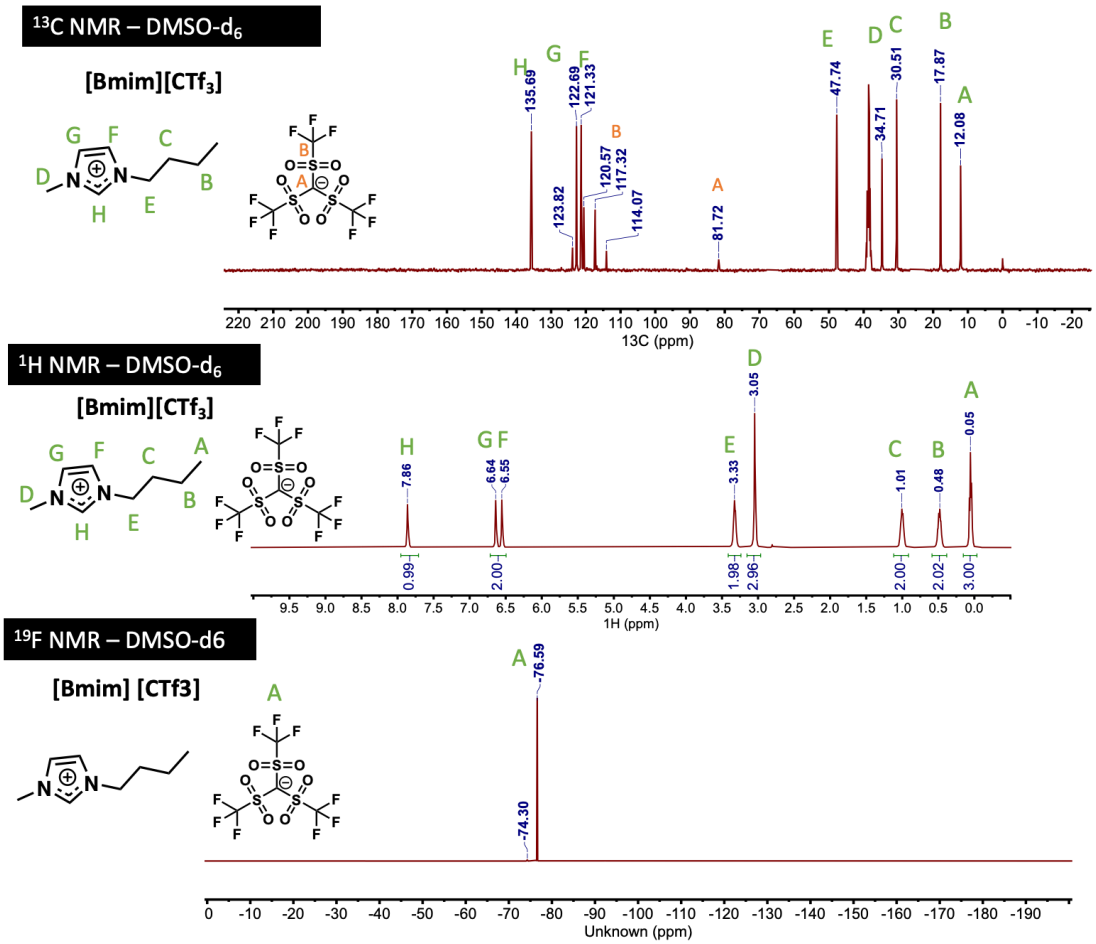

Figure 4.3 ^{13}C NMR Spectroscopy of [Bmim][CTf_3] IL in DMSO-*d_6*

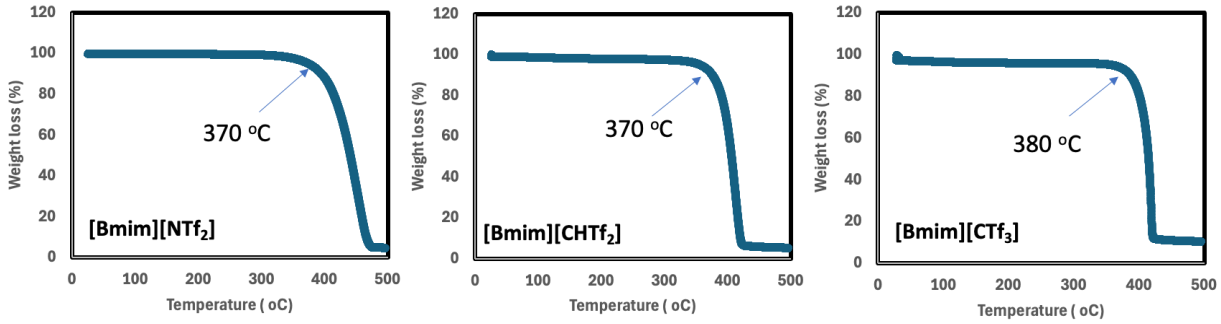

Figure 4.4 The TGA analysis of ILs, being collected under N_2 atmosphere with a ramping rate of 5 °C min^{-1}.

relaxation time is the time constant of the exponential relaxation process for spins to return to the equilibrium state along z from a non-equilibrium state. For the estimation of T_1, PW90 was measured for each sample and was in the order of 10 μs. For every sample, T_1 was measured by an inversion-recovery pulse sequence with 10 spectra, d_1 = 20 s, and NT = 4. d_2 (relaxation delay) is set to 10 elements varying from 0 to 32 seconds, appearing from bottom to top in the stack plot. The index of the null crossing point for the 126 ppm peak (related to physically-absorbed CO_2) was depicted from the bottom, corresponding to a d_2 (d_2-null). The estimated T_1 value of this ^{13}C chemical shift at 126 ppm was calculated by:

$T_1 = d_{2\_null}/0.693$

The more accurate value was extracted through an exponential fitting to a mono-exponential function using MestReNova software.T_2 was immediately measured thereafter using 10-12 spectra (relaxation delay > 5 × T_1). Integrals were calculated over the area of the peak to increase the signal-to-noise ratio. T_2 relaxation time was determined accurately by choosing integral graphs in data analysis, integrating the 126 ppm peaks, and fitting the magnetization (signal intensities: peak heights and integral values) to a mono-exponential function in MestReNova software. (**Figure 4.5**)

T_1 and T_2 relaxation times were measured for all of ionic liquids in the temperature range of 273- 330 K. (**Figure 4.6A and B**). In-situ NMR spectroscopy was utilized to investigate the formation of carbonyl fuctional group after interaction of the ionic liquid with CO_2. There is not any peak related to chemisorption of CO_2 in [Bmim][CTf_3] and ([Bmim][NTf2]) in NMR spectra after bubbling $^{13}CO_2$ into the ionic liquids. This indicates there is no chemical adsorption occurred in these two ILs. **Figure 4.7** shows that, after bubbling $^{13}CO_2$ into the ([Bmim][$CHTf_2$]), a chemical shift peak shows up at the region of 172.8 ppm, corresponding to carbonate species formation. With the increasing temperature up to 55^{o}C, the peak starts to eliminate and is totally eliminated at 55 °C.

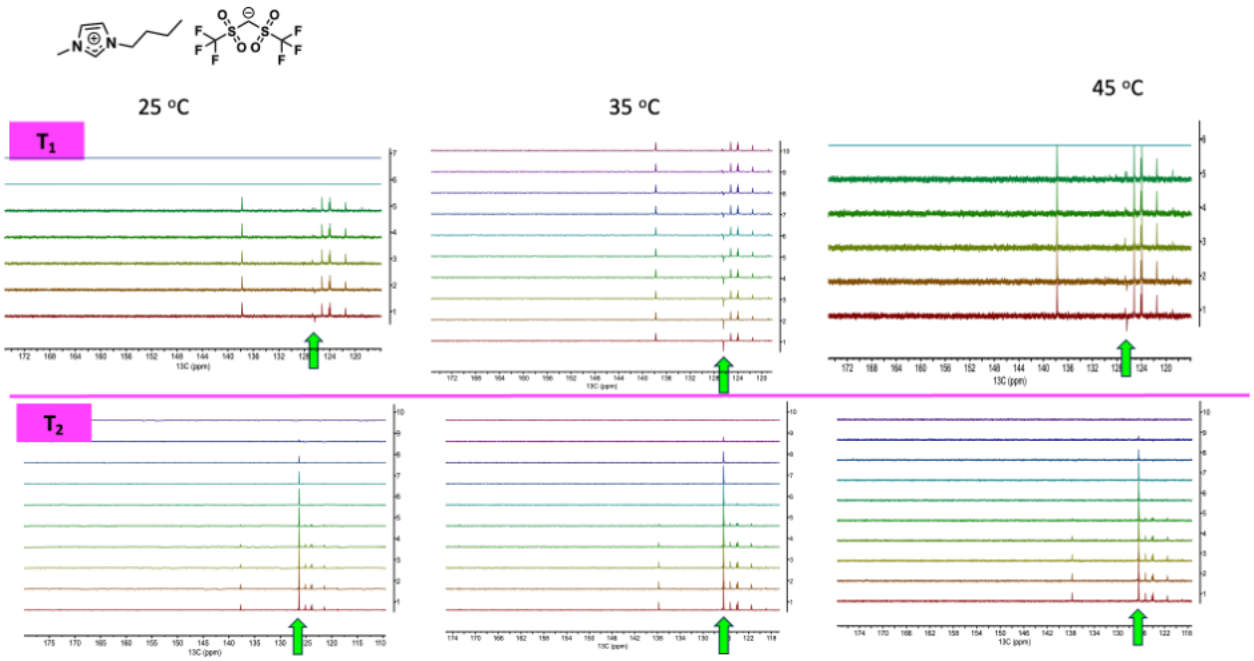

Figure 4.5 T_1 and T_2 spectra- ^{13}C NMR Spectroscopy of [Bmim][$CHTf_2$] IL

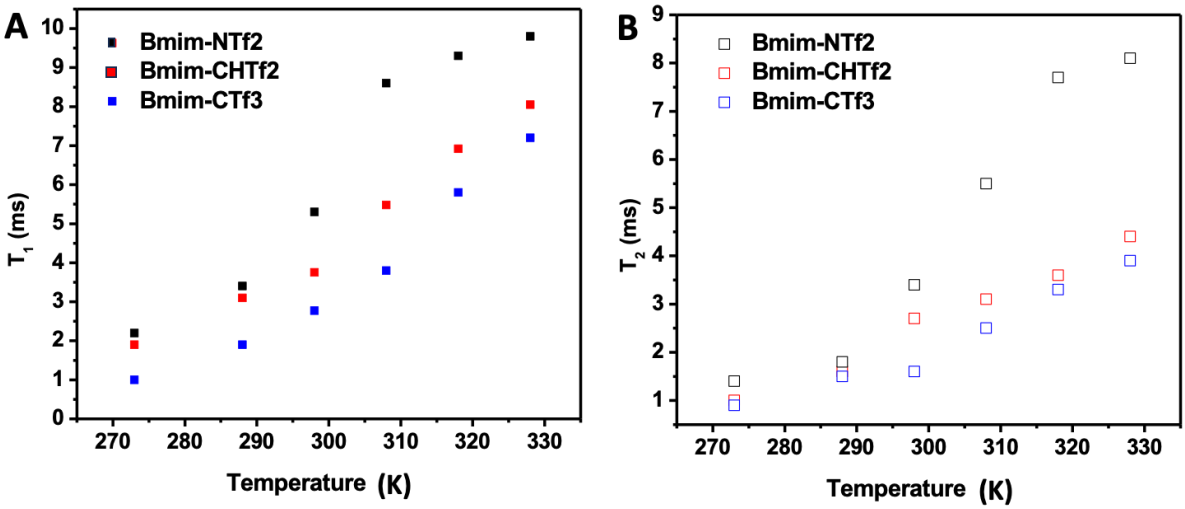

Figure 4.6 (A) T_1 relaxation for three ionic liquids at variable temperatures, (B) T_2 relaxation for three ionic liquids at variable temperatures

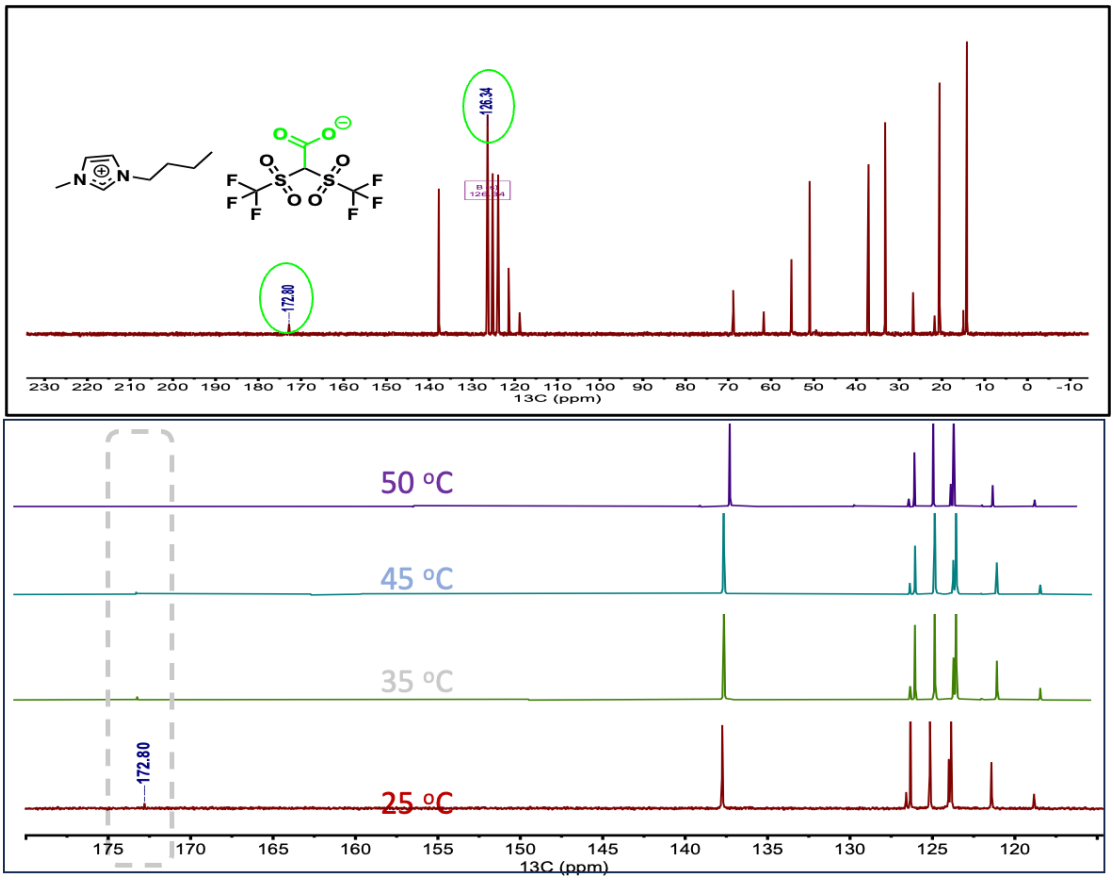

Figure 4.7 In-situ ^{13}C NMR spectroscopy of [Bmim][$CHTf_2$] in variable temperature after bubbling $^{13}CO_2$ into the ionic liquid

4.3 Results and Discussion

Key factors influencing CO_2 uptake in supported IL systems include the nature of the ionic liquid components, particularly in terms of active sites, and the mobility of confined CO_2, which is directly linked to the viscosity and molecular interactions within the ILs. To investigate this relationship, we employed ^{13}C NMR relaxation studies, particularly T_1–T_2 relaxation correlation experiments, to probe the local molecular dynamics of CO_2 within ILs of varying viscosities. These measurements provide insight into the timescales of molecular motion and interaction strength between CO_2 and IL components. Our findings reveal that ILs with lower viscosity, such as [Bmim][NTf_2], exhibit longer T_2 values, suggesting faster CO_2 diffusion and weaker interactions. This behavior is attributed to the relatively weak interaction of the NTf_2^- anion with CO_2, allowing for easier diffusion and hopping between coordination sites. In contrast, more viscous ILs [Bmim][$CHTf_2$] and [Bmim][CTf_3] demonstrate shorter T_2 relaxation times, indicating stronger CO_2 binding and hindered transport due to steric hindrance imposed by the three trifluoromethane sulfonyl groups and electronic effects. In-situ NMR spectroscopy of [Bmim][$CHTf_2$] revealed a peak corresponding to CO_2 chemisorption at 172.8 ppm. With increasing temperature up to 55°C, this peak gradually diminishes, indicating a reversible interaction. Notably, the NMR spectra show that the peak disappears completely at 50°C, suggesting that CO_2 desorption occurs at this temperature. This behavior aligns with the dynamic nature of CO_2 binding in ionic liquids, where temperature-dependent equilibrium shifts influence CO_2 uptake and release. Such insights provide valuable information on the thermal stability and regeneration potential of IL for CO_2 separation applications.

Interestingly, [Bmim][$CHTf_2$] exhibited an intermediate behavior, with CO_2 appearing to transfer more readily between coordination domains compared to [Bmim][CTf_3]. This facilitated CO_2 hopping mechanism contributes to higher sorption capacities (0.108 mol CO_2/mol IL) and faster CO_2 uptake rates. The enhanced mobility in [Bmim][$CHTf_2$] suggests that while the presence of electron-withdrawing groups affects CO_2 interaction

strength, their spatial arrangement and steric accessibility play a critical role in governing overall CO_2 transport dynamics.

These findings highlight the intricate balance between electronic effects, steric constraints, and molecular mobility in IL-based CO_2 capture systems. The observed variations in T_1–T_2 relaxation behavior provide fundamental insights into how anion selection can be leveraged to optimize IL performance for gas separation applications. By fine-tuning anionic structures, it is possible to enhance CO_2 solubility while maintaining favorable diffusion characteristics, offering new strategies for designing next-generation IL-based membranes with superior separation efficiency.

4.4 Conclusion

As advancements in gas separation material science continue to enhance the selectivity, permeability, and stability of CO_2 separations, for example, membrane-based technologies—especially those incorporating ionic liquids—are expected to play a critical role in mitigating climate change. By enabling cost-effective and energy-efficient CO_2 capture, these technologies offer significant potential for large-scale implementation in various industries, contributing to global efforts to achieve carbon neutrality and combat climate change. The incorporation of electron-withdrawing groups diminishes nucleophilicity and suppresses chemisorption, leading to a lower CO_2 binding strength. For correlating NMR relaxation behavior with membrane permeability measurements, our study provides a deeper understanding of how IL structural properties impact gas transport performance. T_1–T_2 relaxation correlation experiments revealed that [Bmim][NTf_2] exhibits the longest T_2 relaxation times, indicating higher CO_2 mobility and weaker CO_2–anion interactions, which can facilitate enhanced gas transport and result in the high permeability. In contrast, [Bmim][$CHTf_2$] displays intermediate T_2 values, signifying a balanced interaction strength that supports moderate CO_2 hopping and permeability. [Bmim][CTf_3] demonstrates the shortest T_2 relaxation times, reflecting restricted CO_2 mobility due to stronger interactions within IL and steric hindrance from the bulky trifluoromethane sulfonyl groups, leading to the lowest permeability. These findings highlight the critical role of anion structure in governing CO_2 dynamics and

transport properties in ionic liquid-based membranes, providing fundamental insights into designing ILs with optimized CO_2 separation performance.

References

[1] Keeler, James. Understanding NMR spectroscopy. John Wiley & Sons, 2011.

[2] Moon, H. J., Sekiya, R. S., & Jones, C. W. (2023). Probing the morphology and mobility of amines in porous silica CO2 sorbents by 1H T 1–T 2 relaxation correlation NMR. The Journal of Physical Chemistry C, 127(24), 11652-11665.

[3] Castiglione, F., Saielli, G., Mauri, M., Simonutti, R., & Mele, A. (2020). Xenon dynamics in ionic liquids: a combined NMR and MD simulation study. The Journal of Physical Chemistry B, 124(30), 6617-6627.

[4] Moore, J. K., Marti, R. M., Guiver, M. D., Du, N., Conradi, M. S., & Hayes, S. E. (2018). CO2 adsorption on PIMs studied with 13C NMR spectroscopy. The Journal of Physical Chemistry C, 122(8), 4403-4408.

[5] Eidmann, G., Savelsberg, R., Blümler, P., & Blümich, B. (1996). The NMR MOUSE, a mobile universal surface explorer. Journal of Magnetic Resonance, Series A, 122(1), 104-109.

[6] Russell-Parks, G. A., Leick, N., Marple, M. A., Strange, N. A., Trewyn, B. G., Pang, S. H., & Braunecker, W. A. (2023). Fundamental Insight into Humid CO2 Uptake in Direct Air Capture Nanocomposites Using Fluorescence and Portable NMR Relaxometry. The Journal of Physical Chemistry C, 127(31), 15363-15374.

[7] Moore, J. K., Guiver, M. D., Du, N., Hayes, S. E., & Conradi, M. S. (2013). Molecular motions of adsorbed CO2 on a tetrazole-functionalized PIM polymer studied with 13C NMR. The Journal of Physical Chemistry C, 117(44), 22995-22999.

[8] Li, E., Ganesan, A., Liu, H., Ivanov, A. S., He, L., Nalaoh, P., ... & Dai, S. (2025). Sub-5 Ångstrom Porosity Tuning in Calixarene-Derived Porous Liquids via Supramolecular Complexation Construction. Angewandte Chemie International Edition, 64(11), e202421615.

CHAPTER 5: CONCLUSIONS, SUMMARY, AND FUTURE WORK

5.1. Conclusions and Summary

The DAC procedure represents a promising technique to mitigate the emitted CO_2 directly from the air atmosphere and diminish their impact on climate change. Depending on the performance of the sorbents, this can even outperform the impact of natural processes, and the captured CO_2 might be used as feeding stocks in industrial production processes that are specifically designed to produce value-added chemicals, such as fuels, solvents, and plastics, reducing the overall carbon footprint. Although state-of-the-art DAC procedures are still relying on liquid sorbents such as aqueous amines/alkaline hydroxide/carbonates, their inherent drawbacks (e.g., inferior stability and high energy consumption) triggered the development of alternative advanced sorbent systems. Comparatively, solid sorbents could provide solutions to some of the issues and have attracted extensive studies towards enhanced DAC of CO_2 procedure by structural engineering. As summarized and compared in the introductory of the thesis, amine-modified scaffolds, iminoguanidine-derived sorbents, and SIL-functionalized systems are three promising categories. The IL-derived sorbents exhibited large tuning capability in terms of interaction strength with CO_2 and improved anti-oxidation and thermal stability. Despite all these achievements, there are still unsolved issues and space to further improve the DAC of CO_2 performance, particularly deploying customized solid sorbents. This thesis explored the design, synthesis, characterization, and performance evaluation of ionic liquid (IL)-modified carbonaceous materials for enhanced direct air capture (DAC) of CO_2. The major findings and contributions are summarized as follows:

Design and Engineering of IL-Modified Sorbents:

A family of superbase and imidazolium-based ILs were synthesized and supported on porous carbonaceous scaffolds using wet impregnation techniques. The combination of strong CO_2-reactive ILs and tunable carbon porosity resulted in composite sorbents with favorable properties for DAC, including high CO_2 affinity and thermal stability.

Porosity and Structure–Performance Relationships:

Through detailed porosity analysis and wide-angle X-ray scattering (WAXS), it was shown that the morphology of carbon supports, particularly mesopore size and pore

volume, governs the IL distribution and CO_2 accessibility. Larger mesopores promote greater CO_2 uptake by exposing more active IL binding sites to the gas phase, while IL layering in micropores can hinder accessibility.

Performance in DAC Conditions:

Breakthrough experiments under simulated ambient conditions confirmed that IL-modified sorbents exhibit reversible CO_2 uptake, with performance enhanced by optimized IL loading and pore structure. The measured sorption capacity and desorption kinetics emphasize the potential for these systems in practical DAC technologies.

Chemical and Physical Interactions with CO_2:

Operando NMR techniques, including ^{13}C T_1–T_2 relaxation correlation, were deployed to investigate the chemical and physical dynamics of CO_2 within IL-modified systems. It was demonstrated that shorter T_2 values correspond to reduced CO_2 mobility, indicative of stronger binding environments. The diversity in T_1–T_2 profiles among ILs provided molecular-level insight into CO_2 hopping and binding dynamics, strongly correlated with IL viscosity and chemical composition.

Collectively, this work confirms that rational integration of superbase ILs with carbon scaffolds offers a viable pathway toward next-generation sorbents capable of efficient and reversible CO_2 capture from ultra-dilute environments.

5.2. Future Work

Building on the promising results of this study, future research efforts should focus on refining the structure and functionality of the ionic liquids (ILs) to further enhance their performance in direct air capture (DAC) applications. One particularly promising direction lies in the molecular-level design of ILs by tailoring their anion and cation pairs. Such structural optimization could allow precise tuning of properties like basicity, viscosity, and CO_2 binding strength—parameters that directly impact sorption capacity and regeneration efficiency. Specifically, ILs containing multidentate anions or fluorinated functionalities may provide synergistic enhancements in both CO_2 affinity and thermal stability.

At the same time, a more detailed mechanistic understanding of CO_2 interactions within confined IL environments is essential. This can be achieved by coupling experimental observations with molecular dynamics (MD) simulations and density functional theory (DFT) calculations. Computational modeling would help reveal the nature of CO_2 binding under varying humidity levels and temperature ranges, and clarify the effects of confinement and support-IL interactions on CO_2 transport and reaction dynamics. These insights would support the rational design of next-generation sorbents with predictive control over performance metrics.

As this work has primarily focused on CO_2 as a single-component system, it is also crucial to evaluate the performance of these materials under realistic ambient air conditions, which contain moisture and various other gases. The presence of water vapor, in particular, can significantly influence IL behavior, potentially altering the sorption mechanism and affecting long-term material stability. Conducting multicomponent gas breakthrough studies under varied humidity levels will provide a clearer picture of operational robustness and practical applicability.

Furthermore, while this research demonstrates the fundamental potential of IL-modified carbonaceous materials, translating these findings into scalable technologies will require a focus on fabrication strategies that enable uniform IL distribution and mechanical durability in structured sorbents, such as pellets, monoliths, or fibers. These formats are more amenable to integration in fixed-bed DAC systems and could improve process efficiency by reducing pressure drop and enhancing gas-solid contact.

Finally, to evaluate the true potential of these materials for deployment, future work should also consider techno-economic analysis and life cycle assessment (LCA). These studies would quantify the cost, energy requirements, and environmental impact of IL-based DAC materials, providing crucial metrics to compare their feasibility against other carbon capture technologies. The combination of advanced material engineering, mechanistic insight, and systems-level analysis will be essential to bring IL-modified carbon sorbents closer to real-world DAC applications.

VITA

Narges Mokhtarinori was born in Tehran, Iran. She earned her bachelor's degree in chemistry from Azad University. Following graduation, she worked as a research assistant at Tehran University of Medical Sciences (TUMS) under the mentorship of Professor Ahmad Reza Shahverdi. During her time at TUMS, she also pursued and completed her master's degree.

After gaining industry experience as a technical supervisor at a medical equipment manufacturing company, she was admitted with full funding to the graduate program at the University of Tennessee, Knoxville. She joined Dr. Sheng Dai's research group in Spring 2022 to pursue her thesis work.

Her research focuses on carbon dioxide capture, including the synthesis of novel materials and ionic liquids for enhanced CO_2 adsorption. Throughout her graduate studies, she successfully published multiple first-author papers and contributed to several collaborative projects with research groups both across the U.S. and internationally.